PLIO-PLEISTOCENE STRATIGRAPHY AND PALEOGEOGRAPHY FOR

HOMININ REMAINS FROM AREAS 130 AND 133, KOOBI FORA, KENYA

by

CHRISTOPHER J. LEPRE

A Dissertation submitted to the

Graduate School-New Brunswick

Rutgers, The State University of New Jersey

in partial fulfillment of the requirements
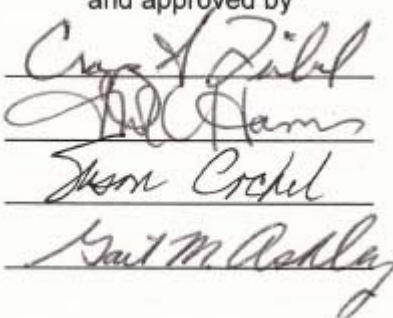
for the degree of

Doctor of Philosophy

Graduate Program in Anthropology

written under the direction of

Craig S. Feibel

and approved by

_____

_____

_____

_____

New Brunswick, New Jersey

October 2009

ABSTRACT OF THE DISSERTATION

Plio-Pleistocene stratigraphy and paleogeography for hominin remains from

Areas 130 and 133, Koobi Fora, Kenya

by CHRISTOPHER J. LEPRE

Dissertation Director:

Craig S. Feibel

The Koobi Fora Formation archives a record of hominin evolution for a three-million-year period (ca. 4-1 Ma) within the northeast Turkana Basin, Kenya. Assessing probable controls on the fossil or archaeological patterns in the formation requires an understanding of the spatial-temporal contexts of the hominin remains and detailed knowledge of the paleoenvironmental settings in which evolution occurred. Toward these ends, research was conducted in the basin to interrelate paleoanthropological sites from collection Areas 130 and 133, refine the paleogeography of the north-central Karari Escarpment, and ultimately provide a framework for establishing associations between hominin adaptations and habitats features in the Koobi Fora region. Results of sedimentological and stratigraphic analyses demonstrate that deposits of the upper Burgi/lower KBS members (~1.9 Ma) accumulated within a low-lying floodbasin setting, covering an area of about 8 km^2 for the northern Karari. This setting supported vertisols and was locally incised in northern Area 133 by a channel that attained a minimal depth of 3 m and lateral extent of ≥100 m. Beginning in the middle KBS Member

ii

and continuing to the upper KBS Member, the landscape experienced repeated dissection, aggradation, and prolonged (10^3-10^5 years) calcic soil formation. Channel systems during this interval extended laterally for ≥2 km and evolved from a deeply incised (up to 8 m of erosive relief) sandy complex to a shallower braided network carrying abundant basaltic gravel. Deposits of the upper KBS/lower Okote members (~1.6 Ma) accumulated within a meandering channel and associated proximal floodplains. This landscape mainly aggraded through crevasse-splay sedimentation and supported immature alluvial soils. A similar floodplain style in Area 133 persisted to or resumed in the upper Okote/lower Chari members (~1.4 Ma). The oldest and youngest hominin remains are potentially represented by surface occurrences of stone tools in Area 133. Most hominin remains from Area 130 derive from both braided- and meandering-river environments of the upper KBS to lower Okote members. The paleogeography represented by the reconstructed depositional systems was influenced by monsoon-driven seasonality in an otherwise semi-arid climate, in addition to instances of extra-basin volcanism that caused rates of sediment supply to episodically increase. Additional controls may have stemmed from lake-level oscillations and/or increased regional aridity occurring at 1.8-1.7 Ma.

ACKNOWLEDGMENTS

TABLE OF CONTENTS

LIST OF TABLES

LIST OF FIGURES

1. Introduction

A comprehensive understanding of the environmental factors of East African hominin evolution remains elusive despite decades of multidisciplinary research. Many unresolved questions exist and compromise interpretations of the adaptive meaning and significance of fossil and archaeological materials. Such issues range from fundamental ones, like the habitat preferences of hominin genera (Haile-Selassie, 2001; Wood and Strait, 2004), to complex problems that deal with the role of environmental change in producing the long-term patterns and key junctures of evolution (Vrba, 1995, 1999; Potts, 1996, 1998). At least some of this uncertainty derives from the need to refine the sedimentological and stratigraphic context of hominin sites (Feibel, 1997; Potts, 1998). Sedimentological analysis is a basis for reconstructing the environments of deposition and assessing the taphonomic factors of preservation, prevailing climatic conditions, and ecological constraints on habitat structure. Stratigraphy not only provides a means for establishing spatial and temporal relationships between different hominin sites, but also facilitates the integration of local, regional, and global records for examining likely controls on environmental change. Moreover, sedimentology and stratigraphy are the rudiments to the geological framework upon which different types of environmental data are assimilated.

Central to the understanding of the environmental context of East African hominins from the Plio-Pleistocene is the Lake Turkana Basin of northwest Kenya and southwest Ethiopia (Figs. 1 and 2). Within the northeast part of the

Fig. 1: Geopolitical location of the Lake Turkana Basin. Note
shaded outline of the lake within the boxed area labeled Fig. 2.

Addis Ababa

ETHIOPIA

5° N

Fig. 2

SOMALIA

Mogadishu

KENYA

0°

INDIAN

Nairobi

OCEAN

TANZANIA

5° S

35° E

40° E

45° E

100 km
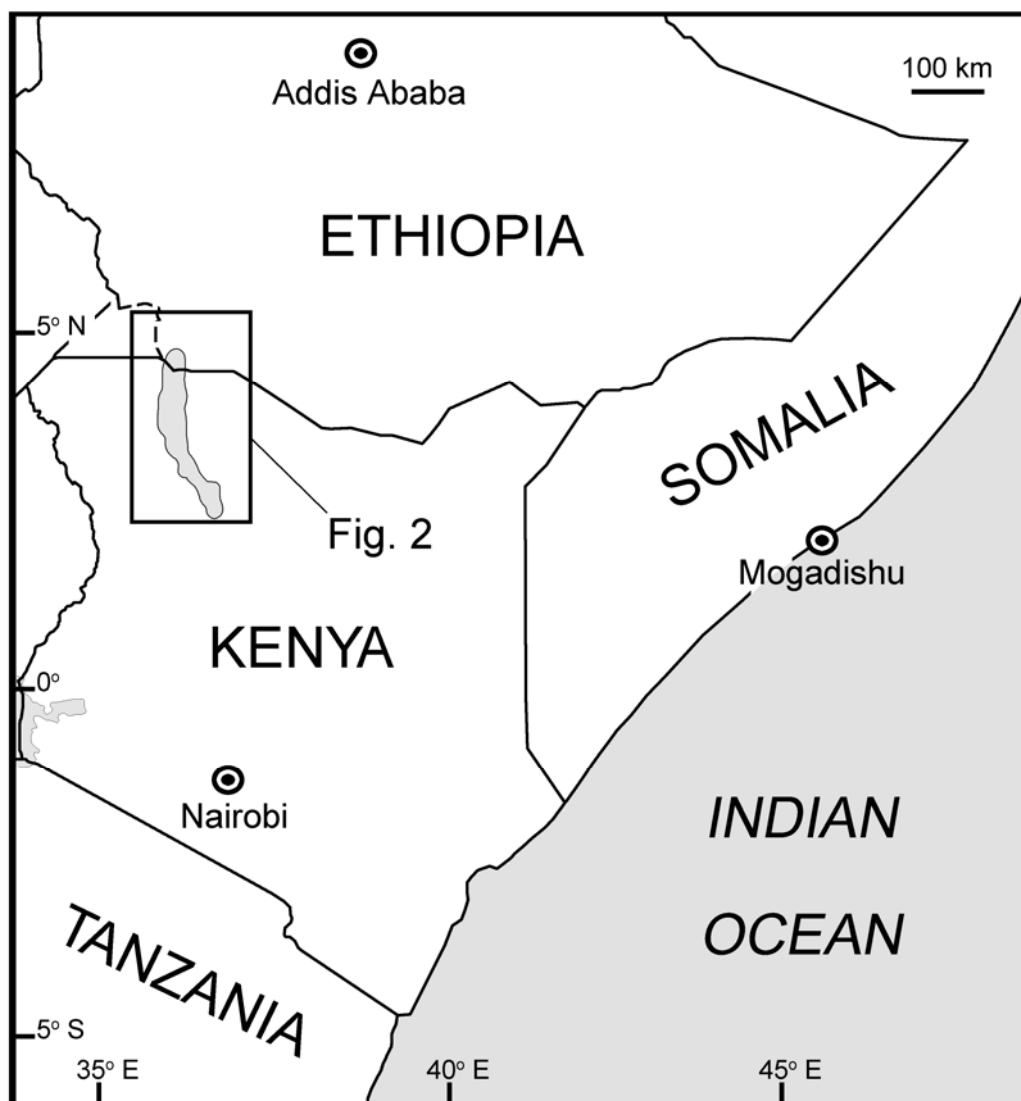
Fig. 2: Modern tectonic and hydrographic setting of the Lake Turkana Basin. Fault patterns and structure from Frostick and Reid (1990) and Frostick (1997). Extent of Plio-Pleistocene sedimentary formations (crosshatched areas) after Brown and Feibel (1991).

Shungura Fm.

Omo River

N

5° N

0   (km)   60

Ileret

Nachukui Fm.

Koobi Fora Fm.

4° N

Fig. 3

Lodwar   Turkwell River

3° N

Kerio River

Loiyengalani

36° E   37° E
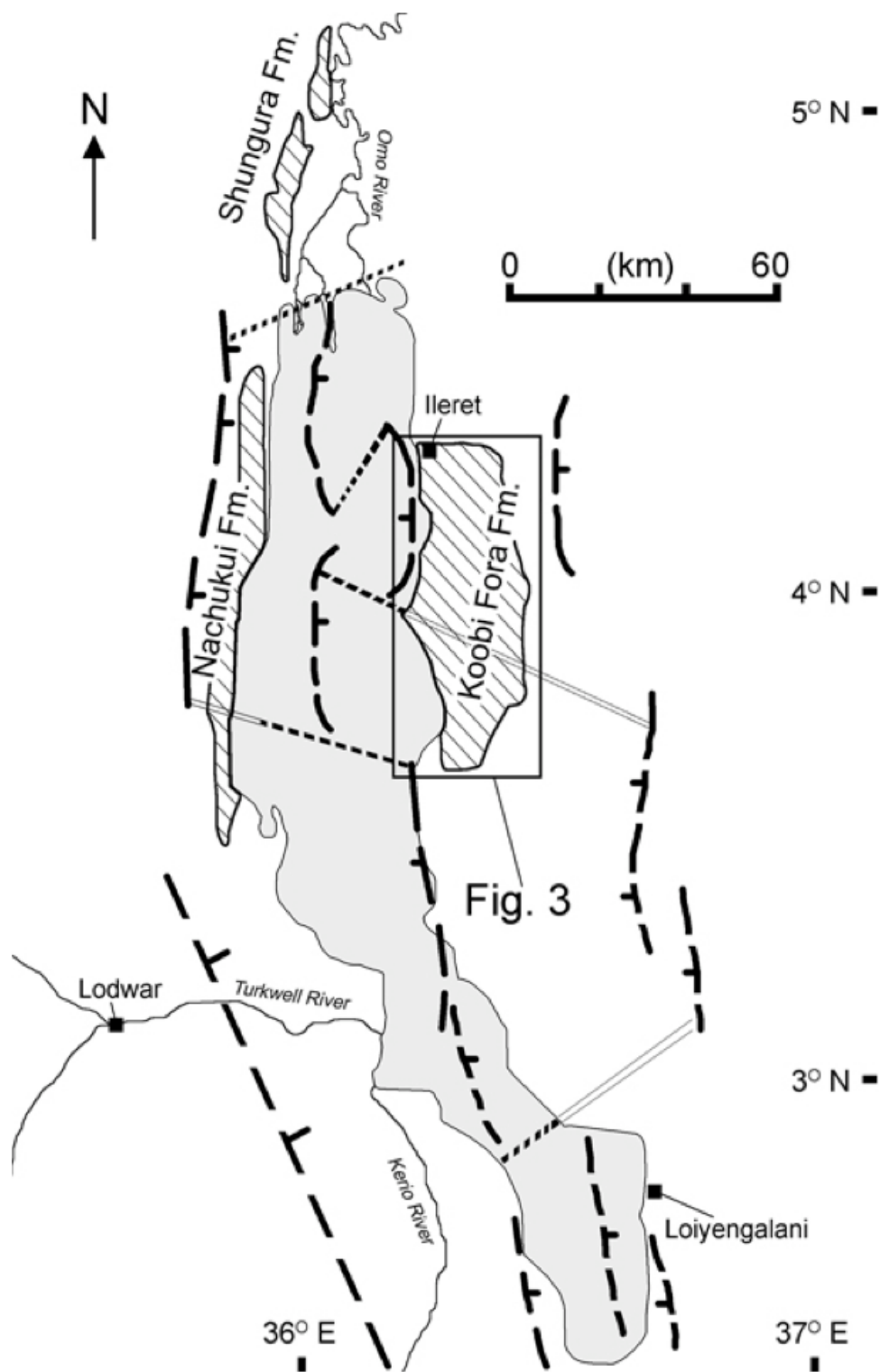
basin, in Kenya, is the important paleoanthropological locality of Koobi Fora (Fig. 3). Sedimentary successions of the Koobi Fora Formation (Fig. 4) contain multiple environmental, fossil and archeological records, which are instrumental for interpreting the tempos, modes, parameters and thus reasons behind hominin evolution and human origins (Leakey and Leakey, 1978; Harris, 1983; Wood, 1991; Isaac and Isaac, 1997). During a three-million-year period of Pliocene and early Pleistocene time, several hominin species evolved and stone tool industries were developed within a range of habitats encompassed by river, delta and lake-margin ecosystems (Feibel et al., 1991). These ecosystems existed through rift-related volcanism, tectonic events, and climate changes that shaped habitats and presumably directed evolutionary trends to some extent. As a result of post early Pleistocene rifting and erosion, the sedimentary records of these ecosystems are now exposed along a series of ephemeral streams, fault blocks and escarpments, and distributed across an area greater than 2000 km^2 (Brown and Feibel, 1986, 1991). However, even though research at Koobi Fora has been extensive and multidisciplinary, there are still geological issues that complicate interpretations of the hominin remains. This is especially true for paleoanthropological collection Areas 130 and 133 of the Karari Escarpment.

The Karari Escarpment is a roughly NE/SW trending promontory of hominin-bearing sediments that abuts the northeast basin margin. It is 20-25 km inland from the modern shoreline of Lake Turkana. The escarpment extends for ~20 km from contacts with basin margin volcanic highlands, like the Suregei Cuesta. At its north-central portion, the Karari is subdivided E-W by the northern part of

Fig. 3: Aerial distribution of Koobi Fora Formation sediments within the northeast Lake Turkana Basin (modified from White et al., 1981). Examined outcrops of the "upper" Koobi Fora Formation are exposed along the Karari Escarpment in Areas 130 and 133, which are just to the south of the Suregei Cuesta.

Legend:

- mainly early Pliocene & older volcanic (basalt) rocks
- "lower" Koobi Fora Formation (Plio-Pleistocene) sediment: Lonyumun to Burgi Members
- "upper" Koobi Fora Formation (Plio-Pleistocene) sediment: KBS to Chari Members
- Pleistocene-Holocene Galana Boi Formation (sediment)
- Holocene colluvium
- fault
- ephemeral stream
- unpaved road

4°19'N
36°32'E

Ileret

Suregei Cuesta

Kokoi Horst

TURKANA

Karari Escarpment

1 3 0

1 3 3

Museum camp

LAKE

Allia Bay

Ranger post

NORTH

20 km

36°10' E
3°39' N

Fig. 4: Plio-Pleistocene formations of the Omo Group (based on Brown and Feibel, 1986, 1991; Feibel et al., 1989; McDougall et al., 1992; McDougall and Brown, 2006; McDougall and Brown, 2008). Timescale is from Lourens et al. (2004). For this study the examined stratigraphic interval generally covers the upper Burgi to lower Chari Members, Koobi Fora Formation. See Figs. 2 and 3 for aerial distributions of the formations.
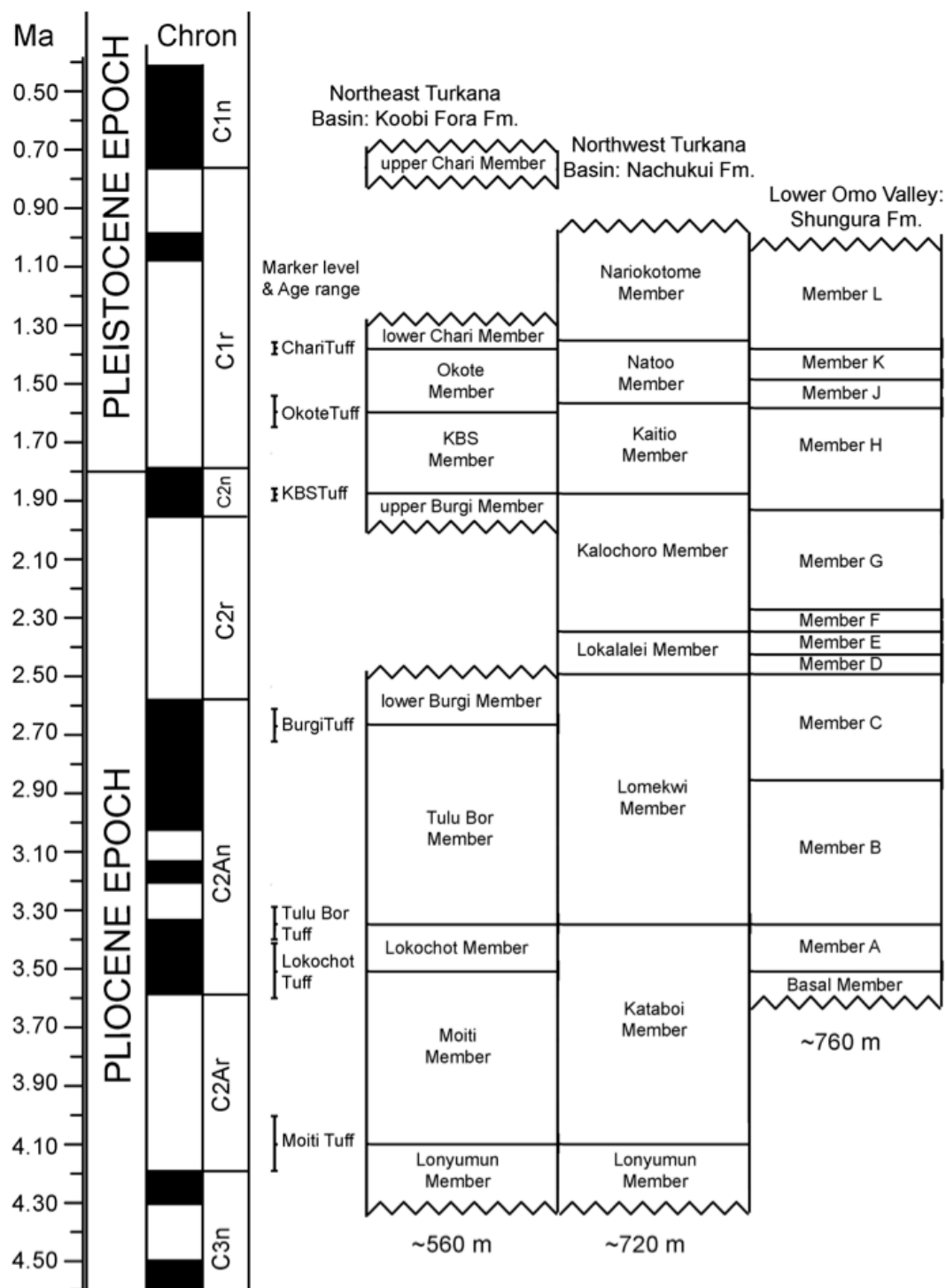
Area 133 and the entirety of Area 130 (Fig. 3) (Leakey and Leakey, 1978; Burggraf et al., 1981; White et al., 1981; Brown and Feibel, 1991). Outcrops are well exposed in Area 130 and rich in hominin remains, including multiple stone tool and fossil sites (Isaac and Harris, 1976; Leakey et al., 1978). However, although the site-specific (Harris et al., 1997) and regional (Rogers et al., 1994) settings are documented, the paleogeographic context of the hominin remains at the landscape scale is not fully understood. Furthermore, the few studies focusing on this level of analysis (e.g., Isaac and Behrensmeyer, 1997) are problematic and assimilate sites from disparate chronostratigraphic positions into the same landscape reconstruction. As landscape-scale geological data is key for assessing hominin activities and ecological causes over narrow spatial intervals (Potts et al., 1999), it therefore necessary to further interpret the paleogeography of Area 130.

The eastern boundary of Area 130 is the western extent of northern Area 133, as defined by the major dirt road that runs along the N/S axis of the Karari (Fig. 3). Collection Area 133 comprises a subtle terrain on the backslopes of the Karari. Surface archaeological occurrences and, to a lesser extent, *in-situ* stone tools are documented from the sedimentary outcrops in the northern portion of this collection area. Besides microstratigraphic work at one archaeological site (Harris et al., 1997) and cursory geological survey (Frank, 1976), there is little basis for understanding the possible sedimentological and stratigraphic context of the archaeology. Furthermore, Area 133 is thought to reflect the Plio-Pleistocene location of a somewhat unique arid and upland environment. Such

interpretations are founded on a small sample of ungulate fossils, and the proximity of Area 133 to the modern basin margin (e.g., Rogers and Sorkowitz, 1992; Feibel et al., 1991). If these interpretations are correct, then the archeological remains might allow for interesting research on hominin behavior in an under-sampled environmental context.

Fieldwork was conducted in collection Areas 130 and 133 to help address the above issues. The following dissertation reports on the sedimentological and stratigraphic observations, analytical methods, and interpretations for both areas. It also discusses and interprets electron-microprobe analyses on glass shards from collected northern Area 133 tuffs. The research builds on previous work by providing new fluvial architectural and tephrostratigraphic data as well as additional details on sedimentary facies, paleosols, and lithostratigraphy. The goals of this dissertation are (1) to describe and interpret the Plio-Pleistocene fluvial sediments from Areas 130 and 133, (2) to document centimeter- to decameter-scale trends in the fluvial sediments that were produced by variations in channel and overbank deposition, and (3) to assess the scales, processes and genetic factors for the paleo-geomorphology of the north-central Karari Escarpment. Results of these studies are used to improve the geological contexts of the fossil and archaeological sites. The findings will permit paleoanthropologists to better resolve the hominin remains according to adaptive meaning, taxonomic/technological affinities, and evolutionary factors.

2. Geological overview

Situated between the Ethiopian and Kenyan domes, the Turkana Basin is located in the eastern branch of the East African Rift System. It extends north/south, mainly through northwestern Kenya but also within a part of southwestern Ethiopia (Fig. 1). Today, the Turkana Basin is occupied by hydrologically closed Lake Turkana and chiefly fed by the perennial Omo River (Fig. 2). For at least the last five million years or so, the river has drained southwards off the Ethiopian dome, flowed through the broad zone of rifting that connects the Main Ethiopian Rift to the Kenyan Rift, and entered the northern end of the basin (WoldeGabriel and Aronson, 1987; Brown and Feibel, 1991). A series of roughly N/S normal faults and NE/SW transfer faults divide the basin into southern, central, and northern sub-basins (Dunkelman et al., 1988; Morley et al., 1992). The Area 130 and 133 study locations are located within an easternmost portion of the northern sub-basin, referred to as the northeast Turkana Basin (Fig. 3). This sub-basin has an overall half-graben structure, with a normally faulted escarpment margin to the west and a flexural margin at the east (Fig. 2) (Frostick and Reid, 1990; Frostick, 1997). A succession of late Paleogene to early Pliocene uplifted basalt rocks and, to a lesser extent, ignimbrites and sediments define the eastern limits for this northern sub-basin of Turkana (Fig. 3) (McDougall and Watkins, 2006). Such volcanics, particularly the basalts, are extensive in the subsurface and underlie much of the accumulated Pliocene to Recent sediment of the northeast basin (Dunkelman et al., 1988; Haileab et al. 2004).

Rift-related volcanism and crustal extension in the Turkana region began in early Cenozoic times (Ebinger et al., 2000; Chorowicz, 2005). For the northeast Turkana Basin, rifting proceeded through a series of pulses. The earliest began near 35 Ma ago and the onset of the most recent one, which continues today, commenced between <13 Ma and >5 Ma (McDougall and Watkins, 2006). Gombe Group flood basalts (Watkins, 1986) comprise a majority of the volcanic highlands marginal to the northeast basin (e.g., the Suregei Cuesta in Fig. 3). They date to 6-4 Ma, and represent an exposed extent to a series of widespread eruptions associated with an early phase to this most recent pulse of rifting (Fitch et al. 1985; McDougall and Watkins, 2006; Haileab et al. 2004). Successive to these basalts is the nearly 560-m-thick Koobi Fora Formation (Fig. 4), which is the Plio-Pleistocene (about 4-1 Ma) sedimentary record associated with this recent pulse of rifting (Behrensmeyer, 1970; Vondra et al., 1971; Bowen and Vondra, 1973; McDougall, 1985; Brown and Feibel, 1986).

The Koobi Fora Formation consists of gravel/conglomerate, sand/sandstone and mudstone, and records fluvial, deltaic, and lacustrine environments of deposition (Brown and Feibel, 1991). Age constraints are from radioisotope dating of feldspar-rich pumices found within fluvial-deposited rhyolitic tuffs (McDougall, 1985; McDougall and Brown, 2006, 2008), magnetostratigraphy (Hillhouse et al., 1977, 1986; McDougall et al., 1992), and tephrostratigraphy (Cerling and Brown, 1982; Brown and Feibel, 1986; Feibel et al., 1989; Brown et al., 2006). The tuffs are particularly important for high-resolution correlation of the Koobi Fora Formation and the other coeval Omo Group formations of the

northern Turkana Basin of Kenya and the adjacent southern Omo Valley of Ethiopia (Figs. 2 and 4). Omo Group tuffs drive from Plio-Pleistocene volcanic centers within the Main Ethiopian Rift (Brown, 1972; WoldeGabriel and Aronson, 1987), and represent the aqueous transport of volcaniclastics in the Turkana Basin via the ancestral Omo River (Cerling and Brown, 1982; Brown and Feibel, 1986, 1991; WoldeGabriel and Aronson, 1987). Therefore, most studies agree that the Turkana Basin tuffs are not representative of volcanism in the basin, but rather reflect eruptions farther to the north.

Except for activity near 2.5 Ma and again at ~1.4 Ma, the deposition of the entire Koobi Fora Formation occurred over a fairly quiescent period of within-basin tectono-volcanism (Brown and Feibel, 1991; Feibel et al., 1991). Furthermore, the general tectonic structure and associated physiography of the northeast Turkana Basin (such as the Kokoi Horst in Fig. 3) formed in the late Pleistocene or Holocene after the deposition of the Koobi Fora Formation (e.g., Morley et al., 1992; Wescott et al., 1996; Ebinger et al., 2000). However, basalts rimming the northeast basin (Fig. 3) were amply deposited as gravels/conglomerates in the Koobi Fora Formation. Basin margin volcanics thus were sediment source areas and to some extent uplifted/exposed in the Plio-Pleistocene (Vondra et al., 1971; Bowen and Vondra, 1973; Brown and Feibel, 1986).

The Koobi Fora Formation (Fig. 4) is divided into Lonyumun, Moiti, Lokochot, Tulu Bor, Burgi, KBS, Okote, and Chari Members (Brown and Feibel, 1986). A disconformity or angular unconformity, which apparently reflects about 500,000

years of missing section over the approximate period of 2.5-2.0 Ma, divides the Burgi Member into upper and lower parts (Feibel et al., 1989; McDougall and Brown, 2008). The origin of this break is hypothesized as a result of regional uplift in southern Ethiopia and associated down-warping of the Turkana Basin (Brown and Feibel, 1991; Feibel et al., 1991). Another similar unconformity occurs higher in the section, within the Chari Member (Fig. 4), but its origin is not well studied as compared to the one from the Burgi Member. Sedimentation pre-dating the Burgi disconformity/unconformity (about 4.0 to 2.5 Ma) is characterized by separate intervals, each lasting on the order of 10^4 to 10^5 years, of fluvial, deltaic and lacustrine deposition (Brown and Feibel, 1991). Contrastingly, the sedimentary interval above the break (about 2.0 to 1.0 Ma) generally reflects a protracted transition from a lacustrine-dominated basin to a fluvial-dominated one (Feibel et al., 1991).

Field research for this dissertation mostly focused on Burgi, KBS, and Okote Member deposits of the Koobi Fora Formation that collectively span an interval of about 300,000 years at 1.9-1.6 Ma (Fig. 4). Basin-scale paleogeography and paleoenvironments have been well documented for this period. Between 1.9 and 1.8 Ma the ancestral Omo River flowed north to south into the basin and terminated at the margin of an axial lake (Brown and Feibel, 1991). Upon entering the northern basin, the ancestral Omo River flowed east-southeast of a northern lake margin and then turned south-southwest to the lake's edge (Fig. 5). Expansive floodbasins flanked the river's course. The lake had an open hydrology at times, with an outlet located near the southeast margin of the basin.

Fig. 5: Paleogeographic map of the Lower Omo Valley and northern Turkana Basin at ~1.87 Ma (after Brown and Feibel, 1991). The three major elements are the ancestral Omo River coming in from the north, a basin-wide axial lake, and the Turkana River exiting the basin toward the southeast.

ancestral Omo-Turkana system

~1.87 Ma

topographic relief

N

60 km
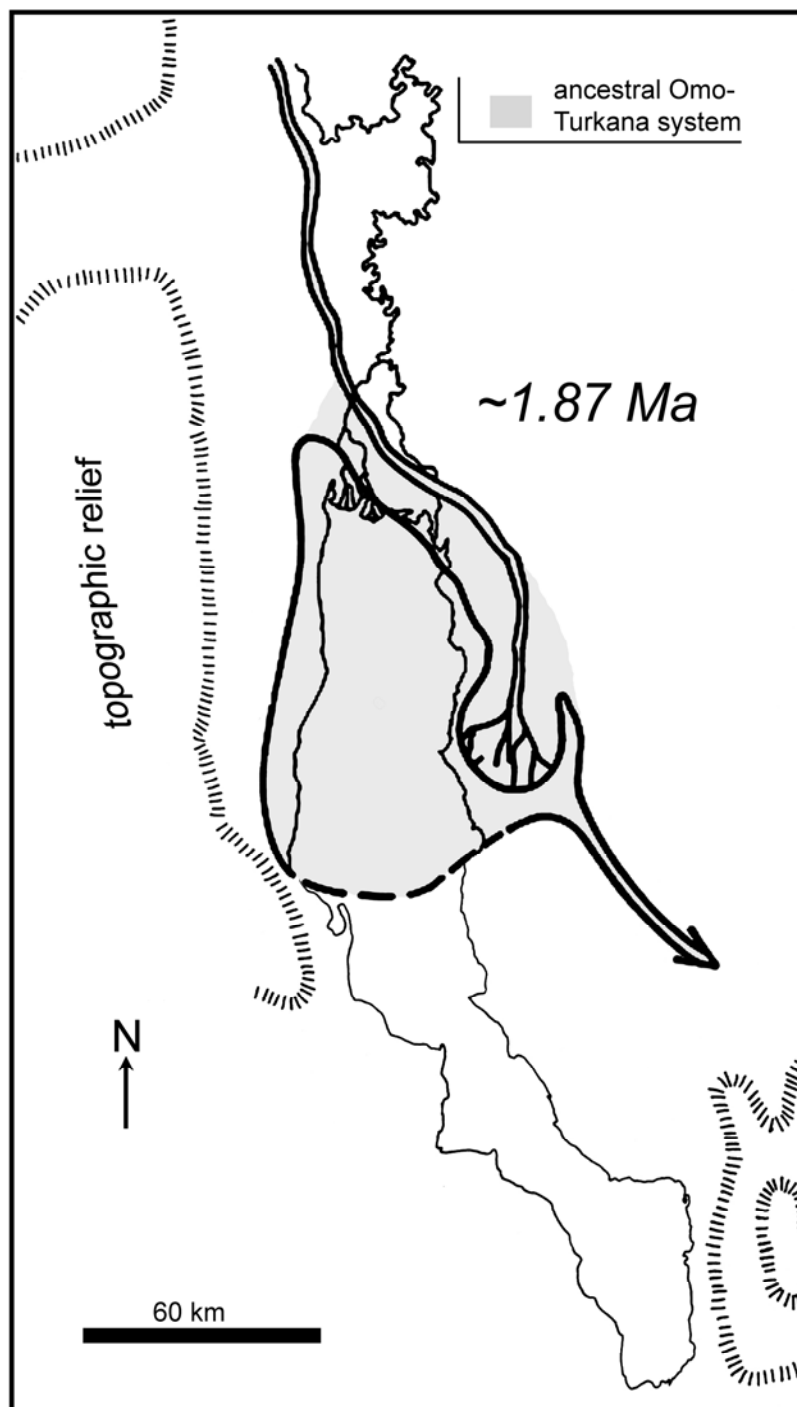
Paleontological studies on stingray remains in the Koobi Fora Formation have indicated a river stemmed from the outlet and connected to the Indian Ocean (Feibel, 1994). Lake waters were somewhat alkaline/saline, but generally fresh, and the lake-margin communities comprised abundant gastropods and bivalves (Williamson, 1982; Feibel et al., 1991).

Around 1.8 Ma, the ancestral Omo River retreated to north/northwest (Fig. 6), probably because the lake filled to its sill and the Omo diverted into the Nile drainage system (Feibel et al., 1991). Sometime after this, the overall level of the lake fell, likely in response to the decreased Omo input (Brown and Feibel, 1991).   The lake appears to have been a mostly closed system, with alkaline/saline waters that often experienced algal blooms and supported a limited biotic community (Abell et al., 1982; Feibel et al., 1991). Lake-level frequently oscillated, conceivably due to global and regional climate changes (Brown, 1995; Lepre et al., 2007). Coinciding with these axial hydrological changes, a multi-threaded channel system emanated from the northeast margin of the basin and emptied into the northeast/east lakeshore (Fig. 6).

By 1.6 Ma the ancestral Omo River reclaimed the northeast basin and the lake was largely infilled (Fig. 7). Shallow lake remnants existed, such as those along the basin's northwestern margin (Harris et al., 1988; Feibel and Brown, 1993). The river flowed through the Turkana Basin along a north-south axis, periodically avulsed east/west, and exited the basin toward the southeast (Brown and Feibel, 1991; Feibel et al., 1991). The river during this episode was largely a meandering system and had expansive overbank areas that included distributary

Fig. 6: Paleogeographic map of the Lower Omo Valley and northern Turkana Basin at ~1.8 Ma (after Brown and Feibel, 1991). Diversion of the ancestral Omo River toward the west is represented by large arrow in upper left-hand corner. Areas of the northeast Turkana Basin include a transverse fluvial system emptying into an axial lake, which oscillated in depth and aerial extent.
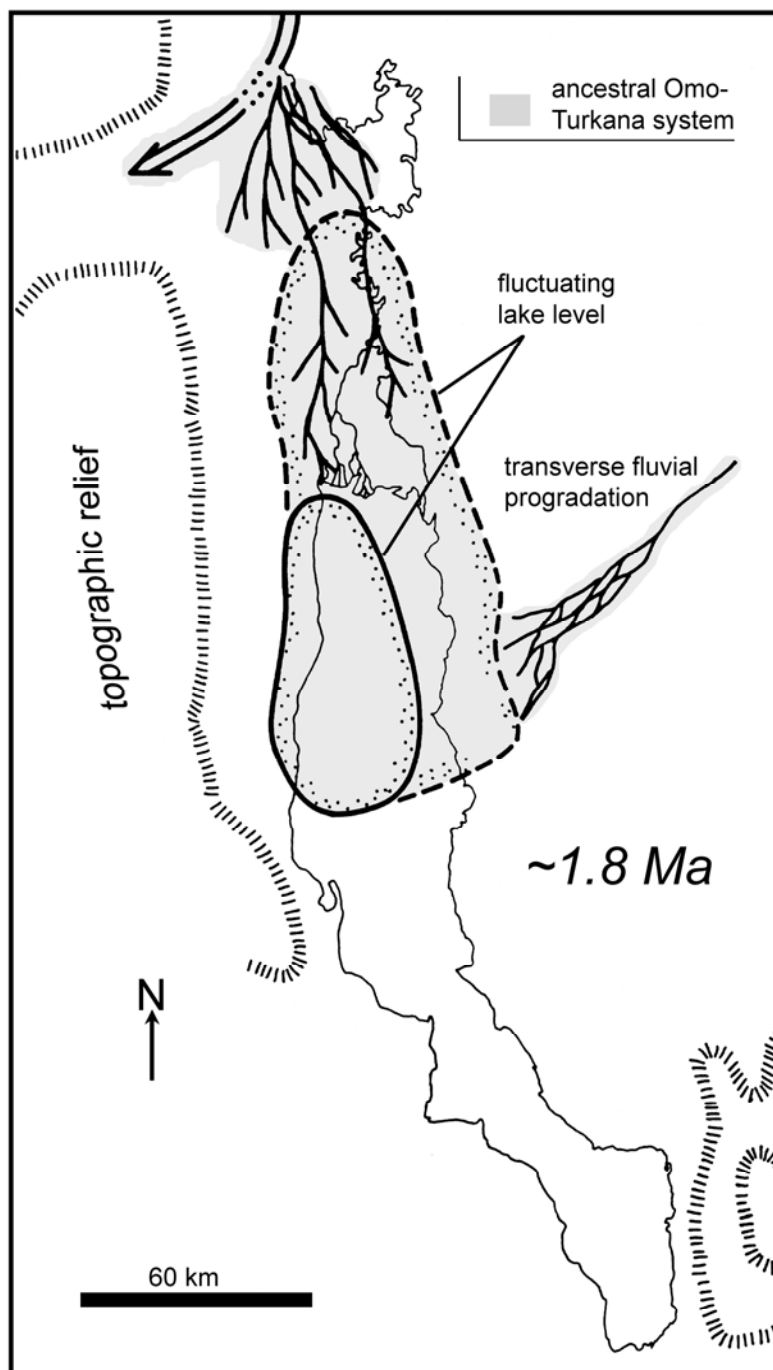
Fig. 7: Paleogeographic map of the Lower Omo Valley and northern Turkana Basin at about 1.6 Ma (after Brown and Feibel, 1991; Rogers et al., 1994). Exiting the basin toward the east is the Turkana River, whereas the ancestral Omo River is within the basin and to the north in the Lower Omo Valley. Anabranching lines represent the lower-ordered offshoots of the Omo's main channel.
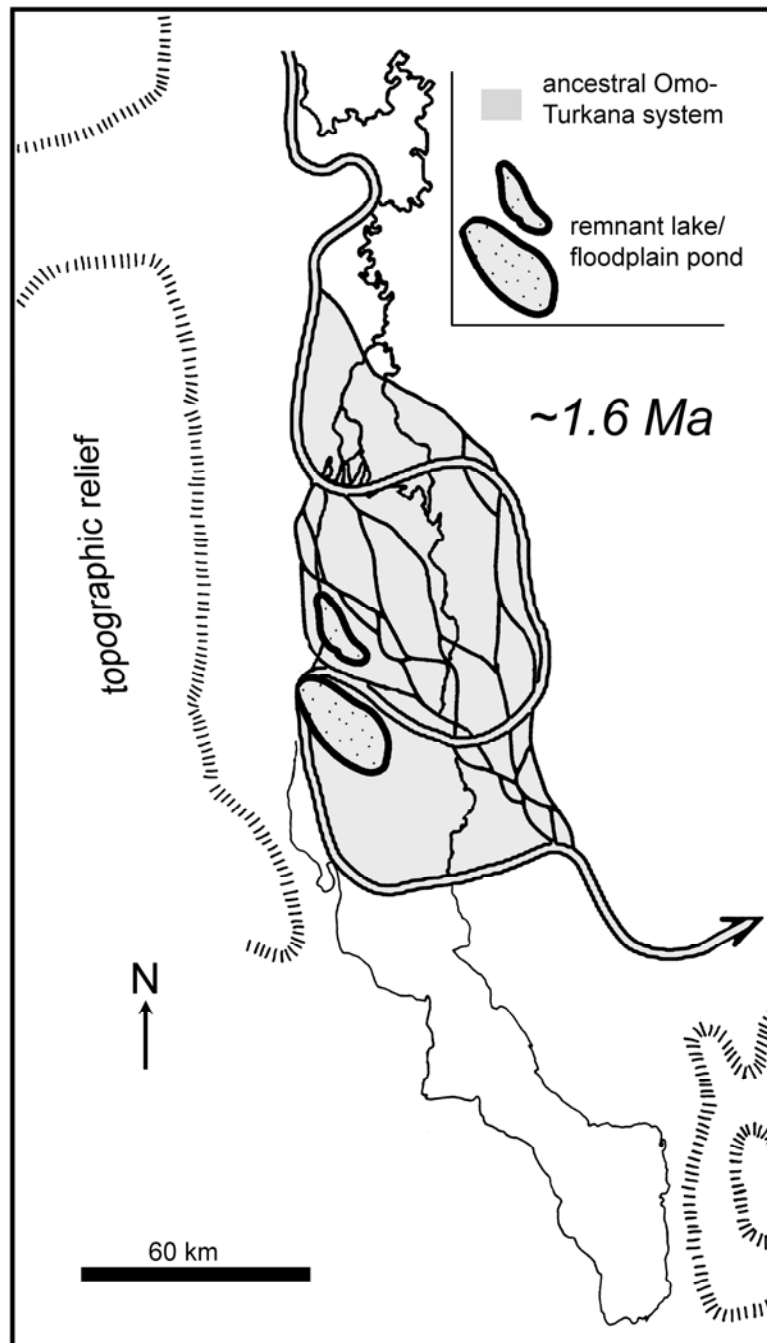
channels, tuffaceous-muddy floodplains, and a series of shallow ponds (Brown and Feibel, 1991; Feibel et al., 1991; Feibel and Brown, 1993; Rogers et al., 1994). Of importance to the timing of this reclamation was the deposition of a series of generally correlative tuff complexes—referred to as the Okote Tuff Complex, Ileret Tuff Complex, and Koobi Fora Tuff Complex—that were largely accumulated in Omo floodplain settings such as crevasse splays (e.g., Findlater, 1978; Burggraf et al., 1981). Tephrostratigraphic studies, and associated radiogenic-isotopic ages, have dated some of the lowest stratigraphic levels of these complexes to about 1.6 Ma (Brown and Feibel, 1985, 1986; Brown et al., 2006; McDougall and Brown, 2006).

This predominantly fluvial phase for the basin persisted past the period of 1.4-1.3 Ma, but the timing for its demise and the development of subsequent lacustrine phases are not precisely understood (Brown and Feibel, 1991; Feibel et al., 1991).

3. Facies, paleosols and architecture of hominin-bearing deposits from Area 130

   3.1. Introduction

   Fluvial sequences from the East African Rift System are important analytical units for paleoenthropological research, as they regularly contain multiple fossil and/or stone-tool sites in close stratigraphic association. Such datasets are key for understanding hominin sympatry, in addition to probable interrelationships between behavioral adaptation, taxa evolution, and environmental constraints. Often, however, there is much variation according to the type of depositional context and assemblage, for example:

   - *Homo*, *Paranthropus*, Acheulean, Oldowan, and zooarchaeological remains within interbedded fluvial, lacustrine, and pyroclastic deposits (Leakey, 1971; Hay, 1976),

   - Similar to above but lacking Oldowan and zooarchaeological components (Asfaw et al., 1992; Suwa et al., 1997),

   - Meandering river and floodplain successions containing Oldowan flakes and *Homo* remains (Kimbel et al., 1996),

   - As above but without *Homo* and including Oldowan cores, flakes, and cut-marked bones (Semaw et al., 2003)

   - Oldowan tools among the intercalated sediments of transverse braided streams, axial meandering channels, and overbank environments (Howell et al., 1987; Kibunjia et al., 1992; Roche et al., 1999)

A necessary first step for evaluating the meanings behind theses associations involves constructing integrative geological frameworks, which provide details on

sedimentary processes, stratigraphic relationships, and depositional controls. This is often laborious and can be problematic at times (Brown and Gathogo, 2002; Quade et al., 2004; WoldeGabriel et al., 2005; Stollhofen et al., 2008) due to poor lateral-vertical exposure resulting from the youthful tectonics and modern sedimentary activity in the rift system. Establishing these frameworks is also complicated by the tendency for different types of fluvial systems to generate similar sedimentary sequences, and the potential for any given system to accumulate an array of disparate sequences (Allen, 1983; Bridge, 1985, 1993a, 2003; Miall, 1996). Despite these complications, ancient fluvial systems and their deposits are commonly likened to one of several types of modern rivers, and interpreted as a certain type according to perceived channel patterns and nature of overbank sediments. One of the more common types is the braided-river system, mainly characterized by multiple interconnected networks of channels separated by bars. Another is the meandering-river system that includes a single channel with point bars and well-developed floodplains. Whereas identifying a rock record indicative of a meandering system can be relatively straightforward, especially when lateral-accretionary deposits are overwhelming apparent (Puigdefabregas, 1973; Willis, 1989, 1993), documenting the sedimentary archive of a braided system is usually more problematic. This largely stems from the inherent complexity of the geometries and processes for multi-channel rivers, and a lack of detailed geological models that demonstrate the potential array of channel and bar forms generated by ancient braided systems (Bridge, 1993b; Bristow, 1987; Bristow and Best, 1993; Jones et al., 2001; McLaurin and Steel,

2007).   Classifying the overbank counterparts for braided or meandering channels is not less complicated (Farrell, 1987; Willis and Behrensmeyer, 1994). Interpreting an ancient overbank deposit as proximal, medial or distal, for example, implies some *a priori* knowledge of the landscape's paleogeography or understanding of the active channel's location (e.g., Nanson and Crooke, 1992), which may not always be the case.   Furthermore, discriminating overbank deposits from fine-grained channel fills can also be challenging and confounded by the overlap in lithological composition, primary sedimentary structures, and flow-regime processes associated with the two (Davies-Vollum and Wing, 1998; Kraus and Davies-Vollum, 2004; Schieber et al., 2007).

Over the past two decades or so, geologists have turned to the analysis of lithofacies architecture and paleosol maturity in an effort to address the interpretive problems concerning fluvial sequences.   These approaches are becoming increasingly preferred over traditional methods that solely rely on the examination of lithofacies successions in vertical outcrop profiles.   Vertical successions of lithofacies are now largely considered mere records of depositional conditions at the bed-form scale and not particularly diagnostic of a certain fluvial style (Bridge, 1985, 2003). Architectural analysis overcomes these limitations through examining large-scale structures and the stratigraphic distribution of lithofacies in multidimensional space (Allen, 1983; Miall, 1985; Brierley, 1996). This approach involves the recognition of a series of boundary surfaces, which subdivide fluvial sequences into superimposed sedimentary bodies, having discrete geometries and lithofacies assemblages (Miall, 1994,

1996; Jones et al., 2001). Contrastingly, the analysis of paleosol maturity focuses on the disparity of post-depositional alterations observable through a suite of overbank deposits (Bown and Kraus, 1987; Kraus, 1987). It is based on the identification of a continuum of ancient soil types, each varying by degree of horizon development, as defined by differences in structure, color, lithology, and profile depth (Marriott and Wright, 1993; Kraus and Aslan, 1999). Separately, these two approaches are very effective for interpreting the channel and overbank constituents of fluvial sequences. Conjunctively, however, they are powerful for elucidating not only fluvial style but also formative controls (Kraus, 2002; Mack and Madoff, 2005).

In the northeast Turkana Basin of Kenya, well-exposed sections of the Plio-Pleistocene Koobi Fora Formation offer ample opportunities for examining fluvial sequences with hominin remains (Brown and Feibel, 1986; Feibel et al., 1989). Particularly noteworthy are those cropping out along the Karari Escarpment within Area 130 of the Koobi Fora region (Fig. 3). Prior research on a ca. 2-km-long by 45-m-high continuous series of outcrops from here documents cranial evidence for *Homo* and *Paranthropus* (Leakey et al., 1978) in addition to multiple archaeological sites with Oldowan and developed Oldowan stone tools (Isaac et al., 1997). This section records sedimentation roughly over a 300,000-year period, from about 1.9-1.6 Ma, and consists of gravels, sands, tuffs, and mudstones overprinted with paleosols (Findlater, 1978; Burgraff et al., 1981; Brown and Feibel, 1985; Wynn, 1998; Brown et al., 2006; McDougall and Brown, 2006). However, little work (e.g., Rogers et al., 1994; Isaac and Behrensmeyer,

1997) has been put forth to incorporate the hominin remains into a comprehensive geological model based on sedimentological, paleosol, and stratigraphic data.

The following chapter reports the results of new field-based architectural and paleosol analyses that provide added clarity into the origins of these hominin-bearing fluvial sequences from Area 130. This part of the dissertation has the following aims: 1) to further describe lithofacies and interpret depositional environments, 2) to better integrate paleosol information with interpretations of depositional environments, 3) to identify and correlate the vertical-lateral stratigraphic distribution of the lithofacies and paleosol units, and 4) to subdivide the Area 130 successions into fluvial architectural units.

3.2. Study area and stratigraphy

The study site is the easternmost edge of fossil collection Area 130 (Figs. 3, 8). This location is nearly 25 km due east from the modern lakeshore, 3-5 km away from the volcanic highlands that form the northeast basin margin, and has an elevation of over 500 m above sea level. Area 130 is a headwater location for ephemeral streams that drain into the Lake Turkana. Tributaries that emanate from the Area 130 outcrops erode back the landscape and expose sections up to 55 m high. Outcrops are a series of rounded badland-like hills that are locally capped with steep cliffs. They extend from the easternmost boundaries of Area 130 for distances of 10's to 100's of m, and can be continuously followed NE/SW for about 2 km.

Fig. 8: Geographic and geologic map (based on Frank, 1976) of the eastern extent of central Area 130. Examined outcrops with Koobi Fora Formation sediments are denoted by thick black lines labeled with stratigraphic marker levels. Marker level j is the KBS Tuff, which is the boundary between the upper Burgi Member and the lower KBS Member. Marker levels o and o_2 approximate the boundary between the upper KBS and lower Okote Members. See Fig. 9 for vertical stratigraphic relationships of all marker levels, archaeological sites, and fossil localities. Note the locations of Figs. 10, 19, 20, 21, 23, 24 and 25. The six stratigraphic sections plotted on this map are drawn in Fig. 22.

Outcrop trace

Stratigraphic marker level O_2

Stratigraphic section   CJL04-130-1

Access road (unpaved)

Ephemeral stream

Fossil locality   1805

Archaeological site   17
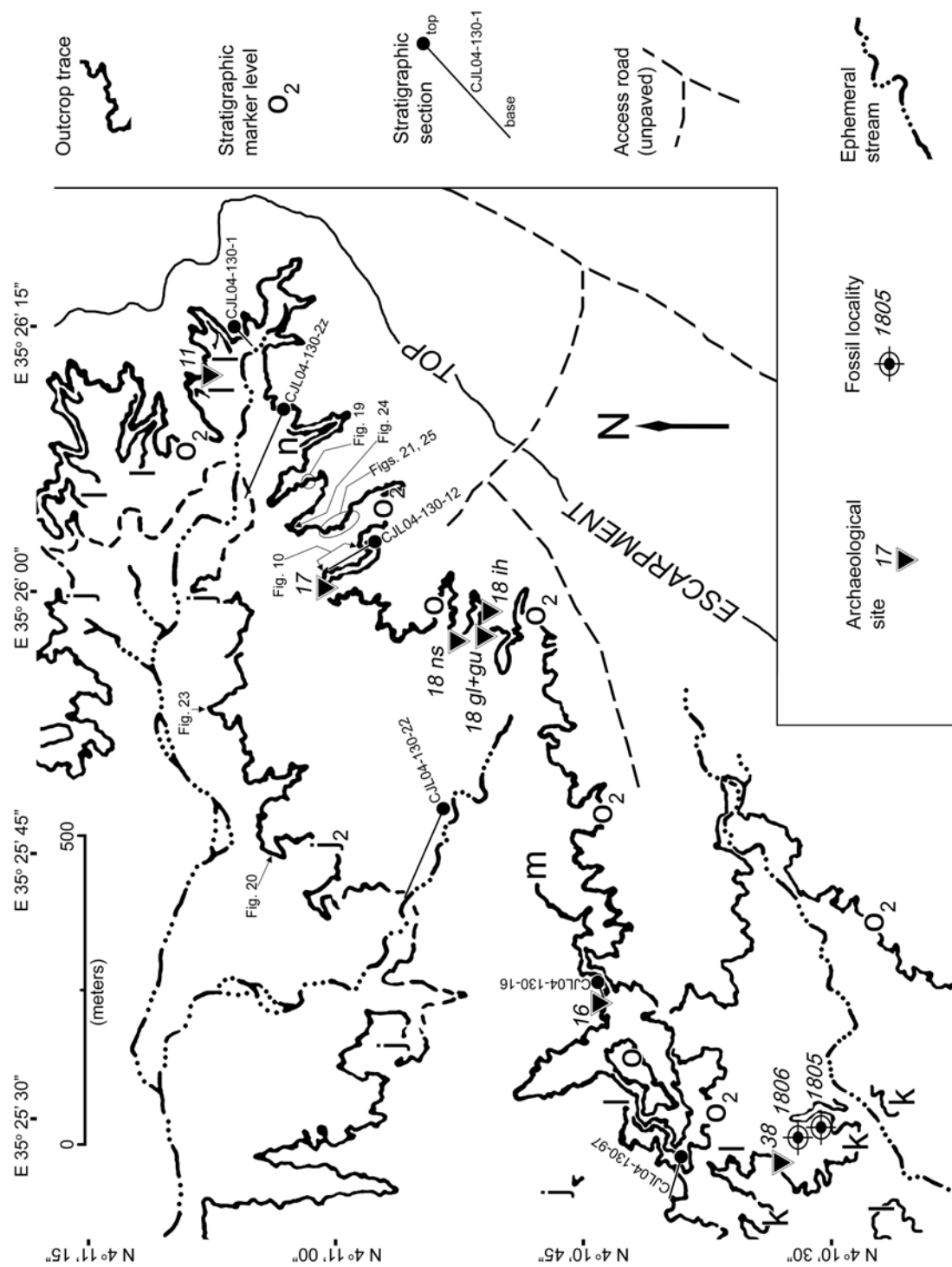
Sediments exposed in Area 130 consist of well-consolidated mudstones interstratified with sands and tuffs, as well as moderately to poorly consolidated gravels and coarse sands. Since initial studies in the 1970s, there have been few, if any, observations of significant tectonic deformation (i.e., dips more than a few degrees). The most detailed stratigraphic framework for the Area 130 sediments is the geological map (Fig. 8) and lithological profiles (Fig. 9) documented by Frank (1976). These profiles were chiefly correlated using alphanumerically coded stratigraphic marker levels—"j", "j_2", "k", "l", "m", "n", "o", and "o_2"—that have local and/or Karari-wide significance. Four of these are described below because of their chronostratigraphic and paleoenvironmental importance for this study.

Marker level j (Figs. 8, 9) is the stratigraphically lowest of the studied successions. It is the KBS Tuff (Frank, 1976; Findlater, 1978; Burggraf et al., 1981; White et al., 1981; Brown and Feibel, 1985, 1986, 1991). This tuff is one of the more geographically widespread in the northern Turkana Basin, known from many Koobi Fora Formation localities in the northeastern basin, and several northern and northwestern basin areas that have correlative Plio-Pleistocene deposits (Fig. 4). It is dated by the single-crystal-sanidine ^{40}Ar/^{39}Ar method to 1.87±0.02 Ma (McDougall and Brown, 2006). The tuff's base is the boundary between the Burgi Member and KBS Member (Fig. 4); hence, the base marks the basal level of the KBS Member and deposits below this level are from the upper Burgi Member (Brown and Feibel, 1986). As preserved in Area 130 and across the Karari Escarpment, the tuff (25-100 cm thick) comprises

Fig. 9: Lithostratigraphic framework for east-central Area 130 (modified from Frank, 1976). Inset map at lower left—with locations of sections, archaeological sites, fossil localities and streams—corresponds to Fig. 8. Ages of tuffs (within the key) after Brown et al. (2006) and McDougall and Brown (2006).

SW

NE

KEY

LOCATIONS OF SECTIONS

CENTRAL AREA 130

1805/ = fossil locality
1806

j = mapping level

KBS = KBS Tuff (1.87±0.02 Ma)

ORT = Orange Tuff (~1.64 Ma)

OTC = Okote Tuff Complex (≤1.56±0.05 Ma)

N7, 5YR8/1,
5Y7/2, 10YR8/1

10YR7/4,
10YR6/4

10YR6/2, 10YR5/4,
5YR5/2, 2.5YR5/6

38 = archaeological site

sand

gravel

tuff

pumice

claystone

silty claystone

siltstone

sandy siltstone
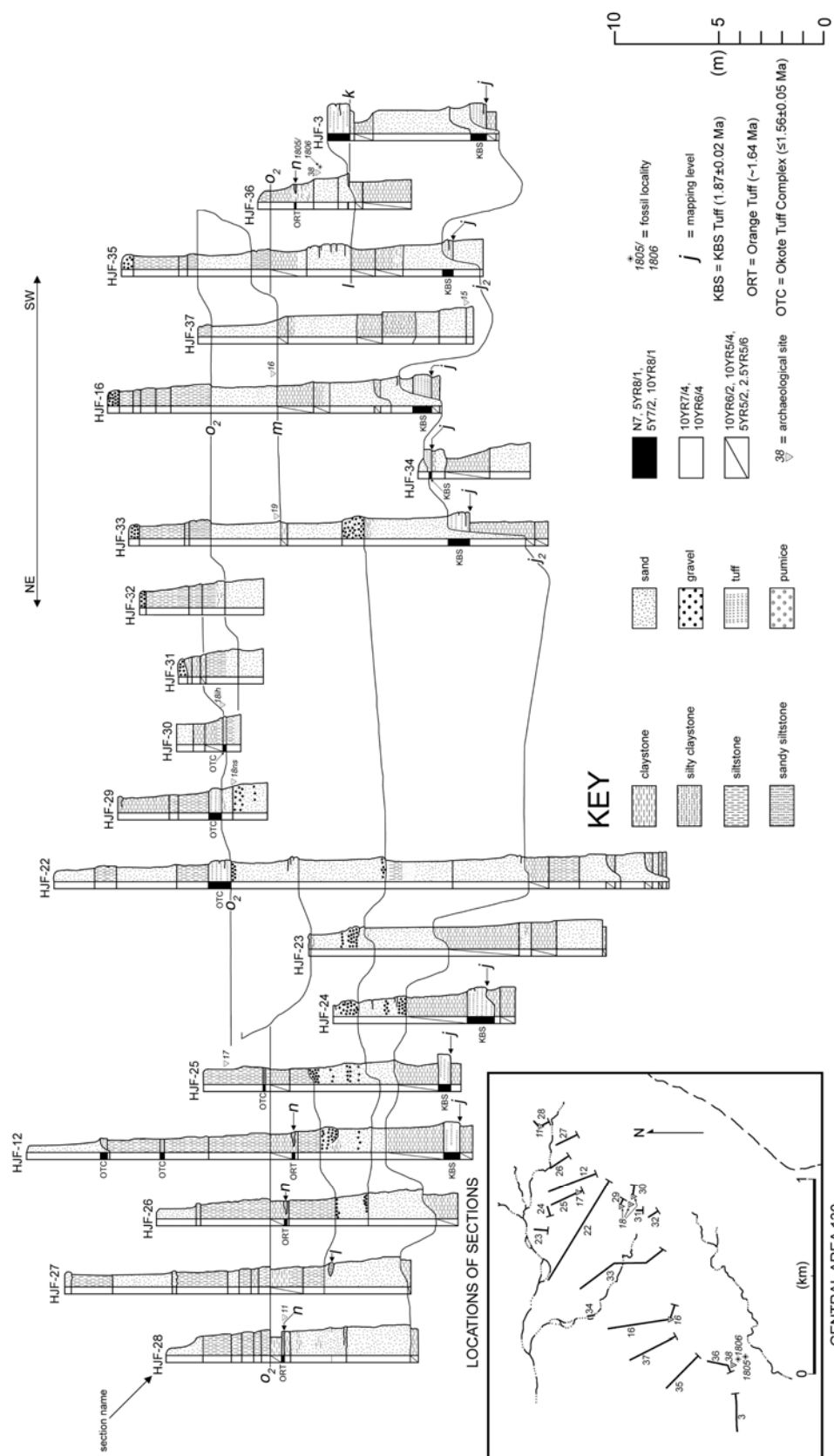
medium- to fine-grained rhyolitic glass shards, and locally includes pumices (White et al., 1981). It is largely found as lenticular units that are surrounded by clayey mudstones overprinted with vertic paleosols. Outcrops of the KBS Tuff are numerous in Area 130 and occur at similar lateral-vertical stratigraphic levels across the exposures (Fig. 9). Stratigraphic marker level j_2 is a widespread marker level within the study area (Fig. 8) and can be traced across the base of the Karari Escarpment for over 20 km (Burggraf et al., 1981; White et al., 1981). Marker level j_2 mainly comprises coarse (lithic arkose) sands, in addition to lesser amounts of moderately to poorly sorted polymictic gravels. These sediments fill scour surfaces that show erosive relief of up to ~8 m in the study area (Fig. 9). Marker level j_2 can be continuously traced through many of the sedimentary exposures within Area 130.

Stratigraphic marker level o is a light gray tuff that crops out locally in Area 130 just to the southwest of archaeological site FxJj 16, and again near the FxJj 18 archaeological site complex (Fig. 8). Tephrostratigraphic studies recognize this level as a constituent of the broadly correlative series of tuff complexes— referred to as the Okote Tuff Complex, the Koobi Fora Tuff Complex, and the Ileret Tuff Complex—that are all allocated to the lower/middle portion of the Okote Member (Brown and Feibel, 1985, 1986, 1991). On the Karari and thus in Area 130, it is referred to as the Okote Tuff Complex (Findlater, 1978; Brown and Feibel, 1985, 1986, 1991; Brown et al., 2006). In Area 130 the o marker level is interstratified with the more laterally widespread stratigraphic marker level designated as o_2 (Figs. 8, 9), which is a series of tuffaceous mudstones

colloquially known as the Okote tuffaceous siltstone complex (Findlater, 1978; White et al., 1981; Brown and Feibel, 1985, 1986; Isaac and Behrensmeyer, 1997). Stratigraphic marker level o_2 is an approximation for the stratigraphic level of the base or lower portion of the Okote Member (Brown and Feibel, 1985, 1986, 1991; Brown et al., 2006). Both stratigraphic marker levels o and o_2 are situated at 10-15 m above the KBS Tuff in Area 130 (Fig. 9). Studies by Brown et al. (2006) surmise an age of ~1.62 Ma for stratigraphic levels of the Karari sediments that lie some 11-12 m above the KBS Tuff. It seems reasonable to then use the age of the base of the Okote Member (i.e., 1.56±0.05 Ma, McDougall and Brown 2006) to approximate the age of stratigraphic marker levels o and o_2 from Area 130.

Thus, under examination here are Area 130 sediments from a stratigraphic interval of the Koobi Fora Formation that includes an uppermost portion of the Burgi Member, the KBS Member, and a lower portion of the Okote Member (Fig. 4). Accordingly, the sediments reflect about 300,000 years of deposition, roughly from 1.9 to 1.6 Ma. Major basin-wide paleographic changes for this stratigraphic/temporal interval are portrayed in Figs. 5, 6 and 7, as modified from Brown and Feibel (1991) and Rogers et al. (1994).

3.3. Methods

Detailed sedimentological and stratigraphic information was collected from a ca. 2-km-long section through the Area 130 outcrops by analyzing the lithostratigraphic framework constructed by Frank (1976; see also Figs. 8, 9 this

study).   This information is described and interpreted here through facies, paleosol, and fluvial architectural analyses.

Sedimentary facies for Area 130 are analyzed here by largely following guidelines described by Miall (1996). Modified versions of his classification and interpretative approaches are used to accommodate the sedimentological features of the study area into five lithofacies (Table 1). Furthermore, five lithofacies associations—representing combinations of lithofacies organized into stratigraphically discrete units with distinctive sizes and geometries—are used to subdivide and interpret the Area 130 strata (Table 2). Each lithofacies association is given an interpretative-free descriptive name and code (sensu Perez-Arlucea et al., 2000), and correlated with previously established lithofacies associations when appropriate (Table 2). Lithofacies associations fall into coarse and fine groups. The coarse group comprises four lithofacies associations. The fine group includes one lithofacies association that is subdivided into two varieties. Besides sedimentological features, the fine lithofacies association is interpreted from the paleosols overprinted on the deposits.

Wynn and Feibel (1995), Wynn (1998), and Quinn et al. (2007) have previously investigated paleoenvironmental and taxonomic aspects of paleosols in Area 130. Area 130 paleosols are examined for this study so as to better understand the depositional settings according to proximity to an active channel (Bown and Kraus, 1987; Kraus, 1987), prevailing aggradation rates (Kraus, 2002; Mack and Madoff, 2005), and environments of sedimentation deduced from facies analysis (Miall, 1996; Bridge, 2003). The paleosols are described and

Table 1
Lithofacies of examined deposits from Area 130

Lithofacies	Description	Interpretation
Gh	Massive, tabular to lenticular sets of gravel with well-defined, near-horizontal upper and lower contacts; clast-supported, cobble- to pebble-sized basalt clasts; moderately to poorly sorted by size; sub-spherical to elongate clast shapes; rare internal horizontal stratification and crude coarsening-up/fining-up trends; individual set thickness at 10-100 cm; rare stacked sets up to 3-m thick.	Rapid fallout of bedload transported by floods; channel lags; gravel sheets; low-relief longitudinal bars (Leopold and Wolman, 1957; Boothroyd and Ashley, 1975; Hein and Walker, 1977; Steel and Thompson, 1983; Rust, 1984; Nemec and Steel, 1984).
St	Lenticular units of trough cross-stratified sands; predominantly coarse to medium sand, with a lesser fraction of granules and/or pebbles; typical set thickness of 10 to 50 cm, but up to 1 m; cosets up to 3 m.	Bedload transport and accumulation; 3-D sinuous-crested dunes; upper part of the lower flow regime; channel-floor dunes (Harms et al., 1982; Collinson and Thompson, 1989; Perez-Arlucea et al., 2000).
Sp	Tabular to wedge-shaped units of planar cross-stratified, coarse to medium sands; locally includes pebbles and granules; 5-30 cm thick sets, with cosets at 1-2 m.	Bedload transport and accumulation; straight-crested 2-D dunes of the lower flow regime; slip-faces for downstream or laterally accreting sand bars (Harms et al., 1982; Steel and Thompson, 1983; Rust, 1984; Collinson and Thompson, 1989).
Sh	Massive coarse or medium (less frequently fine) sand/tuff; locally includes pebbles and granules for coarser examples; arranged into tabular or lenticular sets with well-defined upper and lower, near-horizontal contacts; moderately to poorly sorted by size; rare internal horizontal laminations; crude fining-upward trends; individual set thickness 10-100 cm; commonly, sets stacked up to 3 m.	Plane-bed deposition from the upper flow regime; rapid bedload fallout from sediment-laden sheetfloods; falling-stage flood deposition; plane-bedded simple bars (McKee et al., 1967; Tunbridge, 1981; Bennett and Bridge, 1995; Hjellbakk, 1997).
Mh	Massive siltstone or claystone, often with a fine sand or tuffaceous fraction; rare parallel laminations in coarser sets; locally with carbonate nodules/tubules and slickensided surfaces; arranged into tabular sets with well-defined, upper and lower contacts that are horizontal; set thickness at 10-300 cm, with rare examples up to 500 cm.	Suspension settling dominantly from pooled or standing water; low-energy flows and weak currents; bedding destroyed by pedogenesis and carbonate precipitation (Farrell, 1987; Bown and Kraus, 1987; Kraus, 1987; Kraus and Aslan, 1999).

Table 2
Lithofacies associations of examined deposits from Area 130

Lithofacies association	Lithofacies	Description	Interpretation	Prior designations in the study area
LA1	St	Coarse lithofacies association consisting of cross-cutting lenticular sets of trough cross-stratified sand (St); upward decreases in set size and grain caliber; sheet-like in cross-section; erosive lower contact showing near planar to mildly concave-up contours; upper contact is sharp to gradational with LA2, LA3, or LA4; extends laterally for 10's m; maximum thickness of 3 m.	Deposition of 3-D, sinuous-crested dunes at thalwegs, channel floors, and other basal channel areas (Cant and Walker, 1978; Bluck, 1980; Allen, 1983; Miall, 1996).	"Primary Structure Group One" and lower portion of "Primary Structure Group Three" of the "Polymictic Conglomerate and Sandstone Subfacies" (Vondra and Burggraf, 1978; Burggraf et al., 1981); basal part of the "F1a Fluvial Facies Association" (Feibel and Brown, 1986).
LA2	Gh, Sh	Coarse lithofacies association of horizontally stratified sets of massive gravel (Gh) and massive sand (Sh); tabular to lenticular set shapes, erosive lower contacts displaying cm's to dm's erosive relief; multiple, vertically stacked fining-upward cycles of Gh to Sh; locally, thick uninterrupted gravels successions; extends laterally for 100's m; maximum thickness of 3 m.	Broad and shallow, low-sinuosity fluvial channels; longitudinal gravel bars; gravel sheets or lags; plane-bedded simple bars of sand; composite-compound bars of gravel and sand (Leopold and Wolman, 1957; Boothroyd and Ashley, 1975; Hein and Walker, 1977; Allen, 1983; Allen et al., 1983; Steel and Thompson, 1983; Nemec and Steel 1984; Rust, 1984).	"Lenticular Basalt Clast Conglomerate Subfacies" (Vondra and Burggraf, 1978; Burggraf et al., 1981).
LA3	Sp, Sh	Coarse lithofacies association with planar cross-stratified sand (Sp) and horizontally stratified sets of massive sand (Sh); vertically stacked lenticular, tabular and wedge-shaped sets; nearly planar lower contacts with cm's to dm's of erosive relief; fining-upward cycles (up to 1 m thick) of Sp to Sh; extends laterally for 10's m; maximum thickness of 3 m.	Deposition of 2-D, straight-crested dunes and sand sheets; plane-bedded simple bars, compound bars and composite-compound bars; transverse, linguoid or cross-channel bars (Collinson, 1970; Cant and Walker, 1978; Rust, 1978; Allen, 1983).	"Primary Structure Group Two" of the "Polymictic Conglomerate and Sandstone Subfacies" (Vondra and Burggraf, 1978; Burggraf et al., 1981); lower to middle part of the "F1b Fluvial Facies Association" (Feibel and Brown, 1986).

Table 2 (cont.)
Lithofacies Associations of examined deposits from Area 130

LA4	Sh	Coarse lithofacies association having multiple horizontally stratified sets of massive sand (Sh); vertically stacked, tabular to lenticular sets; minor lenses of Gh occasionally at bases of Sh; nearly planar lower contacts displaying cm's of erosive relief, locally, basal concave-up erosive relief of 25-50 cm; extends laterally for 100's m; maximum thickness of 5 m.	Broad and shallow, low-sinuosity fluvial channels, lateral banks without sizeable relief; simple plane-bedded bars, sand sheets and gravel lags (McKee et al., 1967; Williams, 1971; Miall, 1977, 1996; Tunbridge, 1981; Sneh, 1983; Dreyer, 1993; Hjellbakk, 1997).	None
LA5a	Sh, Mh	Fine lithofacies association comprising horizontally stratified sets of massive sand (Sh) and massive mudstone (Mh); sand sets are classified as "sheets" based on width/thickness ratios (e.g., Friend et al., 1979); sand sheets with cm's of basal erosive relief, but locally up to 25 cm of concave-up relief; fining-upward cycles (up to 1 m thick) of alternating Sh/Mh very common; weakly developed paleosol features for lithofacies Mh; extends laterally for 100's m; maximum thickness of ~20m.	Proximal floodplains; immature paleosols overprinted on mudstones (Bown and Kraus, 1987; Kraus, 1987; Smith et al., 1989; Bristow et al., 1999; Kraus and Aslan, 1999; Perez-Arlucea and Smith, 1999).	"Interbedded Sandstone and Tuffaceous Siltstone Subfacies" (Vondra and Burggraf, 1978; Burggraf et al., 1981); "F2 Fluvial Facies Association" (Feibel and Brown, 1986).
LA5b	Mh	Fine lithofacies association consisting of horizontally stratified sets of massive mudstone (Mh); vertically stacked, tabular to lenticular sets overprinted with abundant carbonate nodules/tubules and slickensides; locally, lenses of lithofacies Sh embedded within thick mudstone successions; extends laterally for 100's m, up to ~20 m thick.	Overbank depositional settings, such as floodplains/floodbasins at medial-distal locations relative to the active channel(s); mature soil formation (Bown and Kraus, 1987; Farrell, 1987; Kraus, 1987; Kraus and Aslan, 1999).	"Lenticular Mudstone and Sandstone Subfacies" (White et al., 1981).

interpreted using standard procedures for the analysis of ancient soils in fluvial deposits (Mack et al., 1993; Retallack, 2001). Three distinctive paleosol types from Area 130 are recognized. Each of these is diagnosed from a unique array of grain-sizes, colors, peds, carbonate concretions, and slickensides, in addition to profile depths and number of horizons (Table 3).

This study also utilizes fluvial architectural analysis (e.g., Allen, 1983; Miall, 1985, 1994, 1996) to document and interpret the Area 130 successions. Architectural analysis is employed to understand the building blocks of the fluvial geology and subdivide it into discrete stratigraphic units that have distinctive paleo-geomorphic and temporal significance (Dreyer, 1993; Brierley, 1996). The architectural study of Area 130 is based on the concept of the lithosome (e.g., Allen and Fielding, 2007). As defined here, lithosome is a purely descriptive term, referring to 2-D sedimentary bodies, with thicknesses of 5-10 m and extents of 500-2000 m, that are bounded by two discordant contacts (Allen, 1983; Bristow, 1996) or boundary surfaces (Miall, 1994; Holbrook, 2001). Measured and correlated stratigraphic logs of Frank (1976; see Fig. 9 this study) were used as a basis for recognizing boundary surfaces (Table 4) and six lithosomes (Table 5). This involved: relocating outcrop sections, documenting facies and paleosols with new lithostratigraphic logs, identifying and physically tracing boundary surfaces through the strata, and defining the lithosomes (Fig. 10). The resultant fluvial architectural model (Fig. 11), including its recognition and interpretation, also derives from information from previously documented geologic maps, outcrop photos, and newly documented lithostratigraphic logs.

Table 3
Paleosol types of Area 130 deposits

Paleosol type	Diagnosis	Comparable interpretations from the study area
Type I	Developed upon lithofacies association "LA5a"; substrate varies as tuffaceous siltstone, tuffaceous sandy siltstone, sandy siltstone, or clayey siltstone; mainly recognized from a (20-40 cm thick) Bwk horizon, with greenish-gray color mottles, sparse carbonate nodules and rootcasts, and rare (if any) slickensides.	Dite pedotype (Wynn, 1998, 2000): thin surface horizon of darkened clay with crumb ped structure (mollic structure); shallow calcic horizon (<100 cm depth); Mollic Ustropepts (USDA) or Calcic Cambisols (FAO).
Type II	Developed upon lithofacies association "LA5b"; substrate is dark-colored claystone; includes three subordinate B-horizons; 5-15 cm thick Bw-horizon with blocky-columnar peds that are slickensided; 50 to 100 cm thick Bwk-horizons with arcuate slickensided surfaces and carbonate nodules; 75-100 cm thick Bw-horizons with large blocky, angular, and wedge-shaped peds, in addition to densely intersecting networks of arcuate slickensides (mukkara structures).	Aberegaiya pedotype (Wynn, 1998, 2000): vertisol with thick horizons of angular blocky structures, wedge-shaped peds, well-developed network of slickensided dish-shaped fracture planes (mukkara structure); Typic Calciusterts (USDA) or Chromic Vertisols (FAO).
Type III	Developed upon lithofacies association "LA5b"; substrates vary from tuffaceous sandy siltstones, sandy siltstones, and clayey siltstones; mainly recognized from a B-horizon with three subordinate horizons; 10-15 cm thick Bwk-horizon with greenish-gray color mottles and sparse amount of spherical carbonate nodules; ~25 cm thick Bkw-horizons with a moderate number of carbonate nodules or tubules, few greenish-gray color mottles, and 5-15 cm thick Bkw-horizon, masses of interlocking carbonate nodules; 100-150 cm thick Bkw-horizon, masses of interlocking carbonates nodules and tubules, and densely intersecting network of arcuate fractures with slickensides.	Kimere pedotype (Wynn & Feibel, 1995; Wynn, 1998): thick (~100 cm) subsurface horizon of massive carbonates with interlocking nodules; large angular to blocky peds and dish-shaped fracture planes with well-developed slickensides. Typic Calciusterts (USDA) or Aridsols (FAO).

Table 4
Boundary surfaces and features within the examined Area 130 outcrops

Surface name	Across-surface change in lithofacies association	Style & shape	Length (m)
j_2	LA5b to LA1, LA4	erosive; flat and concave-up, up to 8 m of erosive relief	>2000
j_3	LA2, LA3, LA4 to LA5b	non-erosive/accretionary; flat and concavo-convex	≥500
l	LA4, LA5b to LA1, LA2, LA4	erosive; flat and concave-up, up to 3 m of erosive relief	≥2000
l_2	LA2, LA3, LA4 to LA5b	non-erosive/accretionary; flat and concavo-convex	≥900
m	LA3, LA4, LA5a, LA5b to LA1	erosive; flat and concave-up, up to 5 m of erosive relief	~1200
n_2	LA2, LA3, LA4 to LA5b	non-erosive/accretionary; flat and concavo-convex	≥1000
o_2(NE)	LA5b to LA5a	non-erosive/hiatal; flat, mildly concavo-convex	≥900
o_2(SW)	LA5b to LA5a	non-erosive/hiatal; flat, mildly concavo-convex	≥1000
o_2(C)	LA2, LA3, LA4 to LA5a	non-erosive/ accretionary; flat and concavo-convex	~1200

Table 5
Fluvial lithosomes within the examined Area 130 outcrops

Lithosome	Boundary surfaces	Lithofacies associations	Description	Length/thickness (m)
j_2	Lower: j_2 Upper: l, j_3	LA1, LA3, LA4	Coarse lithosome consisting of channel deposits; erosive base with mostly concave-up contours showing up to 8 m of relief, coarse, gravelly and pebbly sands that fine upward to silty sands; vertical lithofacies sequences of St, Sp and Sh	2000/10
j_3	Lower: j_3 Upper: l	LA5b	Fine lithosome comprising abandoned channel fills; non-erosive/accretionary base with nearly horizontal and convexo-concavo contours; dominated by massive mudstones (lithofacies Mh); abundant slickensides and carbonate concretions at uppermost levels; overprinted with very mature (type-III) paleosols	500/5
l	Lower: l Upper: l_2, m, n_2	LA1, LA2, LA3, LA4	Coarse lithosome of channel deposits; erosive base with nearly horizontal and concave-up contours (1-3 of relief); coarse sands and basalt gravel; up to 4 m thick sets of lithofacies Sh locally interbedded with St, Sp and Gh; alternating sets of lithofacies Gh and Sh arranged into 1-3 m thick successions; basal units of lithofacies St and Sh	2000/5

Table 5 (cont.)
Fluvial lithosomes within the examined Area 130 outcrops

	Bounding surfaces	Architectural elements	Description	
l_2	Lower: l_2(NE), m Upper: o_2(NE), m	LA5b	Fine lithosome comprising abandoned channel fills; non-erosive/accretionary base with nearly horizontal and concavo-convexo contours; thick uninterrupted sets of lithofacies Mh overprinted with slickensides and carbonate concretions; very mature (type-III) paleosols developed at topmost levels	900/5
n_2	Lower: n_2 Upper: o_2(SW), m	LA5b	Fine lithosome comprising abandoned channel fills; non-erosive/accretionary base with nearly horizontal and concavo-convexo contours; 1-5 m thick successions of lithofacies Mh; abundant slickensides and carbonate concretions; uppermost levels overprinted with very mature (type-III) paleosols	1000/5
m	Lower: m Upper: o_2(C)	LA1, LA2, LA3, LA4	Coarse lithosome of channel deposits; nearly horizontal erosive base and concave-up lateral-most margins showing ~5 m of erosive relief; coarse sands and basalt gravels; basal sets of lithofacies St vertically grading to Sh, followed by Gh or Sp; topmost levels of well-developed sets and cosets of Sp extending laterally for 10-100 m	1200/5

Fig. 10: Steps involved in constructing the fluvial architectural framework of Area 130. Example is from outcrops at archaeological site FxJj 17 (see Fig. 8 for map view). Sections correlate with the middle to upper part of lithostratigraphic logs HJF-12 and HJF-25 portrayed in Fig. 9. Lower panel—transect of lithostratigraphic log CJL04-130-12 that records detailed facies and paleosol information (Fig. 22). Middle panel—recognition of the lateral extent, style and morphology for boundary surfaces that mark contacts between major changeovers in facies and paleosols (Table 4). Upper panel—interpretation of the stratigraphic distribution of lithosomes defined by boundary surfaces, facies and paleosol components (Table 5). A lower boundary surface for coarse lithosome I is not preserved at these exposures. Type-III paleosol is overprinted on fine lithosome I_2. Upper successions of LA5a are not incorporated into a lithosome because an uppermost Plio-Pleistocene boundary surface could not be identified.
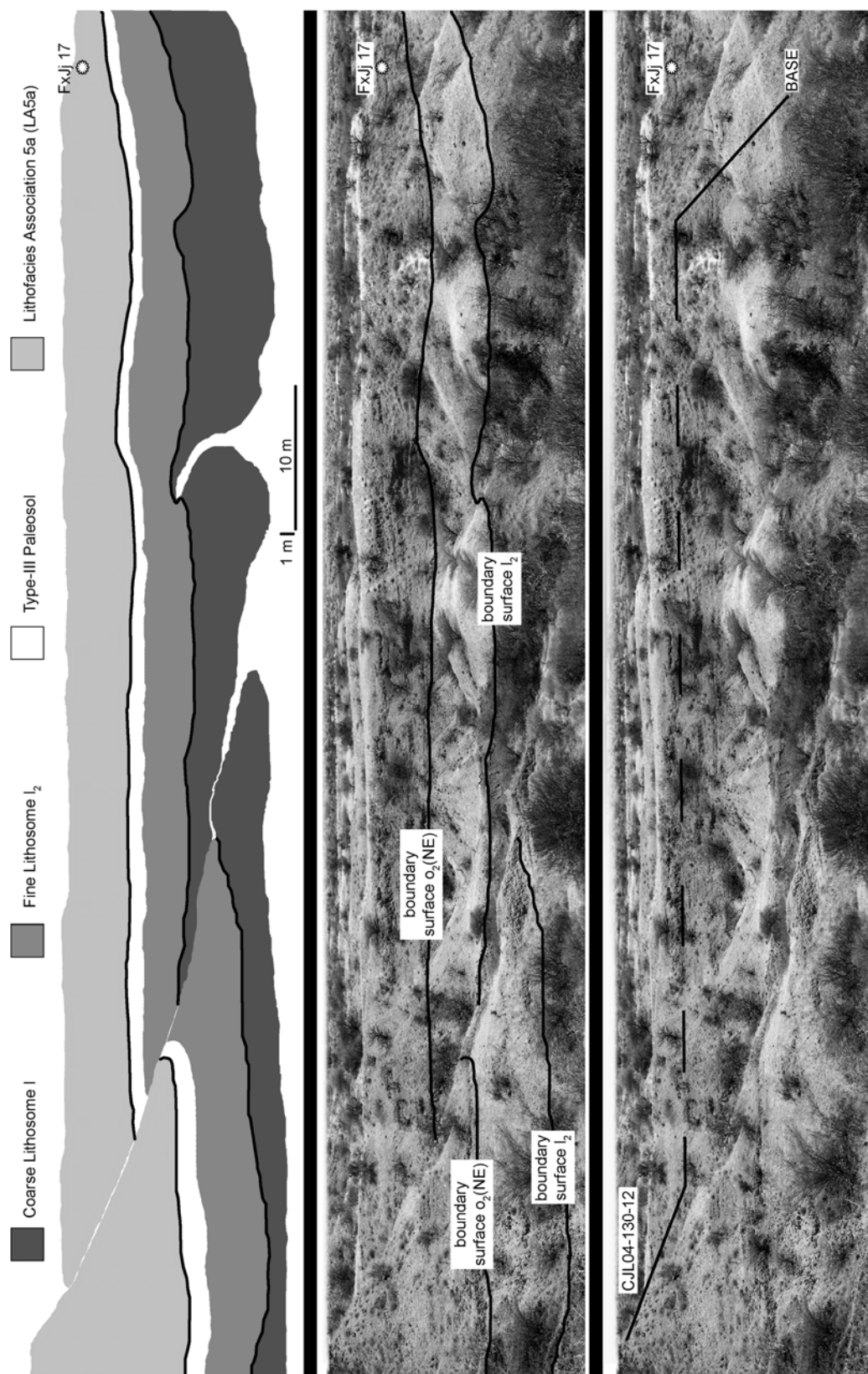
Fig. 11: Fluvial Architectural model for examined deposits of Area 130 (modified from Fig. 9). See Tables 4 and 5 for details on boundary surfaces and lithosomes. Light gray indicates coarse lithosomes, and dark gray is fine lithosomes.
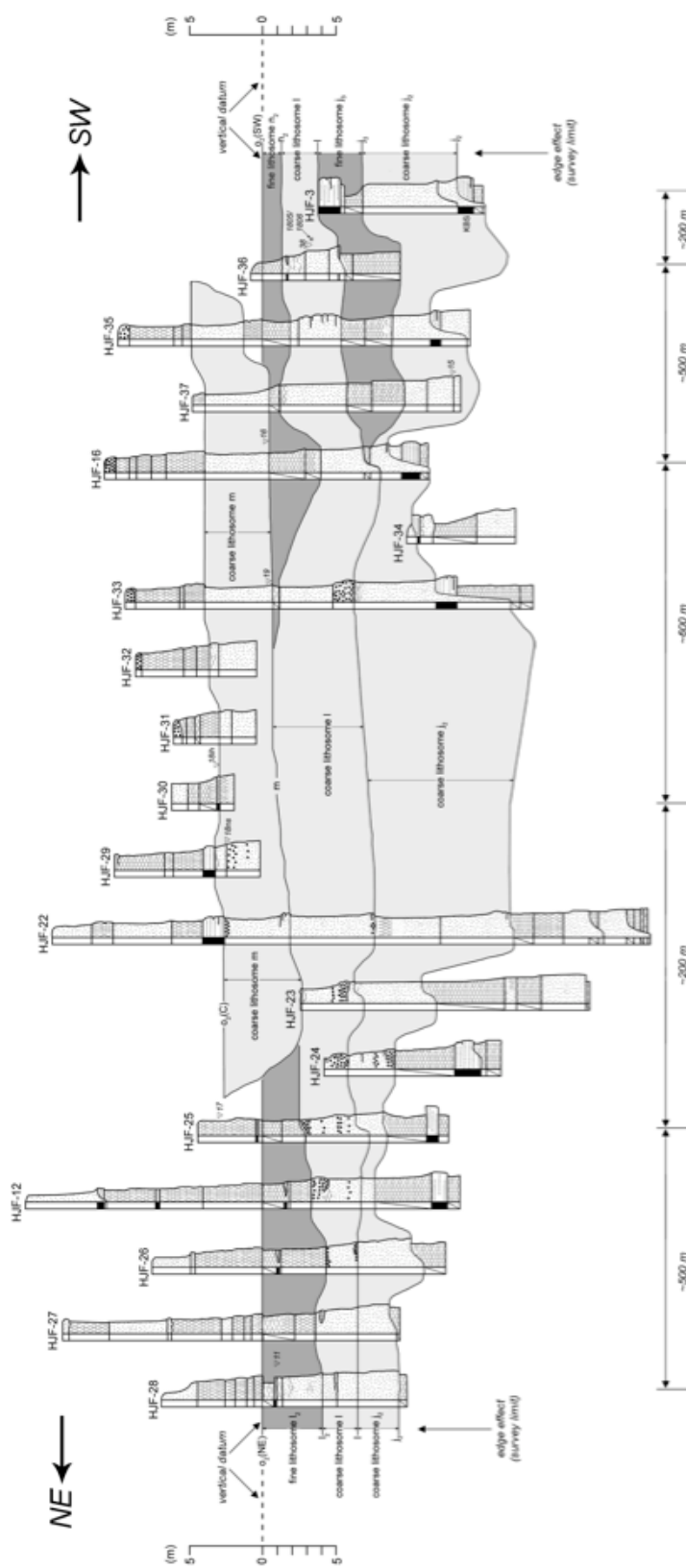
The six lithosomes identified within the successions of Area 130 fall into either a coarse lithosome or fine lithosome category. These distinctions reflect a predominate composition of either coarse lithofacies associations or fine lithofacies associations. Besides lithofacies associations, lithosomes are distinguished by bounding surfaces, size, geometry, vertical-lateral stratigraphic relationships, and paleosols. They thus comprise a group of genetically related strata that has sedimentological and post-depositional information. A lithosome is considered here as a representation of one of several geomorphic units for the ancient fluvial landscape and reflects a certain form-process association that can be used to assess depositional controls and reconstruct the ancient geography of Area 130 (e.g., Dreyer, 1993; Brierley, 1996; Miall, 1996).

First presented below are the descriptions and interpretations of the lithofacies associations. This is followed by the analysis of the Area 130 paleosols, with attention to profile features and developmental times. Thirdly, the identified boundary surfaces and lithosomes are discussed.

3.4. Sedimentology: lithofacies associations

Salient features of the Area 130 sedimentary successions are described and interpreted through lithofacies analyses. This approach allows for the identification of five lithofacies (Table 1), which in various vertical and lateral stratigraphic combinations form lithofacies associations (Table 2).

Coarse and fine lithofacies associations subdivide the Area 130 successions. Coarse associations include Lithofacies Association 1 (LA1), Lithofacies

Association 2 (LA2), Lithofacies Association 3 (LA3), and Lithofacies Association 4 (LA4). The single fine lithofacies association consists of two varieties: Lithofacies Association 5a (LA5a) and Lithofacies Association 5b (LA5b). As used here, "set" follows the terminology of Bridge (1993a, his Fig. 2). Moreover, three lithofacies in Table 1 (i.e., Gh, Sh and Mh) are described as horizontal sets of massive sediment. This means the sets have nearly horizontal upper and lower contacts but preserve no internal primary sedimentary structures.

3.4.1. LA1: lenticular sets of trough cross-stratified sand

Description: LA1 (Fig. 12) measures 50-300 cm thick and stretches across the outcrops for meters to tens of meters. It comprises multiple lenticular sets of trough cross-stratified sands (lithofacies St). LA1 commonly occurs as the basal fill on erosive relief that has concave-up, channel-form contours. Grain size generally decreases upward in the lithofacies association. Lower strata consist of pebbly to granular coarse sands, and upper ones are composed from coarse to medium sands deficient in gravels. Upward trends also include a decrease in scale for the trough cross-stratifications. Lenticular sets of trough cross-stratified sands are 0.25-1.0 m thick, up to 2.0 m in apparent width, and ≤4.0 m in length (Vondra and Burggraf, 1978).

Interpretation: LA1 is interpreted to reflect deposition in thalwegs and other channel-floor settings. This is based on its composition of trough cross-stratification and occurrence on basal concave-up, erosive relief (cf., "in-channel deposition" of Cant and Walker, 1978; "in-channel deposits" of Bluck, 1980;

Fig. 12: Cartoon of Lithofacies Association 1 (LA1) illustrating characteristic crosscutting lenticular sets of trough cross-stratified sand (lithofacies St), which upwardly decrease in scale and grain size. See Tables 1 and 2 for additional sedimentological details. Key is also for lithofacies associations in Figs. 13-17.

LA1

10 m

KEY

lithofacies Gh

lithofacies St

lithofacies Sp

lithofacies Sh

tuff (lithofacies Sh)

massive siltstone with rare
laminations (lithofacies Mh)

massive claystone
(lithofacies Mh)
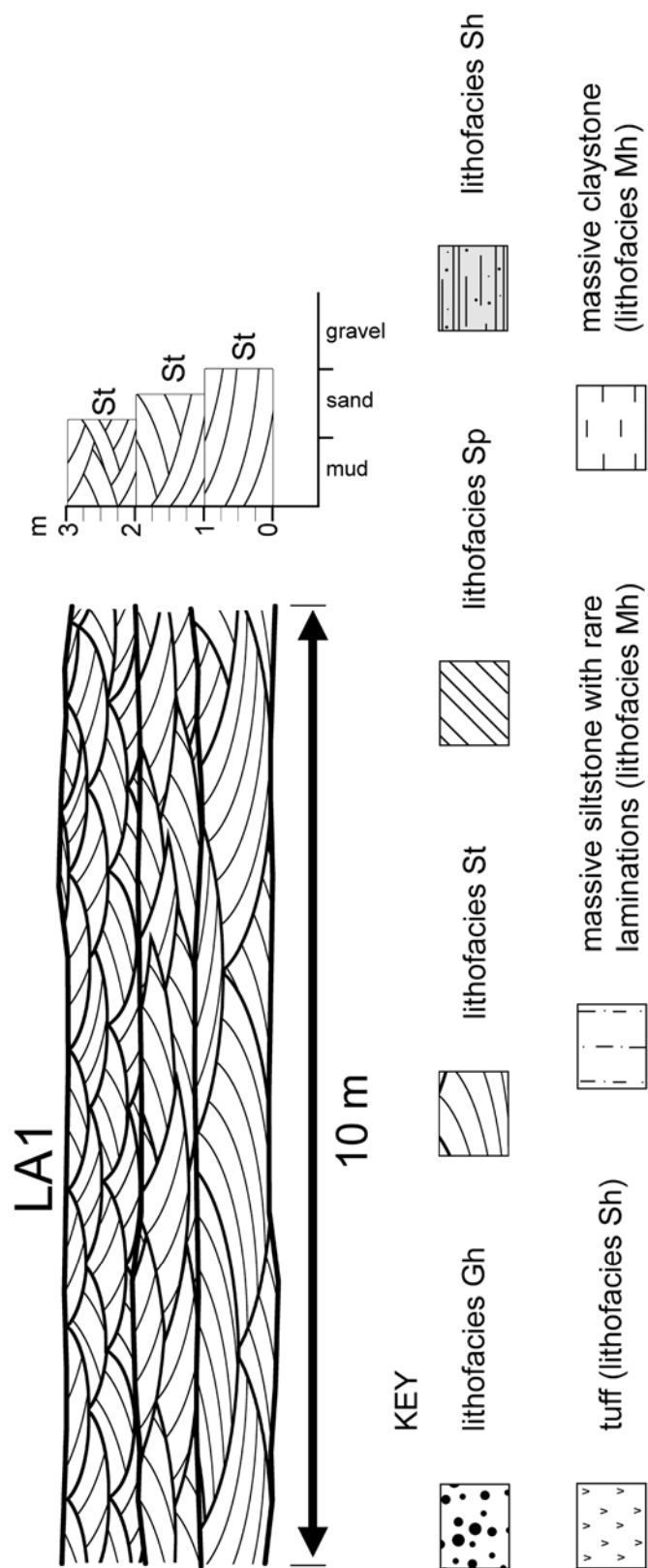
"element 2" of Allen, 1983; "channel-floor dune fields" of Miall, 1996).   As indicated by the ubiquity of lithofacies St, LA1 formed from bedload sediment transport and accumulation, through the migration of 3-D sinuous-crested dunes formed in the lower flow regime (Harms et al., 1982; Collinson and Thompson, 1989; Perez-Arlucea et al., 2000).

3.4.2. LA2: horizontal sets of massive gravel and massive sand

Description: LA2 (Fig. 13) is a sheet-like deposit that has a thickness of 1-3 m and overall lateral extents of 100's of m.   This lithofacies association comprises 10-100 cm thick sets of massive gravel (lithofacies Gh) and massive sand (lithofacies Sh).   Individual sets are tabular or lenticular in cross-section, and extend for meters to tens of meters across the outcrops.   They have planar or slightly convex-up tops and planar erosional bases that locally show centimeter-scale irregular relief or up to ~25 cm of concave-up relief.   These sets vertically stack to form either successions of gravel or alternating gravel and sand layers.

Gravel clasts of lithofacies Gh are poorly sorted by size and include small cobbles to pebbles that are sub-spherical to elongate, and well rounded. Sedimentary structure is lacking and clast fabric is poorly organized. Lithofacies Sh consist of coarse to medium sands that locally include a pebble/granule fraction. As these sand sets are mainly situated between layers of basalt gravel, their bases follow the irregular grain topography at the tops of the underlying gravel sets. Upper contacts are at erosive bases of the gravel sets. Internally,

Fig. 13: Cartoon of Lithofacies Association 2 (LA2); see Fig. 12 for key, and Tables 1 and 2 for sedimentological descriptions and interpretations. LA2 consists of sets of massive gravel (Gh) and massive sand (Sh).
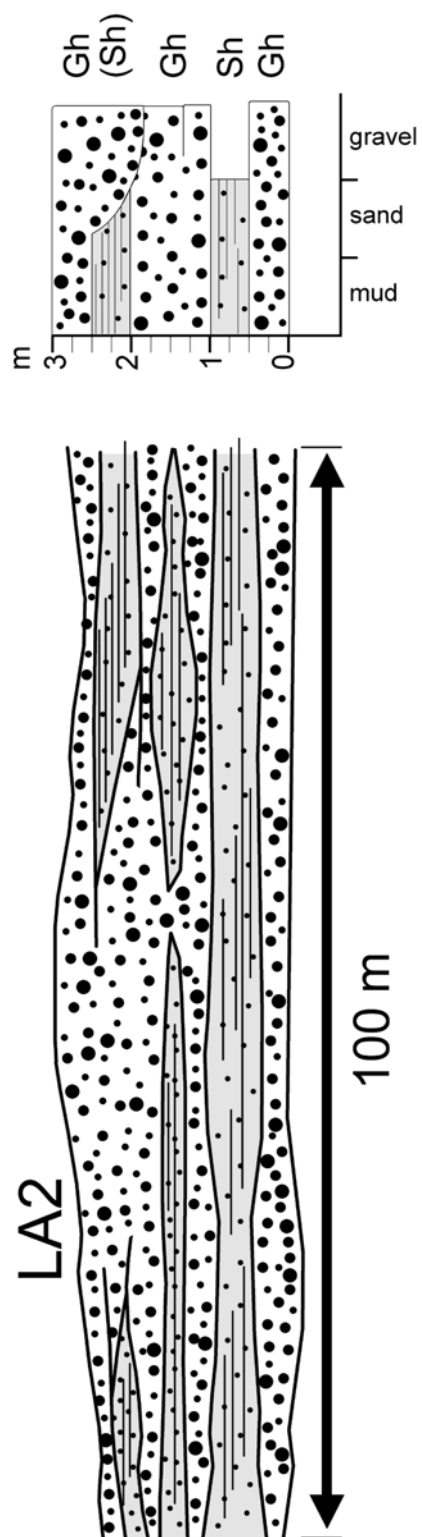
the sand sets infrequently exhibit weakly apparent fining-upward trends.

Interpretation: The massive fabrics and coarse grain sizes of LA2 suggest it was deposited by high-velocity flows. Poor grain sorting and a lack of primary sedimentary structures imply rapid deposition. Sets of lithofacies Gh indicate bedload transport and the deposition of gravel sheets, lags, and longitudinal bars that vertically accreted and elongated in downstream directions (Leopold and Wolman, 1957; Hein and Walker, 1977). Lithofacies Sh indicates deposition from upper plane-bed flows that formed on broad channel areas confined by very shallow margins (McKee et al., 1967; Tunbridge, 1981; Hjellbakk, 1997). Alternating sets of gravel and sand are comparable to composite-compound bars of Allen (1983). The sand sets are interpreted to represent the bar-top sediments deposited at low-flow conditions and/or during the falling-stage portions of floods that accumulated the gravels (Allen et al., 1983). Lithofacies, stacking patterns of lithofacies sets, and geometries of LA2 are comparable with the deposits of broad and shallow, low-sinuosity fluvial channels (Boothroyd and Ashley, 1975; Hein and Walker, 1977; Steel and Thompson, 1983; Rust, 1984). The decimeter-scale thicknesses of the individual gravel sets probably imply channels were no more than a meter or so deep (Nemec and Steel, 1984).

3.4.3. LA3: sets of planar cross-stratified sand and horizontal sets of massive sand

Description: LA3 (Fig. 14) is a tabular or wedge-shaped deposit that measures 30-300 cm thick. The lithofacies association fundamentally comprises

Fig. 14: Cartoon of Lithofacies Association 3 (LA3). See key in Fig. 12, and Tables 1 and 2 for detailed sedimentological descriptions and interpretations. LA3 is composed from planar cross-stratified sand (Sp) alternating with sets of massive sand (Sh).
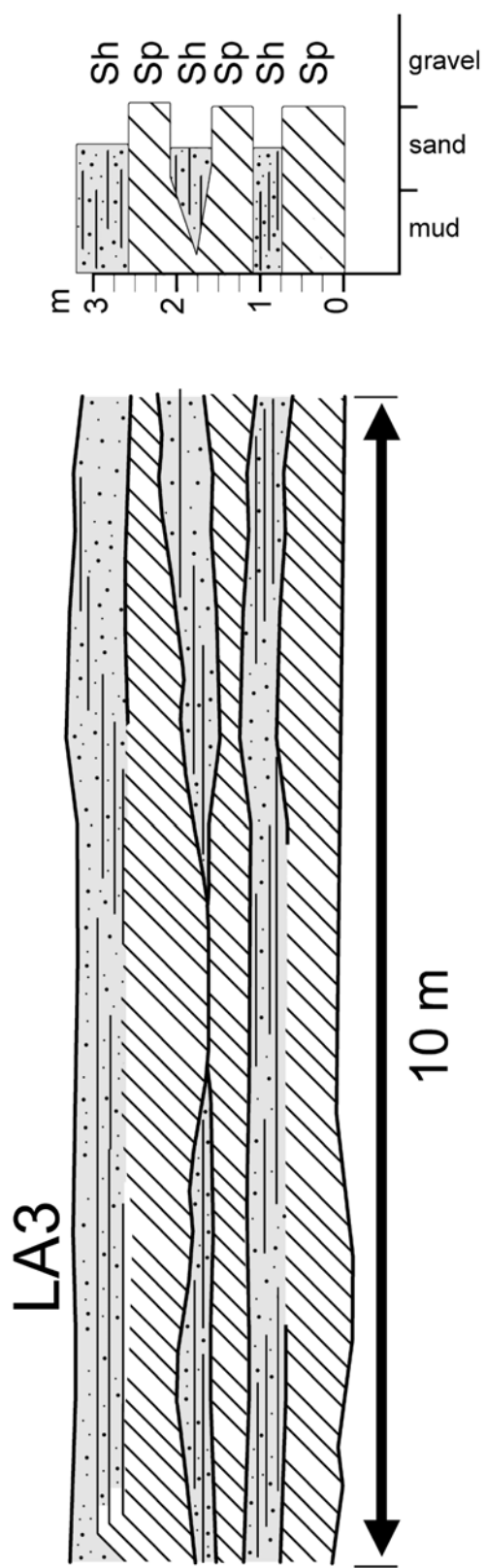
a basal set of planar cross-stratified sands (lithofacies Sp) and an upper set of horizontally stratified, massive sands (lithofacies Sh). The basal set consists of coarse to medium sands that may be pebbly or granular; overlying horizontally stratified sets are finer. The base of the horizontally stratified set may have a sharp, non-erosive contact with the top of the cross-stratified set. Alternatively, the transition between the two is gradational. LA3 can be found as single cross-strata and horizontal-strata couplet, or two such couplets stacked upon each other. It is also found as a cross-stratified coset, overlain with a single horizontal set above.

Interpretation: LA3 is interpreted as a bar deposit similar to the transverse, linguoid and cross-channel bars (Collinson, 1970; Cant and Walker, 1978; Rust, 1978), and the compound and composite-compound bars (Allen, 1983; Ramos et al., 1986; Jo and Chough, 2001) described from river systems with gravelly and sandy streambeds.

The couplets of lithofacies Sp-Sh suggest LA3 formed from the migration of straight-crested 2-D dunes of the lower flow regime, followed by plane-bed deposition of the upper flow regime (Harms et al., 1982; Collinson and Thompson, 1989; Ashley, 1990). Sets of lithofacies Sp are interpreted as the growth increments of bar margins that had avalanching slip faces (Kirk, 1983; Steel and Thompson, 1983; Rust, 1984). Overlying sets of lithofacies Sh are interpreted as indicating deposition at stoss sides or bar tops, and within small bar-top channels (Cant and Walker, 1978). LA3 probably formed in response to

different stages of the same flood and/or seasonal discharge variations (e.g., Steel and Thompson, 1983; Rust, 1984).

3.4.4. LA4: horizontal sets of massive sand

Description: LA4 (Fig. 15) is a sheet-like deposit that measures up to 5 m thick and extends laterally for hundreds of meters. It mainly comprises stacked units of lithofacies Sh, which are moderately to poorly sorted, coarse or medium sands. It also has lenses of lithofacies Gh to a lesser extent. Sets of Sh range in thickness from 10-100 cm. Individual sets are based at a near-horizontal erosive surface, which locally shows centimeter-scale relief and concave-up relief of a few decimeters.

Units of lithofacies Gh are lenticular. These sediments are not typical components of LA4. The lenses commonly measure 5-25 cm thick by 1-25 m long. When present, these gravel lenses can be observed to line the base of lithofacies Sh.

Interpretation: A predominance of lithofacies Sh and coarse to medium sands suggests LA4 was formed with plane-bed flows of the upper flow regime (Harms et al., 1982; Collinson and Thompson, 1989; Bennett and Bridge, 1995). A lack of internal primary sedimentary structures, moderate to poor sorting, and coarse grain sizes suggests the sets formed through rapid fallout from short-lived flows that were laden with sediment (Hjellbakk, 1997). The lenticular units of lithofacies Gh are interpreted as indications of gravel lags that accumulated by floods.

Fig. 15: Cartoon of Lithofacies Association 4 (LA4). See
Fig. 12 for key to symbols, and Tables 1 and 2 for further
sedimentological details. LA4 comprises sets of massive
sand (Sh), and rare lenticular units of massive gravel
(Gh) that line the bases of Sh sets.
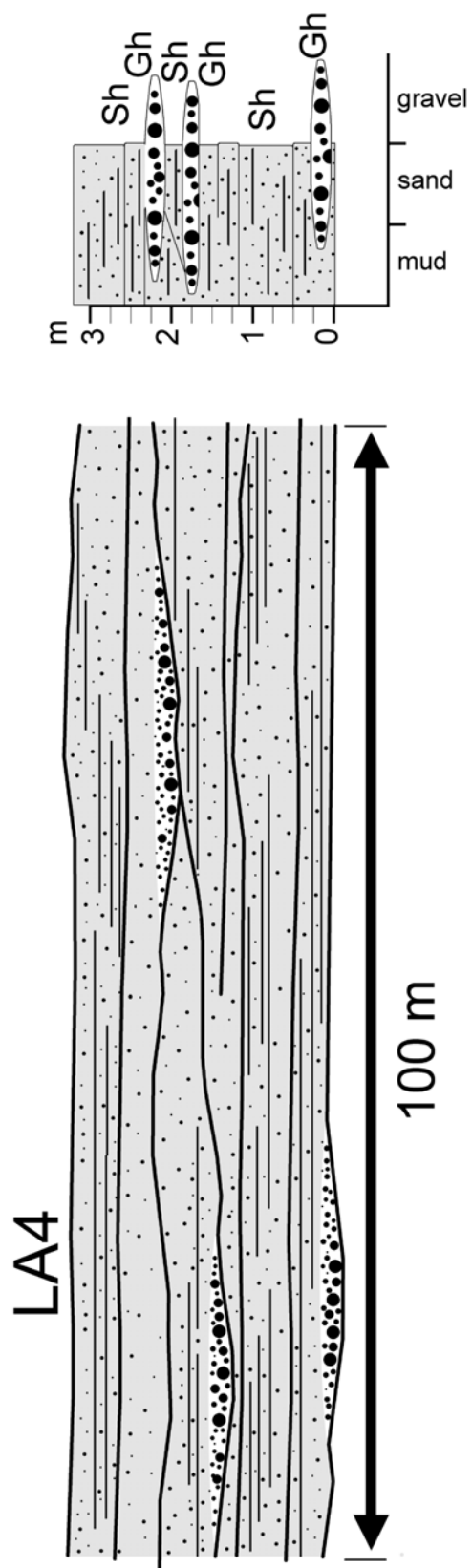
LA4 is interpreted as the result of high-energy, short-lived floods occurring within shallow and broad channel areas with subtle banks (McKee et al., 1967; Miall, 1977, 1996; Tunbridge, 1981). The depositional system may have been ephemeral to some extent, and operated under arid to semiarid climatic conditions (Williams, 1971; Sneh, 1983; Dreyer, 1993).

3.4.5. LA5: thin ribbon or sheet sands, and mudstones with paleosols

Description: One fine lithofacies association, designated as LA5, is documented from deposits of the study area. Two sub-varieties of this lithofacies association are recognized within the examined successions. The first is LA5a (Fig. 16), interpreted to represent deposition in a proximal floodplain. And the second is LA5b (Fig. 17), which reflects a floodbasin area. But as discussed in the later portion of this study (i.e., fluvial architecture), some deposits of LA5b represent infills for abandoned channel segments. Differences between LA5a and LA5b are also based on variations in grain size, lithology, and paleosols. Successions of LA5 are 5-20 m thick and 10 to 1000 m long.

Sands and tuffs of LA5 have near-planar basal erosive surfaces that locally show centimeter-scale irregular relief. These surfaces also display concave-up contours that have up to 25 cm of erosional relief. Most commonly, these deposits consist of medium to fine sands, tuffaceous sands and tuffs, and are dominated by lithofacies Sh. Usually there is a fining-upward trend, culminating with the uppermost one or two decimeters of the sand body having a

Fig. 16: Cartoon of Lithofacies Association 5a (LA5a). See Fig. 12 for key to symbols, and Tables 1 and 2 for additional sedimentological details. This association consists of sets of massive sand/tuff (Sh) alternating with sets of massive mudstone (Mh). Sets stack to form fining-upward cycles up to 1 m thick, which are overprinted with color mottles and carbonate rhizoliths/nodules of immature (type-I) paleosols in Fig. 18.
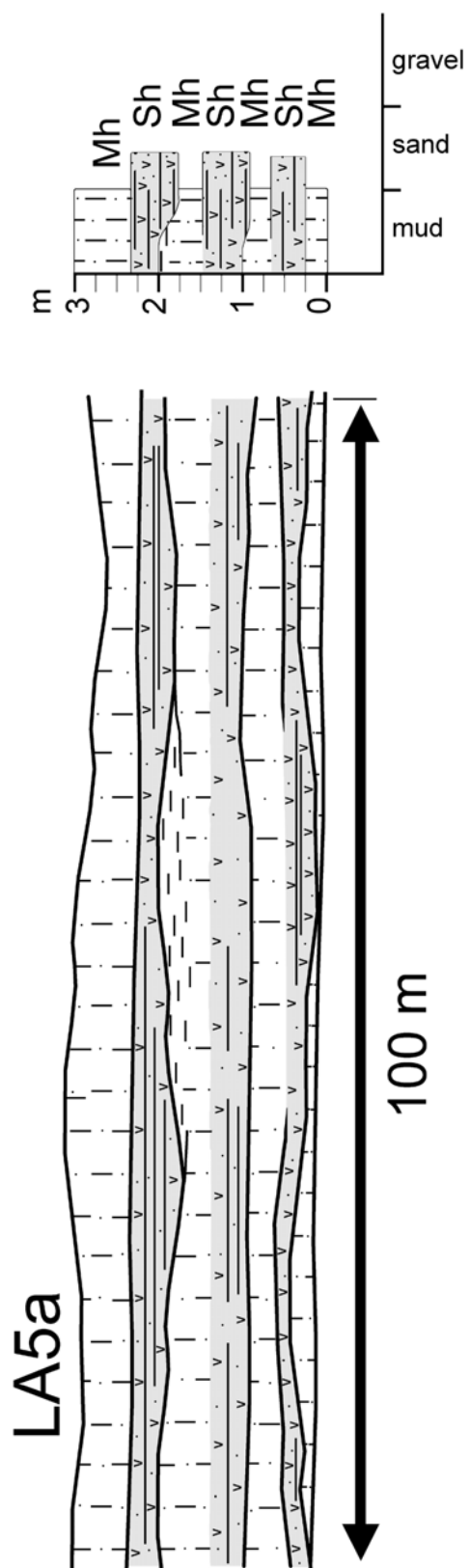
Fig. 17: Cartoon of Lithofacies Association 5b (LA5b). See Fig. 12 for key, and Tables 1 and 2 for further sedimentological details. The lithofacies association comprises thick successions of massive mudstones (Mh) with occasional lenticular sets of massive sand/tuff (Sh). Mudstones are overprinted with well-developed slickenside and/or carbonate horizons of mature (type-II) and very mature (type-III) paleosols in Fig. 18.
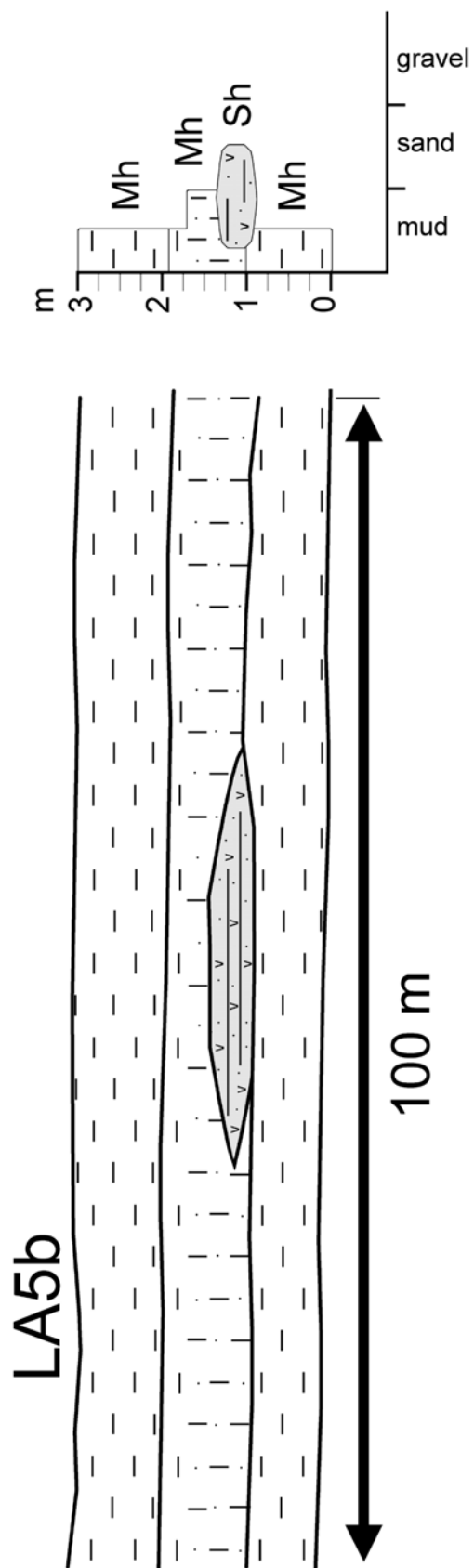
50-75% fraction of sandy silt and/or silty sand. Lateral and upper contacts with the mudstones vary from sharp to diffuse.

Individual mudstone sets of LA5 range from centimeters to decimeters in thickness, and have lateral extents of 10's to 100's of m. A set usually consists of a massive silty claystone or sandy-clayey siltstone. Mudstones of LA5 are usually overprinted with carbonate nodules, tubules and/or slickensides. Slickensides are observable on the surfaces of blocky, angular, wedge-like, or columnar structures. Best-developed slickensides show arcuate geometries that can be followed for 10's of cm through a mudstone. Calcic tubules and nodules have diameters at 1-10 cm. Tubules have lengths of 5-10 cm, and commonly display vertical to sub-vertical orientations relative to depositional layers. Nodules are largely spherical, but can be elongate and have lengths of 5-20 cm. The direction of elongation can be parallel to sedimentary layers. The largest elongate nodules form thick carbonate horizons, and display vertical to sub-vertical orientations.

Lithofacies association LA5a (Fig. 16) is formed by multiple fining-upward cycles, characterized by sheet- or ribbon-like sands/tuffs alternating with mudstones. Sheets are more typical. Paleosol overprinting is common for the mudstones in these cycles, but it is not as well developed or mature as all of the examples from LA5b.

LA5b (Fig. 17) derives most of its thickness from mudstones, with sand or tuff lenses accounting for the rest. Many of the mudstones have paleosol horizons, recognized from well-developed arcuate slickensides, and a small to

moderate amount of largely nodular carbonate. Some examples of LA5b, however, include meter-thick paleosol horizons with large-scale accurate slickensides and/or masses of carbonate nodules that interlock.

Interpretation: Settings that range from proximal channel areas to distal floodbasins are interpreted for LA5. Poorly developed paleosol features, a proportionate mudstone to sand ratio, and constituent fining-upward sedimentary cycles suggest proximal floodplain settings for LA5a (e.g., Farrell, 1987; Bown and Kraus, 1987; Kraus, 1987; Kraus and Aslan, 1999; Fig. 6.1 in Bridge, 2003). Sediment in these proximal settings probably accumulated through processes related to overbank flooding, leading to high-energy sheet flows and eventual suspension sedimentation (Smith et al. 1989; Bristow et al., 1999; Perez-Arlucea and Smith, 1999; Kraus and Aslan, 1999). Weakly developed paleosols on the mudstones of the stacked fining-upward cycles suggest a relatively short period between successive flood events (e.g., Bown and Kraus, 1987; Kraus, 1987). LA5a is interpreted as reflecting the deposits of crevasse splays, splay channels, levees and sheet flows typically known from proximal floodplain settings (Smith et al. 1989; Bristow et al., 1999; Perez-Arlucea and Smith, 1999; Kraus and Aslan, 1999; Bridge, 2003). Features of LA5a to support this interpretation include: multiple vertically stacked, fining-upward cycles composed from alternating units of sand/tuff and mud, laterally extensive tabular sand sheets that are interbedded with mudstones of equal size, and weakly developed paleosols overprinted on the mudstones.

LA5b is interpreted as indicating deposition in a floodbasin setting. A high ratio of mudstone to sand, in addition to the abundance of claystones suggest LA5b accumulated through suspension deposition in a lower energy environment. Sedimentation is thought to have been in areas away from active channel processes and brought about by flooding and the pooling of shallow waters. Abundant and strongly developed paleosol features, found on the mudstones of LA5b, suggest low sediment and water input to the environment after deposition (Bown and Kraus, 1987; Kraus, 1987). The slickensides, ped structures, and carbonate nodules/tubules collectively indicate a well-drained landscape. Slickensides point to a climate with wet/dry seasonality, whereas the nodular and tubular carbonates imply net deficits in effective moisture and a dry climate (Mack et al., 1993). Sedimentological and post-depositional features of LA5b suggest floodbasin settings that were further removed from the active channel(s) as compared with the proximal floodplains represented by LA5a.

3.5. Paleosol analysis

Fine lithofacies associations LA5a and LA5b (Table 2, Figs. 16 and 17) from the Area 130 deposits are overprinted with paleosols (Table 3, Fig. 18). Interpretations of the fine lithofacies associations suggest the paleosols formed in proximal floodplain settings (LA5a), and floodbasins (LA5b). The parent materials included silty claystones and sandy-clayey siltstones. Tuffs were also deposited and comprise some of the coarser fractions of the mudstones. Paleosol color varies with grain size, or rather clay content, with clay-rich

examples being brown (7.5YR 4/2) to yellowish brown (10YR 5/4) and coarser paleosols being light yellowish brown (10YR 6/4) and very pale brown (10YR 7/4). Most of the ancient soil matrix is typified by these browns, but smaller areas of contrasting colors are known from greenish-gray mottles (Gley1 5/1 to 6/1, and Gley2 5/1 to 6/1). Identified paleosol carbonates are palish white (2.5Y 8/1) and grayish white (5Y 8/1).

3.5.1. Type-I paleosols: description

Type-I paleosols (Table 3 and Figs. 18, 19) are developed upon LA5a (Fig. 16). Profile depths are decimeters thick. The overprinted substrate varies as tuffaceous siltstone, tuffaceous sandy siltstone, or sandy-clayey siltstone. In most cases two master horizons can be discerned, and are mainly identified through variations in carbonates, slickensides, grain sizes, and color mottles.

B-horizons (10-40 cm thick) have a low to moderate number of greenish-gray color mottles, a low to moderate number of carbonate nodules (1-3 cm in diameter) and rootcasts (1-3 cm in diameter by at most 5 cm long), and rare slickensides. It is further interpreted as a Bwk-horizon because, at most outcrop the color mottles are more numerous and strongly developed than other features.

C-horizons lack pedogenic features and either are massive or have poorly preserved sedimentary structures. It is coarser and lighter in color than the overlying B-horizon. Contacts between the two are either over a diffuse zone with a thickness of centimeters to a few decimeters or at a sharp break.

Fig. 18: Generalized profiles of the Area 130 paleosols described in Table 3. Paleosol maturity increases from left to right (see text for discussion). Type-I paleosols are overprinted on LA5a (Figs. 16, 19), type-II and type-III paleosols are overprinted on LA5b (Figs. 17, 20, 21).

INCREASING MATURITY →

TYPE I : weakly developed

clay silt sand

cm
0
20
40
60
80
100

5Y 7/2

Bwk (10YR 6/4)

10YR 7/4

C (5Y 7/2)

TYPE II : moderately developed

10YR 7/4

Bw (10YR 5/4)

Bwk (7.5YR 4/2)

Bw (7.5YR 4/2)

TYPE III : strongly developed

5Y 7/2

Bwk (10YR 7/4)

Bkw (10YR 6/4)

Bkw (10YR 6/4)

greenish-gray mottles

blocky peds

slickensides

mukkara

carbonate rootcasts

carbonate nodules

claystone

siltstone

sand

tuff

sedimentary layering

Fig. 19: Lithostratigraphic log and photo for section through an upper part of the Area 130 successions (see Fig. 8 for geographic location). Section illustrates sets of massive sand (lithofacies Sh) and massive mudstone (Mh) typical of lithofacies association LA5a, and facies features characteristic of fine lithosome I_2. Note abrupt changeover in facies style and paleosol type across boundary surface o_2(NE). See Fig. 18 for key to symbols.

LITHOFACIES, LITHOLOGIES & OTHER FEATURES

boundary surface O_2(NE)

type-I paleosol   type-I paleosol   type-I paleosol   type-I paleosol   type-III paleosol

1 m

sand | silt | clay

Mh Sh Mh Sh Mh Sh Mh Sh Mh Sh   Mh

LA5a   LA5b

LITHOFACIES ASSOCIATIONS

FINE LITHOSOME I_2
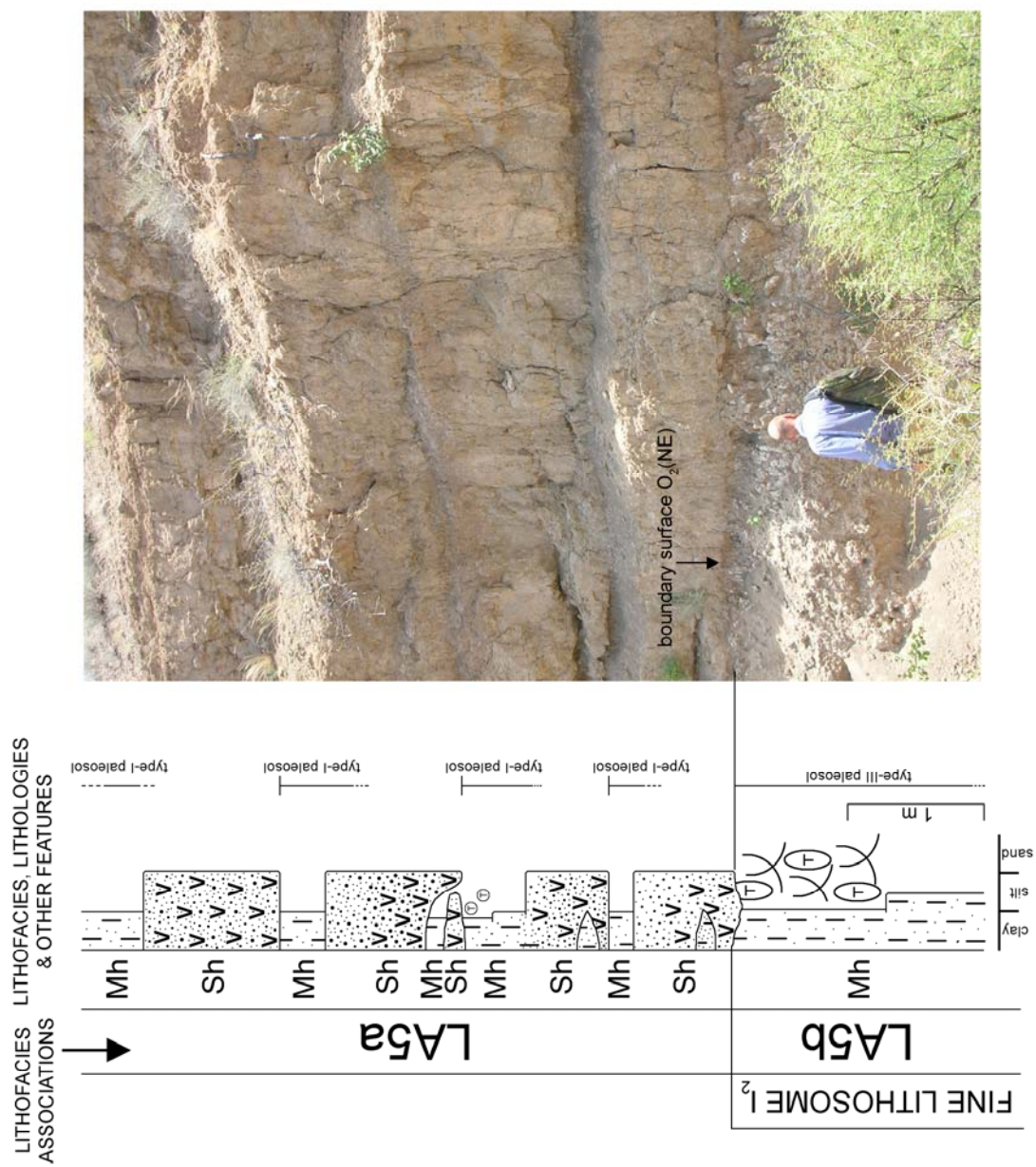
At some outcrop examples a thin A-horizon can be located from crumb structure, which Wynn (1998, 2000) likened to a mollic epipedon resulting from herbaceous vegetation. This horizon is rarely preserved though because of an upper erosive contact with an overlying unit of lithofacies Sh (Fig. 19).

3.5.2. Type-II paleosols: description

Type-II paleosols (Table 3 and Figs. 18, 20) are overprinted on LA5b (Fig. 17). Profile depths range from 100 to 200 cm, through dark-colored claystones. The paleosol can be divided into at least three subordinate structured B-horizons, including an upper Bw-horizon, a middle Bwk-horizon, and a lower Bw-horizon. A ubiquitous and diagnostic feature for all the B-horizons is slickensides. These structures form large pseudo-anticlines in the lower Bw-horizon.

Upper Bw-horizons have thicknesses of 5-15 cm. It is not often present though, because the upper limit of the paleosol is defined by contacts with sands with erosive bases (Fig. 20). Upper Bw-horizons are discerned from blocky-columnar peds (typically 3-5 cm long/wide by 5-15 cm high) that are slickensided. Bwk-horizons have thicknesses that range from 50 to 100 cm. They are recognized from arcuate fractures, which have slickensided surfaces, and carbonate nodules (Figs. 20a, 20b). Arcuate, slickensided fractures range from 15 to 100 cm long/high. These fractures show a moderate to high degree of intersection and define curvilinear and wedge-shape structures for the overprinted claystone. Carbonate nodules are sparsely to moderately abundant in the Bwk-horizons. Nodules are spherical, with typical diameters of 1-5 cm.

Fig. 20: Photos of mature, type-II paleosols overprinted on fine lithofacies association LA5b (map location in Fig. 8). (a) Lithofacies association LA5b overprinted with large-scale arcuate, slickensided fractures (designated by arrows) infilled with carbonate; note upper contact with coarse lithosome j_2 at boundary surface j_2. (b) Close-up of features in (a) with "NC" designating nodular carbonate. (c) LA5b characterized by lithofacies Sh bracketed by sets of Mh; upper Mh set lacks paleosol features but lower one has well-developed mukkara structure (e.g., boxed area); uppermost contact of LA5b as in (a); note backpack at lower left of boxed area and pen inside boxed area for scales. (d) Close-up of boxed area in (c).

LITHOFACIES
ASSOCIATIONS

COARSE LITHOSOME j₂

LA1

boundary surface j

LA5b

150 mm

a

b

150 mm

NC

NC

NC

NC

NC

LITHOFACIES
ASSOCIATIONS

COARSE LITHOSOME j₂

LA1

boundary surface j

LA5b

c

Mh

Sh

Mh

d

150 mm
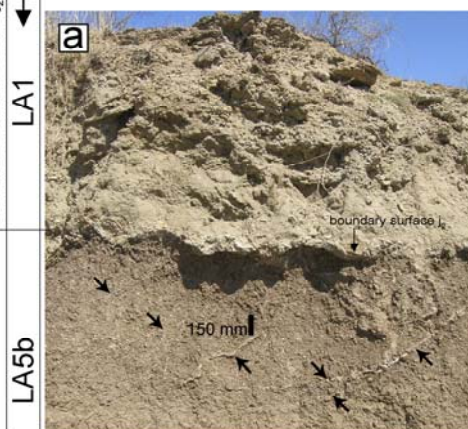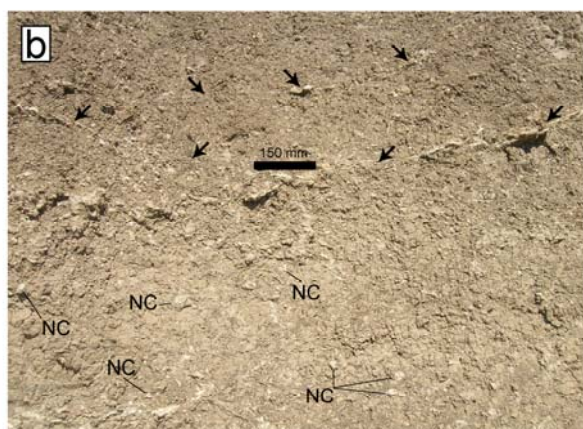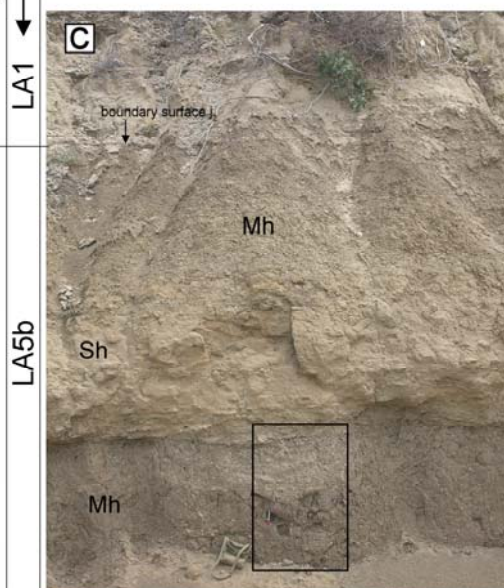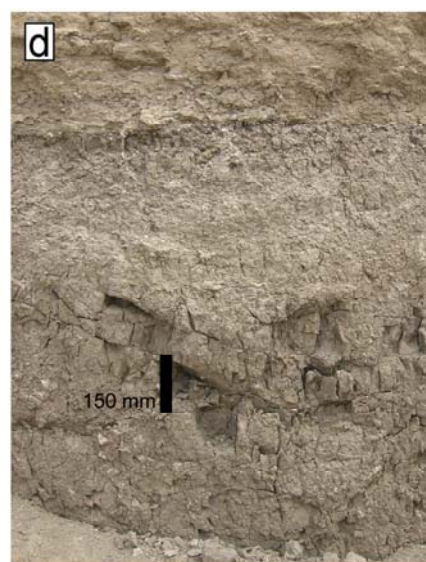
Lower Bw-horizons are 75-100 cm thick. They are identified from zones of large blocky, angular, and wedge-shaped peds (Figs. 20c and 20d). These peds are defined from densely intersecting networks of slickensides fractures. As noted by Wynn (1998), these Bw-horizons resemble mukkara structures described by Paton (1974).

3.5.3. Type-III paleosols: description

Type-III paleosols (Table 3 and Fig. 18) are developed upon units of LA5b (Fig. 17) that typically consist of clayey siltstones, silty claystones, and sandy-silty claystones. The most diagnostic feature of these paleosols is a calcic B-horizon, which comprises three subordinate horizons that are distinguishable from differences in carbonate development, slickensides, and color mottles. Subordinate horizons include an upper Bwk-horizon, a middle Bkw-horizon, and a lower Bkw-horizon. Type-III paleosols are 100-200 cm thick.

Type-III paleosols start with a 10-15 cm thick Bwk-horizon (Fig. 21b). It is considered a colored and then a carbonate horizon because of its moderate number of greenish-gray color mottles and few spherical carbonate nodules (1-3 cm in diameter). At some levels along this horizon, however, the carbonate nodules coalesce and form 5-10 cm long, vertically elongated nodules (Fig. 21c). The overprinted substrate is often a sandy siltstone that is poorly sorted and locally tuffaceous. A tuffaceous sand or silty tuff typically overlies this uppermost paleosol horizon (Figs. 21a, 21b). This coarse sedimentary unit has an erosive

Fig. 21: Photos of very mature, type-III paleosols (map location in Fig. 8) overprinted on fine lithofacies association LA5b that forms the upper levels of fine lithosomes. (a) Close-up view of section in Fig. 19 showing boundary surface o_2(NE) and abrupt changeover from very mature type-III paleosol to LA5a overprinted with immature type-I paleosols. (b) Close-up view of changeover at boundary surface o_2(NE), tuffaceous silt/silty tuff above and type-III paleosol below; Bwk-horizon = grayish-green mottles and carbonate nodules; upper Bkw-horizon = carbonate nodules and grayish-green mottles; lower Bkw-horizon = masses of interlocking carbonate nodules/tubules dissected by slickensides. (c) Close-up view of Bwk-horizon in (b); MT designates mottles of grayish green, and NC stands for nodular carbonate. (d) Close-up view of lower Bkw-horizon in (b) showing carbonate tubules (labeled CT) and carbonate nodules with slickensided surfaces (labeled SS).

a

LITHOFACIES ASSOCIATIONS

LA5a

LA5b

FINE LITHOSOME I₂

boundary surface O₂(NE)

150 mm

b

PALEOSOL HORIZONS

Bwk

Bkw

Bkw

tuffaceous silt

silty tuff

80 mm

c

NC

NC

NC

MT

50 mm

d

SS

SS

CT

base; therefore, the entirety of the uppermost portion of the paleosol profile is probably not preserved. At a number of outcrop localities, such coarse units directly overlie the middle horizon of the paleosol and, presumably, the topmost horizon has been removed by paleo-erosion. In any case, Bwk-horizons diffusely grade downward into middle Bkw-horizons.

Middle Bkw-horizons (Fig. 21b) are developed upon ~25 cm of sandy siltstones or clayey siltstones. This horizon is distinguished by an abundance of carbonate nodules or tubules and greenish-gray color mottles to a lesser extent. Some of the smaller carbonate forms in this horizon coalesce to form blocky masses that are 10-20 cm thick. Middle Bkw-horizons diffusely grade downward into lowermost Bkw-horizons.

The lowermost Bkw-horizon (Figs. 21b and 21d) for type-III paleosols is most frequently developed on 100-150 cm of sandy-clayey silt or sandy-silty clay. It is firstly characterized by a mass of interlocking carbonates nodules and tubules. Secondly, it can be recognized through a densely intersected network of fractures and associated slickensided surfaces. Each slickensided fracture is large scale, typically extending through 25-50 cm of the substrate. Nodular carbonates are spherical (1-5 cm in diameter) and elongate (10-20 cm long and 5-10 cm in diameter). The elongate nodules have sub-vertical to vertical orientations in comparison to sedimentary layering. Tubules occur with diameters of 1-3 cm and lengths of 5-10 cm. They are curvilinear and are commonly sub-vertically orientated in relation to the horizontal layering of the

sediments.   Carbonate nodules are sometimes slickensided on their outer

surfaces (Fig. 21d).

3.5.4. Interpretation of paleosols

Collectively, the greenish-gray color mottles, carbonate accumulations,

and slickensides indicate the paleosols formed under seasonal episodes of

wetting and drying.   Greenish-gray color mottles suggest the soil matrix was

saturated with moisture at times, probably due to poor drainage and/or a shallow

water table (Mack and James, 1992, 1994).   Well-developed slickensides

overprinted on clay-rich mudstones are indicative of vertisol horizons

(Gustavson, 1991; Retallack, 2001).   As expected (Ahmad, 1983; Wilding and

Ruben, 1988), slickenside abundance increases when the clay content of an

Area 130 paleosol increases, likely due to a higher amount of 2:1 clay minerals

necessary for the shrink-swell process.   Modern vertisols commonly occur in

areas with seasonal climate changes, because marked variations between dry

and wet periods are needed for the shrink-swell process (Yaalon and Kalmar,

1978; Wilding and Ruben, 1988). When desiccation occurs—such as after rains

or floodwaters have entered soil channels and saturate the matrix—paleosol

carbonates are precipitated (Mack et al., 1993, 2000).

Depositional environments as inferred from lithofacies associations (i.e.,

LA5b and LA5a) also certainly played a role in paleosol development. Paleosols

are formed upon the siltstones of crevasse-splay, levee and related deposits of

LA5a (Fig. 19).   Overbank floods and the associated currents were probably too

strong for the fallout of clay-sized particles, which may explain why claystone is generally absent from LA5a. This might also suggest there are few 2:1 clay minerals for shrink-swell processes, and point to one cause for the rarity of vertic horizons in LA5a. Comparatively, a predominance of paleosols with vertic horizons in LA5b is attributable to clays composing a significant fraction of this lithofacies association (Fig. 20). Deposition in LA5b occurred with weak currents and from grains falling out of suspension, as indicated by a predominance of massive claystones (lithofacies Mh).

Paleosols of Area 130 have differences in carbonate accumulation, slickenside formation, and horizon differentiation that likely reflect varying degrees of maturity and thus developmental times (e.g., Gile et al., 1981; Machette, 1985; Bown and Kraus, 1987; Kraus 1987; Marriott and Wright, 1993; Kraus and Aslan, 1999; Kraus, 2002; Mack and Madoff, 2005). Type-I paleosols from the study area are interpreted as weakly to moderately developed, and hence the least mature or most immature (Fig. 18). This contention is based on thin profiles and limited horizon differentiation, as well as the few to common carbonate nodules that resemble the assemblage of carbonate accumulations described for youthful calic soils in dry settings (e.g., Gile et al., 1981; Machette, 1985). A probable influence on the limited development has to do with the frequency of overbank flooding and associated high rate of sediment accumulation in the proximal-floodplain setting (Bown and Kraus, 1987; Kraus and Aslan, 1999) interpreted for the type-I paleosols. The overprinting of type-I paleosols upon the proximal-floodplain mudstones and the positions of these

overprinted strata between the erosive bases of coarser sand/tuff sheets (Fig. 19) suggests soil formation was arrested by erosion from overbank flooding and burial from sand/tuff deposition. The limited time available for paleosol development is therefore perhaps attributable to successive (annual/seasonal?) events of overbank flooding, erosion, and deposition.

Chiefly due to multiple, thick horizons with sharp boundaries, and ample, well-formed slickensides, type-II paleosols are interpreted as showing signs of moderate maturity. Multiple subordinate slickensided B-horizons and profile depths (~2 m) for type-II paleosols imply longer periods of sub-aerial exposure relative to type-I paleosols (Fig. 18). Type-II paleosols are developed on claystones of LA5b (Fig. 20). These claystones were deposited from weak currents in a setting removed an active channel, as compared with the setting of type-I paleosols. This may suggest the differences between type-I and type-II paleosols are due to channel proximity and the rate of sediment/water input from flooding (e.g., Bown and Kraus, 1987; Kraus and Aslan, 1999).

Laterally persistent (100's of m) and meter-thick calcic horizons for type-III paleosols (Figs. 10, 21) indicate a lengthy episode of paleosol development compared to the other paleosols from Area 130. Large and abundant slickensides of type-III paleosols also suggest prolonged pedogenesis. This paleosol type may have formed in areas away from an active channel, where a low flood frequency produced slow sediment accumulation rates, leading to a more strongly developed paleosol than the type-I or type-II paleosols (e.g., Bown and Kraus, 1987; Kraus and Aslan, 1999). Type-III paleosols are interpreted as

very mature (Fig. 18) based on well-developed slickensides, multiple horizons, and profile depths of nearly two meters. A status of very mature is especially suggested by the massive carbonates and abundant vertically to sub-vertically orientated, interlocking calcic nodules/tubules (Fig. 21), which bear strong similarities to the carbonate accumulations reported for calcic soils with prolonged development (e.g., Gile et al., 1981; Machette, 1985).

Radiocarbon studies coupled with detailed comparisons between modern soils and ancient calcic soils (Gile et al., 1981; Machette, 1985; Mack and Madoff, 2005) suggest that meter-thick calcic horizons for the Area 130 type-III paleosols reflect pedogenesis over times on the order of 10^3 to 10^5 years. However, the formation time is probably closer to the high end of this range, considering the pronounced interlocking nature of the carbonate accumulations. Type-II paleosols contain comparatively fewer accumulations of carbonate; yet, they have strongly developed, meter-thick vertic horizons. Vertic structures begin forming over tens to hundreds of years in modern soils (Ahmad, 1983; Wilding and Ruben, 1988). The well-developed nature of the vertic features, coupled with the multiple vertic horizons suggests a developmental time $\geq 10^2$ years for the type-II paleosols. Because type-III paleosols are better developed and interpreted as forming on the order of 10^3 to 10^5 years, a maximum formation time for the type-II is likely to be on the order of 10^3 years. Finally, the immature type-I paleosols probably indicate a maximum developmental time on the order of 10^0 to 10^2 years.

3.6. Boundary surfaces and lithosomes: fluvial architecture

A distinctive aspect of the sedimentary geology for Area 130 is that it can be subdivided into six, 500-2000 m long by 5-10 m thick lithosomes (Fig. 11). These lithosomes are bounded by a series of discordant contacts (Allen, 1983; Bristow, 1996) or boundary surfaces (Miall, 1994, 1996) that are recognized as either an erosive surface, accretionary surface, or a hiatal surface (Table 4). Two lithosome types are distinguished, a coarse lithosome and a fine lithosome (Table 5).

Area 130's fluvial architectural components probably derive from processes of major channels operating over timescales on the order of 10^3 to 10^4 years (cf., Table 1 of Miall, 1994; Table 9.1 of Miall, 1996; Table 1 of Jones et al., 2001). This interpretation of major channels is based on observations (e.g., Allen, 1983; Miall, 1994; Jones et al., 2001) that flow-regime processes, simple bar development, and local channel switching generate architectural components smaller than those discussed in detail below, but valley or channel-belt systems (e.g., Holbrook, 2001; McLaurin and Steel, 2007) generate units larger than the examples described here for Area 130. Possible exceptions to these interpretations are erosive surface j_2 and hiatal surfaces o_2(NE) and o_2(SW). Surface j_2 might reflect a basal boundary surface for a channel belt or a paleo-valley base (e.g., Miall, 1994; Holbrook, 2001) because it exhibits up to about 8 m of concave-up erosive relief and can be traced outside the study area and mapped continuously across 10's km of lateral exposure (Burggraf et al., 1981; White et al., 1981). Hiatal surfaces o_2(NE) and o_2(SW) are associated with type-

III paleosols that formed over times on the order of 10^3 to 10^5 years. The largest

end of this range is similar to predicted durations for hiatuses caused by channel-

belt or valley abandonment (Miall, 1996; Kraus, 1999; Retallack, 2001).

The three coarse lithosomes recognized from Area 130 (Table 5) are 1000-

2000 m long by 5-10 m thick (Fig. 11). Each is a complex of coarse lithofacies

associations (i.e., LA1, LA2, LA3 or LA4) and thus represents a fluvial channel

deposits. It is expected that with lateral outcrop exposure roughly parallel with

paleo-flow direction, flat basal channel geometries instead of concave-up

channel margins would be a more common observation at fluvial outcrops (e.g.,

Allen and Fielding, 2007). Coarse lithosome m has well preserved channel

margins. Each lateral margin of the lithosome is clearly defined by concave-up,

channel-form relief (~5 m) that is developed against sediment finer than the

lithosome contains. This suggests a paleo-flow direction roughly normal to the

overall NE-SW orientation of the outcrops. Lateral margins for coarse lithosomes

j_2 or l are not preserved within the study area. Despite this deficit, it is argued

that the overall paleo-flow direction for coarse lithosome j_2 is also largely normal

to the NE-SW orientation of Area 130 outcrops. This is because opposing,

concave-up, channel-form margins can be observed at many locations on

erosive surface j_2, which defines the base of the coarse lithosome j_2. Although

such well-developed opposing margins are generally lacking from lithosome l, its

lenticular cross-section and lateral thinning might be evidence of a paleo-flow

axis similar to the other coarse lithosomes. Also supporting this idea are the fine-

grained lithosomes on top of coarse lithosome l . These are interpreted below as

the infills of side-channel bars that flowed around portions of a mid-channel bar represented by coarse lithosome l. The probability of these suggestions will be further examined in the following discussions.

3.6.1. Erosive surfaces: description

Surface j_2: The j_2 surface (Table 4) has a length greater than 2000 m. It forms the base of the stratigraphic marker level j_2 defined by Frank (1976) and thus takes its name from this marker level (compare this study's Figs. 9 and 11). Surface j_2 shows variable erosive relief ranging from concave-up channel-form scours, which are 10's to 100's of m wide and 1-8 m deep, to near-planar contours that stretch across 10's to 100's of m. Surface j_2 is an erosional contact that marks an upward changeover from mudstone-dominated lithofacies association LA5b to sand-dominated deposits (Figs. 22, 23).

Surface l: Surface l (Table 4) takes its name from stratigraphic marker level l that Frank (1976) defined mainly from his logs HJF-35 and HJF-36 in the southwest portion of the study area (Fig. 9). This marker level can actually be continuously traced from these sections, through the central part of the study area, to all of his northeast sections. This total lateral extent of marker level l is designated here as surface l. The l surface defines an erosive contact greater than ~2000 m long. It displays horizontal contours, as well as contours that show concave-up erosive relief at 1-3 m (Fig. 11). It marks a boundary between upper gravel/sand strata and lower strata that consist of either sands or mudstones (Figs. 22, 23).

Fig. 22: Representative lithostratigraphic logs of examined outcrops in Area 130. See Fig. 8 for map locations. Logs are transects through the recognized lithosomes, boundary surfaces, paleosols, lithofacies associations, and lithofacies listed in Tables 1-5 and illustrated in Figs. 10-21, 23-27 and 29. Type-I paleosols are overprinted on LA5a above boundary surfaces o_2(NE), o_2(C) and o_2(SW). Type-III paleosols are overprinted on LA5b between boundary surfaces l_2 and o_2(NE), n_2 and o_2(SW), and j_3 and l. Type-II paleosols are overprinted on LA5b below boundary surface j_2.
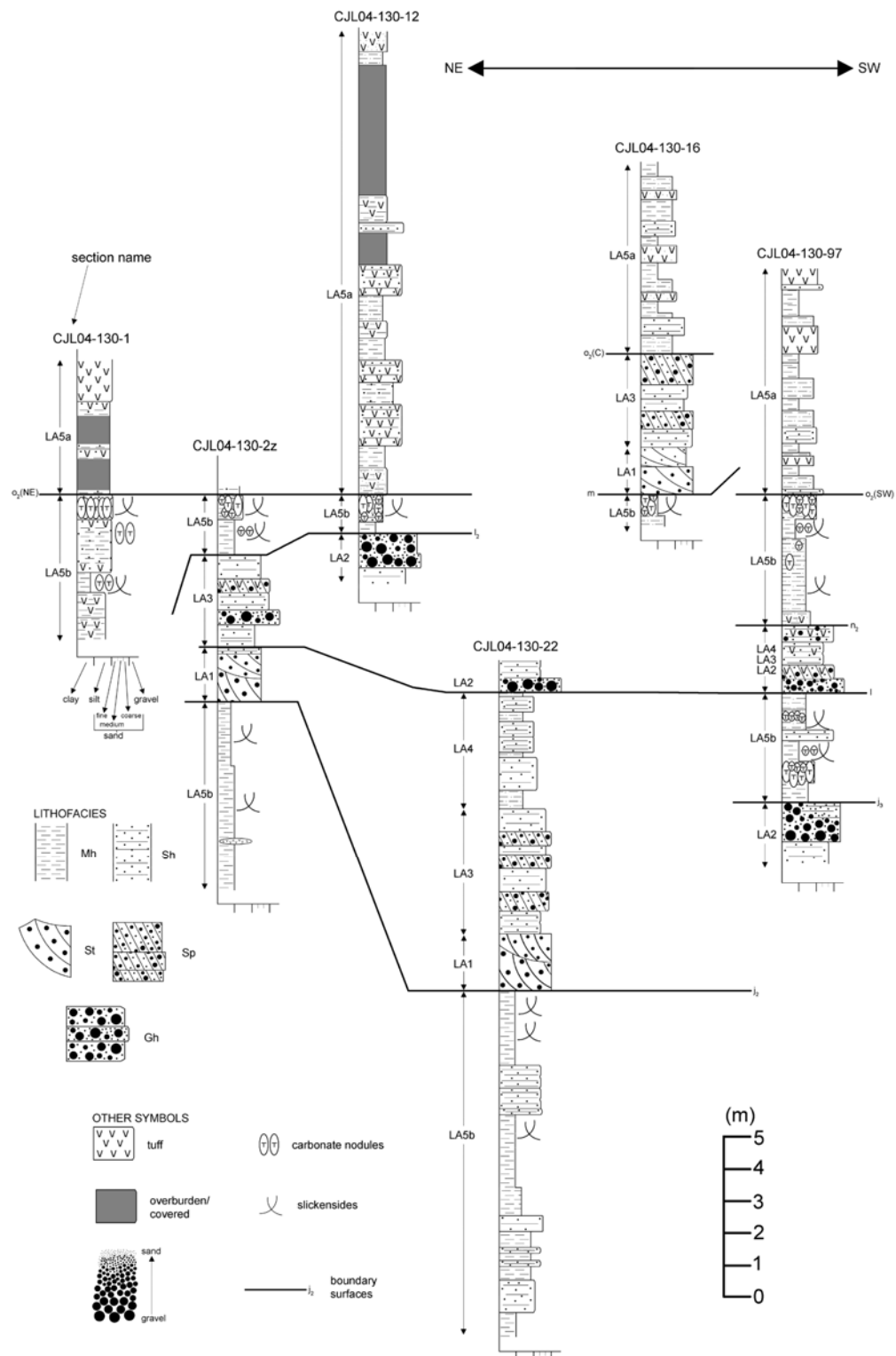
Fig. 23: Photo-mosaic and interpretations for examined Area 130 successions (see Fig. 8 for geographic location). Lower panel: typical badland-like small hills formed when outcrops are dominated by poorly consolidated sands and gravels (labeled LA1, LA2, LA3, LA4 in upper panel) that overlie mudstones (labeled LA5b in upper panel); higher outcrops at far left upheld by mudstones (labeled LA5b in upper panel) and dense carbonate horizon (white area in upper panel); note 50 cm square at lower far left for scale. Upper panel: overlay interpretations showing lithofacies associations (i.e., "LA"), boundary surfaces (horizontal black lines), and carbonate horizon of type-III paleosol (white area); strata with LA5b below surface j_2 are overprinted with type-II paleosols; coarse lithosome j_2 is stratified between surfaces j_2 and l; coarse lithosome l stratified between surfaces l and l_2; fine lithosome l_2 between surfaces l_2 and o_2(NE).
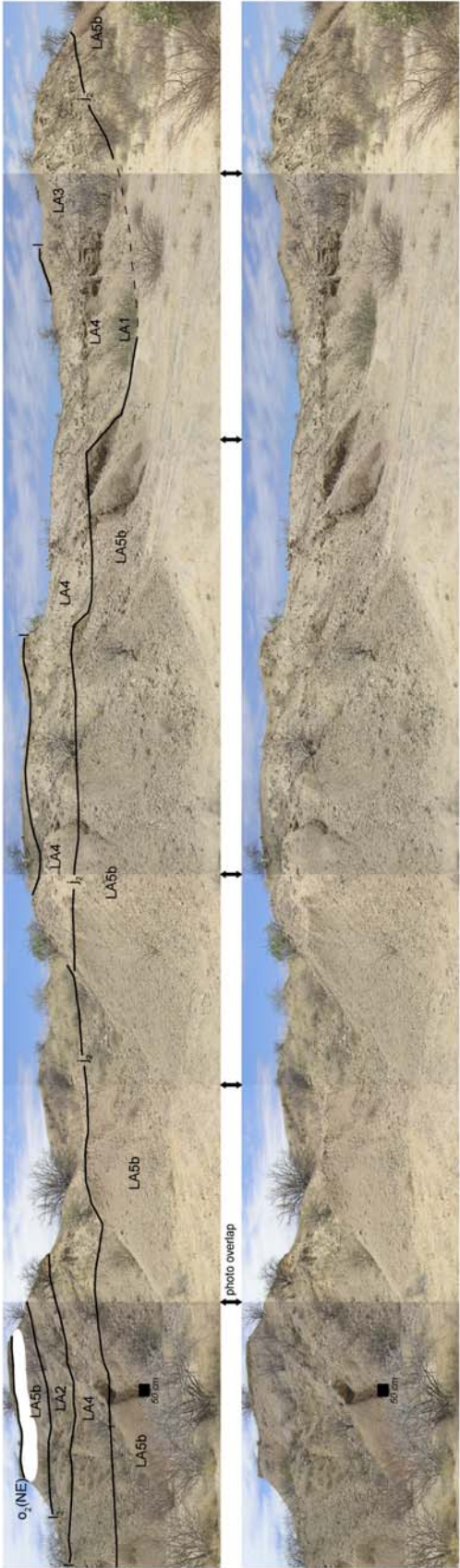
Surface m: The m surface (Table 4) is named from stratigraphic marker level m that was defined by Frank (1976) principally at his logs HJF-33, HJF-16, HJF-37, and HJF-33 (Fig. 9). This present study of Area 130 extends the known lateral range of stratigraphic marker level m. It can be continuously traced to the northeast where it terminates near logs HJF-23, HJF-24, and HJF-25 (Fig. 11). Surface m defines a ca. 1200 m long discordant erosional contact that is nearly flat lying, but it has lateral-most concave-up margins that show about 5 m of overall erosive relief. Across the surface there is mainly change from sands/mudstones to sand-dominated strata (Fig. 22).

3.6.2. Erosive surfaces: interpretation

Across-surface grain-size changes, in addition to contours, erosive style and lengths (Table 4) suggest the erosive surfaces j_2, l, and m reflect basal boundaries for major fluvial channels (e.g., Table 1 of Miall, 1994; Table 1 of Jones et al., 2001). Surface segments with nearly flat lying erosive relief probably formed from broad scour and with little downward incision. Concave-up relief, on the other hand, is interpreted to indicate downward incision developed by processes and flow energies typical of thalwegs or other deep parts of a channel.

3.6.3. Accretionary surfaces: description

Surface j_3: Surface j_3 (Table 4) takes it name from the fact that it is the first surface above surface j_2 (Fig. 11). The surface has a length of ~500 m. It is a

flat or concavo-convex, non-erosive contact. The surface marks a boundary between lower coarse strata and upper lithofacies association LA5b (Fig. 22).

Surfaces l_2 and n_2: Surfaces l_2 and n_2 (Table 4) are named as such because they are the first surfaces above stratigraphic marker levels l and n, respectively (compare Figs. 9 and 11 especially at logs HJF-27 and HJF-36). These surfaces extend laterally for over 900 m and are characterized by concavo-convex to nearly horizontal contours. They mark non-erosive contacts for lower coarse strata and upper mudstones of lithofacies association LA5b (Figs. 22 and 24).

Surface $o_2(C)$: The $o_2(C)$ surface (Table 4) takes its name from the observation that it partially correlates with a portion of Frank's (1976) stratigraphic marker level o_2 cropping out in central portion of the study area (compare Figs. 9 and 11). The (C) stands for "central" and is used to nominally distinguish $o_2(C)$ from hiatal surfaces $o_2(NE)$ and $o_2(SW)$.

The $o_2(C)$ surface has a length of about 1200 m. It displays nearly horizontal contours as well as concavo-convex geometries. The surface defines a non-erosive contact. Strata below this contact consist of coarse sediments, whereas strata above it are exclusively composed of fine lithofacies association LA5a (Fig. 22).

3.6.4. Accretionary surfaces: interpretation

Contours, stratigraphic positions, and across-surface sedimentary changes suggest surfaces j_3, l_2, n_2, and $o_2(C)$ are accretionary surfaces at the

Fig. 24: Interpretative lithostratigraphic log and photo of transition from coarse lithosome I to fine lithosome I_2 (see Fig. 8 for map location). Note bag in photo for scale (25 cm). Coarse lithosome I is bounded by erosive surface I (not shown) and accretionary surface I_2. At this exposure, it is formed by LA2 that comprises alternating sets of massive gravel (Gh) and massive sand (Sh). These facies indicate gravel and sand sheets, gravel lags, composite-compound bars, and longitudinal gravel bars. Fine lithosome I_2 is bracketed by accretionary surface I_2 and hiatal surface o_2(NE), and consists of massive mudstones (Mh) of LA5b. Mudstones are overprinted with very mature type-III paleosols at topmost levels. Note the carbonate debris in the lower right half of the photo—especially the boulder-sized nodule in the gully—illustrating the particularly well-developed nature of calcic horizons in the paleosol. Fine lithosome I_2 is the fine-grained infills of abandoned channel segments for the braided river system represented by coarse lithosome I. The transition to fine-grained infilling and abandonment was rather abrupt, as suggested by the marked contrast in lithology, grain size and sedimentary style across surface I_2.
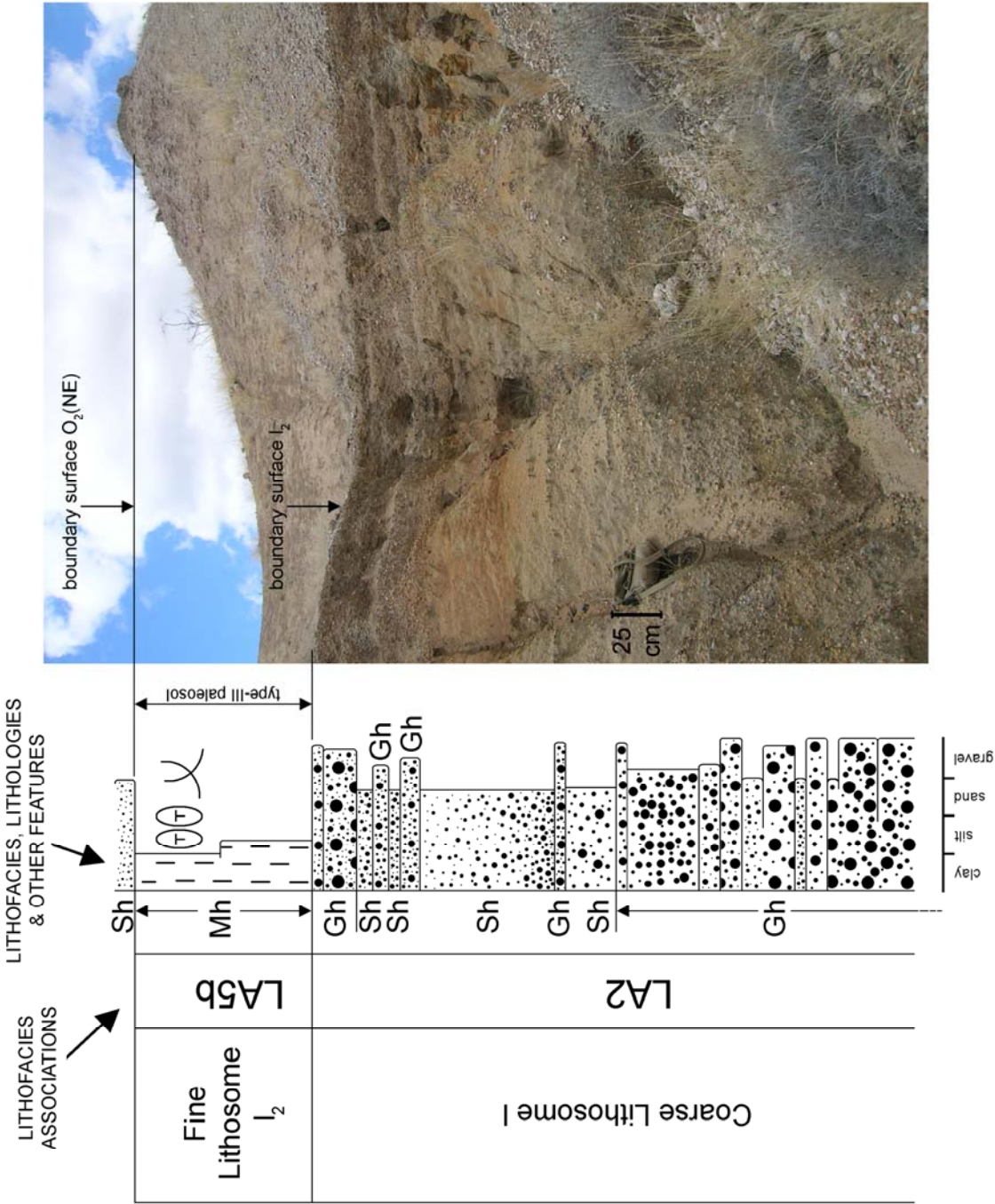
tops of channels (e.g., Miall, 1994; Jones et al., 2001). These surfaces probably started to form at the final phase of channel infilling and/or during abandonment.

3.6.5. Hiatal surfaces: description

Surfaces $o_2(NE)$, $o_2(SW)$: The $o_2(NE)$ and $o_2(SW)$ surfaces (Table 4) take their names from the portions of Frank's (1976) stratigraphic marker level o_2 that crops out in northeast and southwest portions of the study area (compare Figs. 9 and 11). They are ≥900 m long and show nearly horizontal and mild concavo-convex erosive contours. These surfaces mark erosive contacts and mainly separate fine-grained lithosomes from overlying strata of fine-grained lithofacies association LA5a (Figs. 22 and 25). A notable aspect of the contact is that strata directly below the surfaces are overprinted with the mature type-III paleosols, and strata upon the surfaces are overprinted with immature type-I paleosols (Figs. 19 and 21). Surfaces $o_2(NE)$ and $o_2(SW)$ are partially truncated by the m surface and are found at nearly the same vertical-lateral stratigraphic level (Fig. 11).

3.6.6. Hiatal surfaces: interpretation

Paleosol evidence suggests surfaces $o_2(NE)$ and $o_2(SW)$ probably formed during hiatuses, resulting when sediment and water supplies became limited. This may occurred because the active channel system(s) migrated away from the study area. Although some surface aspects may have formed when the overlying sediments were deposited, the contours and erosive features of the hiatal surfaces are interpreted as a partial consequence of landscape weathering

Fig. 25: Photo of uppermost interval of examined Area 130 deposits (map location in Fig. 8). Shown is transition from fine lithosome I_2 to lithofacies association LA5a, which also approximates the changeover from the upper KBS Member to lower Okote Member. Transition occurs at arrows marking the base of LA5a successions (i.e., Okote Tuff Complex/Okote Tuffaceous Siltstone Complex) characterized by very tabular silty-sandy tuffs interbedded with tuffaceous silts and clays, which are overprinted with weakly developed type-I paleosols. Very mature type-III paleosols are developed on the fine lithosome, and indicate a hiatus on the order of 10^3-10^5 years occurred before sedimentation of lower Okote Member deposits of LA5a that represent proximal floodplain settings (e.g., crevasse splays & levees). Section is about 5 m high by 100 m long. Picture is taken from standing at archaeological site FxJj 17 and looking to the ~north (see Fig. 8).

and deflation, during times of pedogenesis and thus negligible aggradation (e.g., Aitken and Flint, 1995; Kraus, 1999). Situated directly beneath the hiatal surfaces are the type-III paleosols with their characteristic meter-thick calcic B-horizons. These mature paleosols suggest that the landscapes where the surfaces formed had limited sediment supplies, and soils were not saturated for significant periods. Large carbonate nodules, and their coalescing patterns, from the type III paleosols suggest sedimentary hiatuses on the order of 10^3 to 10^5 years contributed to surface formation. Hiatal surfaces from Area 130 are interpreted as being analogous to major paleosol surfaces arising from a long-term geomorphic process, such as channel-belt avulsion or paleo-valley abandonment (e.g., Table 1 of Miall, 1994; Table 9.2 of Miall, 1996; Table 1 of Jones et al., 2001).

3.6.7. Coarse lithosome j_2

Description: Coarse lithosome j_2 mainly includes lithofacies associations LA1, LA3 and LA4 (Table 5). It is the sedimentary package from surface j_2 up to surfaces j_3 and I (Fig. 26). Basal contacts are erosive, and scoured into underlying strata that exclusively consist of fine lithofacies association LA5b (Figs. 20, 22 and 23). Concave-up geometries dominate the lowermost part of the lithosome, especially at its center where surface j_2 can exhibit erosive relief up to ~8 m. Upwardly, the lithosome transitions to a more tabular-like shape.

A series of comparatively large, medium, and small channel-form bodies form the lower portion of lithosome j_2. These bodies have bases that conform

Fig. 26: Geometries, boundary surfaces and lithologies of coarse lithosome j_2 and fine lithosome j_3 (modified from Frank, 1976). See Figs. 9 and 11 for key to HJF logs, tephrochronological context, and placement within the overall fluvial architectural model. CJL04 logs (mapped in Fig. 8 and illustrated in Fig. 22.) provide details on constituent facies and paleosols. Coarse lithosome j_2 is bounded by erosive surface j_2, accretionary surface j_3 and erosive surface l.   It is a channel and sheet complex with basal levels formed by at least six concave-up, channel-form bodies of varying size. Accretionary surface j_3 and erosive surface l bracket fine lithosome j_3. The fine lithosome is drawn as removed from its boundary surface context to highlight abandoned channel and fill geometries.
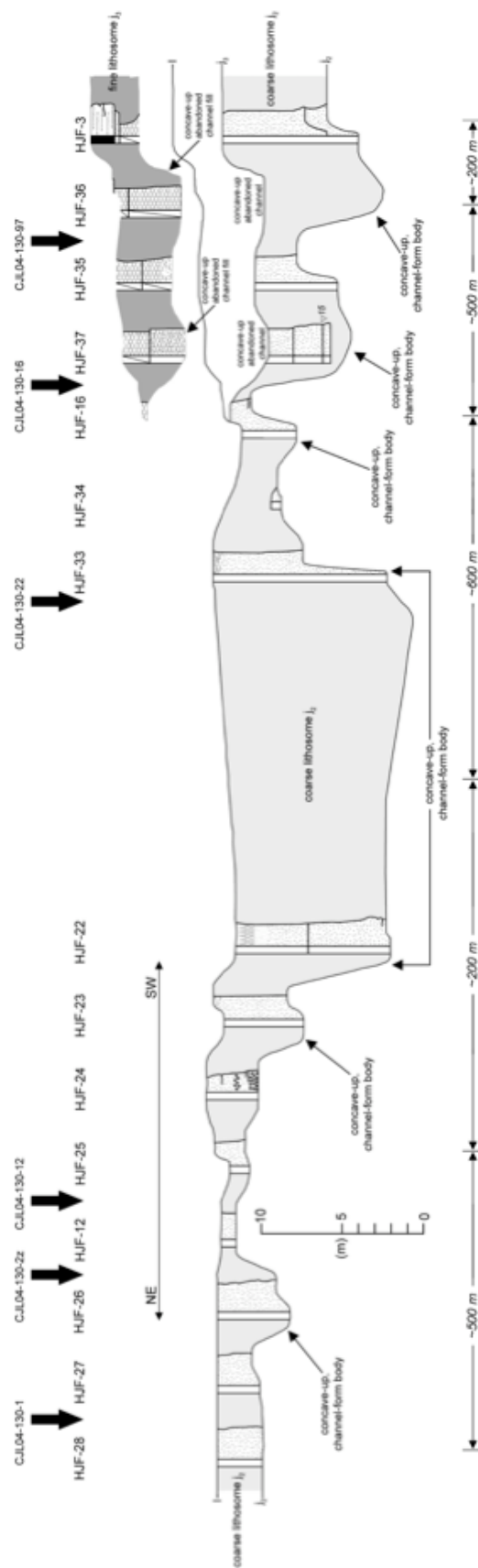
to the base of the lithosome (i.e., erosive surface j_2). At least six such bodies can be recognized on the basis of well-defined, concave-up margins. These display between 1-8 m of erosive relief into underlying and laterally adjacent fine-grained strata. The largest of these channel-form bodies composes most of the central portion of the lithosome (Fig. 26). This body has a mostly flat base, upward-concave lateral margins with erosive relief of ~8 m, and a sheet-like width (~400 m) to thickness (10 m) ratio (e.g., Friend et al., 1979).

Along most areas of the lithosome, there is a somewhat predictable relationship between vertical changes in lithofacies associations (Fig. 22) and geometry. Basal concave-up erosive relief is commonly infilled with channel-floor dunes (lithofacies association LA1). Situated above these dunes are bar deposits of LA3 or sheet-flow deposits of LA4. These two lithofacies associations usually mark the beginning of the more tabular portions of the lithosome, but they do also infill some of the upper extents of the basal concave-up erosive relief. The uppermost tabular geometry of the lithosome generally consists of silty sands of LA4, giving it an overall fining-upward composition.

Interpretation: Vertical geometrical and sedimentological changes for lithosome j_2 suggest a progressive decrease in flow energy and a shift from channelized to comparatively un-channelized deposition (e.g., DeLuca and Eriksson, 1989; Dreyer, 1993). Channel entrenchment is indicated by the lithosome's basal concave-up erosive relief (1-8 m) developed into underlying fine-grained strata. Such relief is typically infilled with large-scale trough cross-stratified sands of lithofacies association LA1, indicating high-energy excavation

of channel floors followed by the deposition by dunes. Above these basal levels the lithosome includes bar (LA3) and sheet-flow deposits (LA4), which are interpreted as evidence of shallower depths and flow expansion. Moreover, the tabular geometries and prevalence of LA4 at uppermost levels of the lithosome suggests the flow became expanded laterally. Deposition of these upper levels likely occurred in shallow and broad channel areas that probably banks with low relief.

The largest channel-form body, which forms the central portion of lithosome j_2, is interpreted to represent an area where most of the flow energies for the channel system were concentrated. Basal erosional relief for the body is the greatest for the lithosome. This aspect probably points to the deepest portion of the channel system and/or where channel thalwegs had the most residence time. The body's steep sides and flat erosive base resemble the morphology of a small valley-like setting, where the migration of one channel or a series of channels was laterally restricted within the confines of well-developed valley margins. Smaller channel-form bodies at lateral areas of the lithosome may represent the scale and deposits of separate channels that were penecontemporaneously active. An alternative is that all of the channel-form bodies, including the largest one from the central part of the lithosome, could be representative of the work of a single channel. This channel may have undergone back-and-forth migration and had multiple temporary positions on the same fluvial plain.

3.6.8. Coarse lithosome l

Description: Coarse lithosome l (Table 5) is defined by surface l at its base and at the top by surfaces l_2, m, and n_2 (Fig. 27). It is a nearly completely preserved sedimentary body. Not considering its lateral margins, it appears that the only original part of the lithosome not preserved in the study area is the uppermost meter or so along its central portion. This part was probably removed by erosion represent by the m surface and incises base of coarse lithosome m. Coarse lithosome l has an overall lenticular shape and a sheet-like width (≥2000 m) to thickness (5 m) ratio (e.g., Friend et al., 1979). The lithosome is exclusively composed of coarse lithofacies associations LA1, LA2, LA3, and LA4.

Basal erosive relief, as marked by surface l, varies between nearly planar and concave-up contours. Concave-up erosive relief occurs as small-scale scours less than a meter deep by a few meters wide, to larger ones with about three meters of depth and extents of 10-100 m. Both types of relief are often filled with trough cross-stratified sands of LA1 and gravel lags of LA2.

As followed along accretionary surfaces l_2 and n_2, the uppermost margins of the lithosome have convexo-concave and nearly horizontal contours (Fig. 27). Deposits accumulated upon these two upper surfaces are mudstone strata of LA5b. These fine-grained deposits are overprinted with the most mature (type-III) paleosols (Figs. 17, 19 and 21-25). An interesting aspect of this upward transition is that most often these fine-grained deposits are accreted directly upon the basalt-clast gravels (lithofacies Gh) of lithofacies association LA2 (Fig. 24).

Fig. 27: Geometries, boundary surfaces and lithologies for coarse lithosome l, and fine lithosomes l_2 and n_2 (modified from Frank, 1976). See Figs. 9 and 11 for key to HJF logs, tephrochronological context, and placement within the overall fluvial architectural model. CJL04 logs (mapped in Fig. 8 and illustrated in Fig. 22.) provide details on constituent facies and paleosols. Coarse lithosome l is bounded by erosive surface l, accretionary surfaces l_2 and n_2, and erosive surface m. It is a lenticular body having uppermost convex-up contours along central parts, which suggest the geometry of a mid-channel bar complex for a braided reach. Fine lithosome l_2 is bounded by accretionary surface l_2, hiatal surface o_2(NE) and erosive surface m. Accretionary surface n_2, hiatal surface o_2(SW) and erosive surface m bracket fine lithosome n_2. Fine lithosomes reflect infills for abandoned channel segments lateral to the mid-channel bar complex. Fine lithosomes are drawn as removed from boundary surface contexts to highlight abandoned channel and fill geometries.
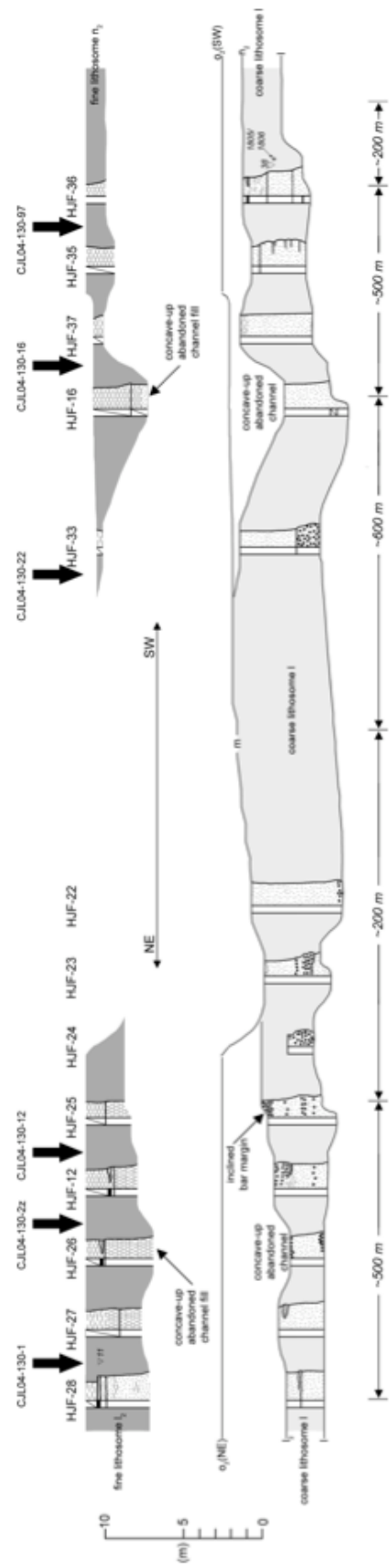
Interpretation: Constituent lithofacies associations for lithosome I indicate sedimentation from both channel (LA1, LA3) and sheet-flow (LA2, LA4) processes. Occurrences of thick successions of basalt gravel and interbedded successions of basalt gravel and sand of LA2 respectively suggest the deposition of longitudinal bars (Leopold and Wolman 1957; Hein and Walker 1977) and composite-compound bars (Allen, 1983; Allen et al., 1983). Comparable assemblages of facies have been documented for coarse-grained, low-sinuosity fluvial systems with braided channels (Williams and Rust, 1969; Collinson 1970; Rust, 1972; Smith 1974; Steel, 1974; Miall, 1977; Cant and Walker, 1978). Moreover, the lithosome's overall lenticular and convex-up geometry (Fig. 27) has strong resemblances with the shapes of a mid-channel braid bar (Bristow, 1987; Bridge, 1993b; Bristow and Best, 1993; Ashworth et al., 2000; Best et al., 2003). Based on these features the lithosome is interpreted as a collection of channel, sheet-flow, and bar sediments deposited by braided streams.

Lateral channel segments of the braided system appear to have been infilled with fine sediment, possibly due to the prolonged growth of the mid-channel bar (Fig. 28). It is envisaged that, as the mid-channel bar vertically aggraded and laterally expanded, flows were progressively diverted around its sides. This probably also caused channel segments to migrate across the landscape in both directions, resulting in the deposition of the northeast and southwest portions of the lithosome. However, sediment supply to these lateral areas eventually became limited, possibly due to the blocking of the main channel entrance from the continued bar growth and/or channel switching to

Fig. 28: Simple genetic model for coarse lithosome I and fine lithosomes l_2 and n_2 (Fig. 27). Time 1: deposition of small bars within a comparatively narrow braided reach; low-stage flows are distributed through channel paths determined by bar topography and surrounding banks. Time 2: prolonged downstream, vertical and lateral growth causes bars to increase in size and overlap, leading to the development of a mid-channel bar complex and the diversion of flows to lateral channel segments, which has the consequence of increasing erosion at the banks and widening the reach. Time 3: blocking of the reach's entrance due to further growth of the bar complex decreases flow competencies and supply rates, and initiates abandonment and fine-grained infilling of lateral channel segments.
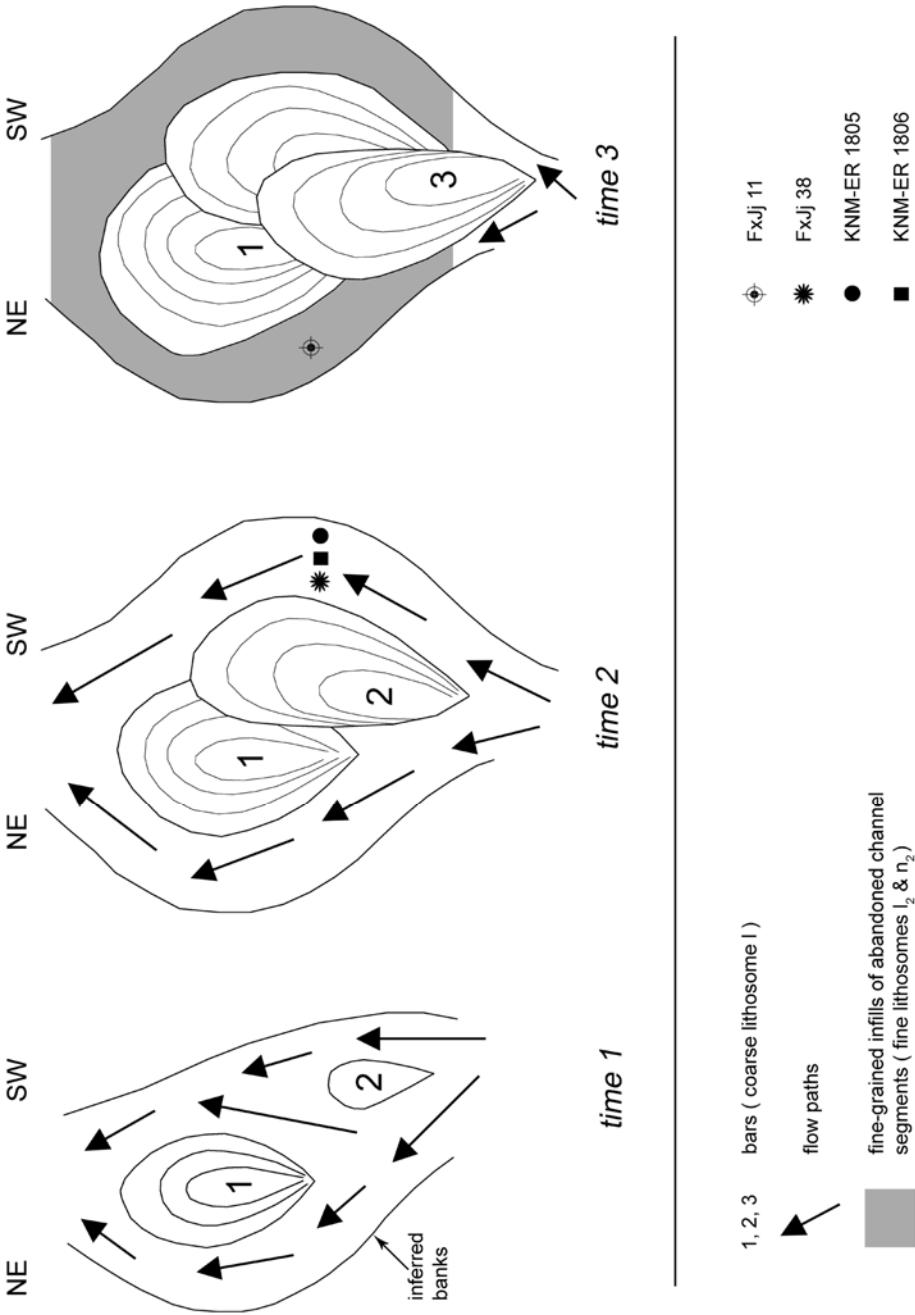
another site (e.g., Jo and Chough, 2001 their Fig. 14). Such a situation at some point would have initiated the fine-grained infilling of the northeast and southwest portions of the braided system. Evidence supporting this interpretation comes from the fine lithosomes l_2 and n_2 on top of the northeast and southwest parts of lithosome l (Fig. 27). Many contacts between lithosome l and the fine lithosomes display a sharp upward transition from gravel to mudstone (Figs. 22, 24, 27). The bases of the fine lithosomes have concave-up shapes that resemble basal, channel-form geometries (Fig. 27). Lithosomes l_2 and n_2 may therefore each reflect the deposition of fine sediments on lateral sides of a large, mid-channel braid bar. Deposition occurred within abandoned channel segments of the braided system represented by the coarse lithosome l (e.g., Fig. 28).

Architectural components (e.g., lithosomes) may only represent terminal-stage characteristics because rivers undergo constant reorganization throughout any given period (Miall, 1996). Accordingly, the braided-river interpretations for coarse lithosome l might be only indicative of how the system was just prior to abandonment. For example, braided rivers commonly evolve from straight or meandering rivers through chute-cutoff events (Bridge et al., 1986; Bristow and Best, 1993; Lunt and Bridge, 2004). Such a circumstance occurs when the bank side of a bank-attached bar (e.g., point bar) is severed from the bank by channel erosion. This results in two separate channels coursing around the bar, and the consequent formation of a mid-channel or braid bar. Coarse lithosome l is ultimately interpreted as a braided-river deposit. But the extent to which this classification characterizes its full developmental history is unknown at present.

3.6.9. Coarse lithosome m

Description: Lithosome m (Table 5) comprises coarse lithofacies associations LA1, LA2, LA3 and LA4. It is a completely preserved channel body, almost entirely encased by fine-grained strata (Fig. 11). The basal boundary is defined by erosive surface m, and the upper boundary by accretionary surface o_2(C). The lithosome is a lenticular sedimentary body with a sheet-like width (~1200 m) to thickness (~5 m) ratio (e.g., Friend et al., 1979).

Basally, the lithosome has near-planar erosive contours at the m surface. At either lateral margin of the lithosome however, the m surface traces up and attaches to accretionary surface o_2(C). These upward-trending contours give each lateral margin a concave-up, channel-form shape that exhibits erosive relief equal to the overall thickness of the lithosome (Fig. 29).

A distinctive series of deposits form the uppermost levels of coarse lithosome m, especially along its medial and southwest portions. These are stacked, tabular sets of planar cross-stratified sands of lithofacies association LA3 (Fig. 22). Each set emanates from the SW margin of the lithosome and extends to the northeast for lateral distances on the order of 10^1 to 10^2 m. At their northeast extents, the sets terminate along accretionary surface o_2(C). These terminal extents are characterized by inclined geometries that take shape from slip faces of planar cross-strata (Fig. 29).

Interpretation: Coarse lithosome m is interpreted as the deposit of a fluvial channel with well-defined banks and bar growth in directions subnormal/normal

Fig. 29: Geometries, boundary surfaces and lithologies for coarse lithosome m; hiatal surfaces o_2(NE) and o_2(SW) included for reference (modified from Frank, 1976).   See Figs. 9 and 11 for key to HJF logs, tephrochronological context, and placement within the overall fluvial architectural model.   CJL04 logs (mapped in Fig. 8 and illustrated in Fig. 22.) provide details on constituent facies.   Coarse lithosome m is bounded by erosive surface m and accretionary surface o_2(C).   It is a lenticular channel body with lateral-most margins interpreted as opposing cut (NE) and accretionary (SW) banks.   Successive inclined geometries on surface o_2 (C) near HJF-31, HJF-32, CJL04-130-22 and HJF-37 represent slip faces for a series of elongated, piggybacked, planar cross-stratified units that begin at the accretionary bank. These units are interpreted as the components of a bar complex growing in directions normal/oblique (generally SW to NE) to the main flow axis of the channel, which suggests the lithosome indicates a meandering reach with a point bar.   Note double inclined margins (at HJF-29) for a small bar and/or channel lag formed by flows diverted around the leading edge of the point bar.   Lowercase roman numerals (i-vii) correspond to features in Fig. 30.
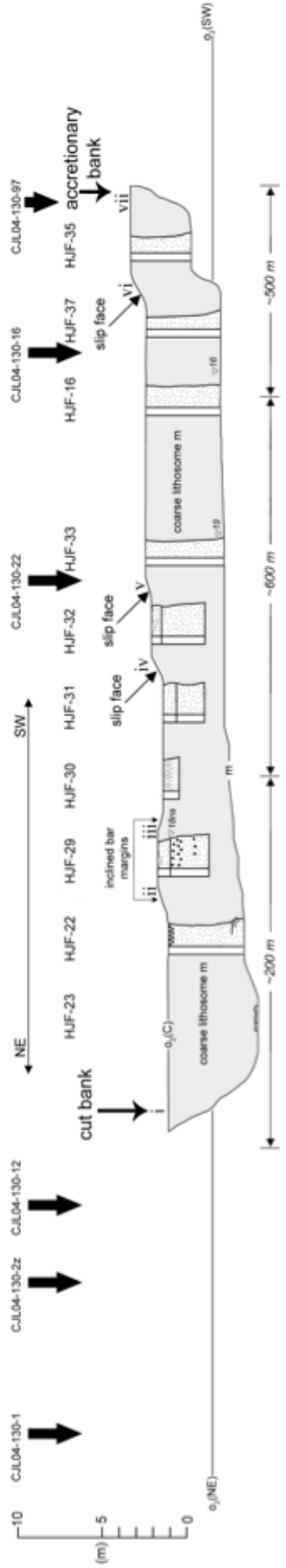
relative to the main paleo-flow axis. Such contentions are based on the contours of the boundary surfaces, sedimentary structures, lithofacies distributions, and overall geometry of the lithosome.

Orientations of the concave-up, lateral-most margins of the lithosome (Figs. 11, 29) suggest the main paleo-flow axis for the channel was generally perpendicular to the overall NE/SW trend of the outcrops. Stacked, planar cross-stratified sets of lithofacies association LA3 (Fig. 22) are interpreted to represent multiple accretionary components of a large barform that propagated across the channel axis. The accretion direction appears to have been mainly toward the northeast, as indicated by the step-like descent and thinning of the sets from southwest to northeast (cf., Carboniferous fluvial bars of Haszeldine, 1983; Kirk, 1983). Moreover, preserved slip faces of the cross-strata generally face toward the northeast (Fig. 29), also implying the sets extend from the southwest and the barform propagated in a northeast direction. The barform likely was laterally opposed by a channelized flow that, as the barform grew in a SW-NE direction, progressively migrated to the northeast. This inference is supported by the nearly horizontal basal contour for coarse lithosome m, which suggests flow processes scoured the channel bed in a lateral—rather than downward—fashion. However, the channel was probably incised and deeper at the northeast, since the m surface dips toward this direction and has concave-up erosive relief of almost 5 m (Fig. 29).

Collectively, the evidence suggests the lithosome reflects a cross-section of a somewhat sinuous channel bend, generated by bar growth along an

accretionary bank and erosion into floodplains at an opposing cut bank (Fig. 30). These interpreted aspects, in addition to the lithosome's near-complete encasement in fine-grained strata and lenticular-like geometry, are consistent with established characteristics (e.g., Table 8.3 of Miall, 1996) of a meandering river. Accordingly, lithosome m is ultimately considered to represent the product of a meandering-style channel with point-bar-like, lateral-accretionary units.

3.6.10. Fine lithosomes: description

Fine lithosomes j_3, l_2, and n_2 (Table 5) have maximum thicknesses of approximately 5 m and lateral extents of 500-1000 m. Fine lithosome j_3 overlies coarse lithosome j_2; fine lithosomes l_2 and n_2 overlie coarse lithosome l (Fig. 11).

The fine lithosomes are based at accretionary surfaces j_3, l_2, and n_2. They have concavo-convex to nearly flat lying bases that follow the paleotopography of the tops of underlying coarse lithosomes (Figs. 26, 27). The upper boundary for fine lithosome j_3 is defined by erosive surface l (Fig. 26). Tops for lithosomes l_2 and n_2 are primarily marked by hiatal surfaces o_2(NE) and o_2(SW), respectively, and secondarily by erosive surface m (Fig. 27).

Internally, these lithosomes are similar in composition and predominated by mudstones of fine lithofacies association LA5b (Fig. 22). Constituent fine-grained sands, tuffs, and especially the mudstones fine upward and become progressively more pedogenically altered towards the top of each lithosome. Additionally, mudstones are often overprinted with a 1-2 m thick calcic horizon of a laterally extensive (100's of m) type-III paleosol (Figs. 21, 22 and 24).

Fig. 30: Map-view model of coarse lithosome m. Lowercase roman numerals are landmarks in Fig. 29 and follow a NE-SW strike section through the lithosome. Numeral i: cut-bank reflected by concave-up geometry of erosive surface m at NE margin of the lithosome. Numerals ii and iii: opposing margins for sandy gravel bar inferred from geometry of accretionary surface $o_2(C)$. Numerals iv-vi: bar crests of individual growth components represented by terminal slip faces for planar cross-stratified units preserved beneath accretionary surface $o_2(C)$. Numeral vii: accretionary bank interpreted through the growth direction of bar components and opposing cut bank.

NORTH

CUT BANK

channel margin

sandy gravel bar

FxJj 18 GL

FxJj 18 NS

i

ii

iii

iv

v

vi

vii

channel-floor sites buried under bar components

FxJj 19

FxJj 16

bar crests

BANK

ACCRETIONARY
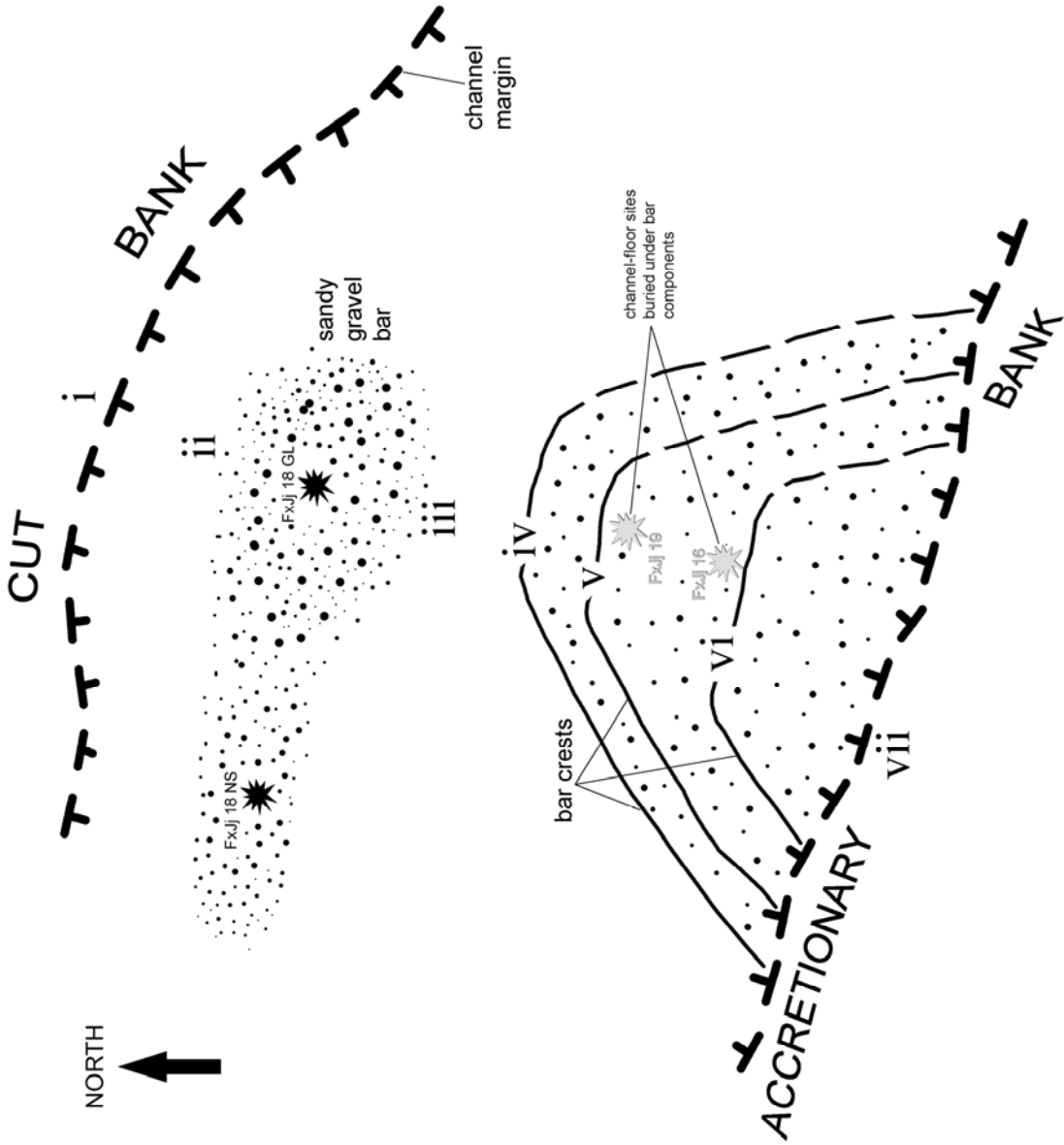
3.6.11. Fine lithosomes: interpretation

Lithofacies evidence indicates that the deposition of the fine lithosomes was mostly a consequence of suspension sedimentation. These lithosomes form the upper parts of fining-upward sequences and directly overlie the channel deposits of coarse lithosomes (Figs. 22, 26, 27). This suggests genetic relationships between the two. Basal geometries of the fine lithosomes are interpreted to reflect preexisting channel topography. The formation of the concave-up basal contours is interpreted as being related to deposition within areas confined by channel margins (e.g., Davies-Vollum and Wing, 1998; Kraus and Davies-Vollum, 2004). Such areas were probably channel segments filled with fine-grained detritus throughout or following episodes of abandonment. In contrast, convex-up geometries are interpreted as basal parts of the fine lithosomes that accumulated on bar tops/sides during low-stage flows or waning phases of floods (e.g., Perez-Arlucea et al., 2000; Jones et al., 2001). However, deposition of the fine lithosomes became progressively decoupled from channel influences. This is evident from the lower flow energies and lack of channel-form contours indicated by the upward increases in finer grain sizes, pedogenic features, and tabular geometries. Uppermost levels of the fine lithosomes may therefore represent overbank areas (e.g., interfluves, floodplains or floodbasins) rather than the within-channel settings interpreted for the lower levels.

4. Sedimentology and tephrostratigraphy of deposits from northern Area 133

4.1. Introduction

The archaeological record of Koobi Fora provides behavioral evidence important for interpreting Plio-Pleistocene tool development (Isaac and Harris, 1976; Toth, 1985), dietary patterns (Bunn, 1981, 1994), and social factors of brain-size evolution for *Homo* (Isaac, 1978, 1984). Stone-tool artifacts within the Koobi Fora Formation occur throughout a stratigraphic interval dated to about 1.9-1.4 Ma, and are contemporaneous with the fossils of several hominin species from at least two genera (Leakey et al., 1978; Brown and Feibel, 1985, 1986; Feibel et al., 1989; Wood, 1991; Isaac and Behrensmeyer, 1997; McDougall and Brown, 2006). Rather than attempting to identify the toolmakers, however, most current research with this archaeological record often focuses on understanding production techniques, strategies of raw-material procurement, and ecological constraints of tool use (Rogers et al., 1994; Ludwig and Harris, 1998; Braun et al., 2008). This requires complementary geological studies that emphasize the construction of paleoenvironmental frameworks and discrete spatial-temporal contexts. Yet, despite a rich and integrative history of research, the geoarchaeology of several areas of Koobi Fora remains underexplored. One notably location is the backslopes of the northern Karari Escarpment, formally known as Area 133. Documented from here are a number of surface sites (i.e., not *in situ*) of stone tools, in addition to a series of tuffaceous sedimentary successions of the Koobi Fora Formation (Harris, 1997; Harris et al., 1997; Isaac and Behrensmeyer, 1997). But there are few detailed reports that reconstruct

environments of deposition from the sediments, establish tephrochronological correlations with the formation, and speculate on the possible geological contexts for the surface archaeological materials.

This chapter represents a contribution towards refining the paleoenvironmental, temporal, and spatial contexts of the archaeology from the northern Karari, and reports on sedimentological and stratigraphic studies from the northern part of Area 133. Northern Area 133 lies just to the east of the better-studied Area 130 (Fig. 3), which preserves *Homo* and *Paranthropus* fossils (Leakey et al., 1978; Wood, 1991), as well as an abundance of stone-tool sites critical for interpreting the transition from the Oldowan to the Developed Oldowan at Koobi Fora (Isaac et al., 1997). Since northern Area 133 is comparatively proximal to possible raw-material sources at the basin margin (Lepre, 2001; Braun et al., 2008), and presumed to have been the location of a relatively arid upland setting (Feibel et al., 1991; Rogers and Sorkowitz, 1992), its geology may provide further insights into the data from Area 130. Moreover, the sedimentological and stratigraphic contributions presented herein hopefully will stimulate renewed research, and provide an impetus for excavation studies on the previously documented surface sites from northern Area 133.

The following chapter deals with the sedimentological descriptions and interpretations for the northern Area 133 deposits. It additionally provides tephrochronological results based on electron-microprobe analysis of glass separates from tuffaceous outcrops. This information is later used (chapter 7) to

interpret possible *in-situ* geological situations for surface archaeological materials previously found lying on the examined outcrops.

4.2. Study area, materials and methods

Northern Area 133 (NA 133) is informally defined here as the portion of Area 133 north of the road to Derati (Fig. 31). It is located about 25 km inland (east) of Lake Turkana and no more than 5 km south or southwest of the volcanic highlands that rim the northeast basin margin (Fig. 3). The area lies 500-550 m above sea level and is a headwater catchment for a series of 6-7 km long, southeast-trending ephemeral streams. These small ephemeral streams incise through the basin fill and expose sections up to 5 m thick. Exposure is best developed in proximal or medial stream reaches, where sections usually attain thicknesses of 1-3 m and lengths of 5-100 m. At a few locations, the outcrops show tilting between 8° and 32°, but commonly they are nearly flat lying.

In NA 133, Isaac and Harris (1976, 1978) and Harris (1997) documented seven sites with stone-tool occurrences on outcrop surfaces and excavated one site with *in-situ* stone tools (Fig. 31). The *in-situ* site is FxJj 23 and derives from sediments of the Koobi Fora Formation's Okote Member (Harris et al., 1997) dated to about 1.6-1.4 Ma (Brown and Feibel, 1986; McDougall and Brown, 2006). This present study focuses on surface sites FxJj 24, FxJj 25, FxJj 26, FxJj 27, FxJj 28, FxJj 29, and FxJj 53. These were relocated using previously reported map data (Isaac and Harris, 1976, 1978; Harris, 1997); and their locations were rerecorded using a handheld GPS device (see Appendix 2).

Fig. 31: Location map of examined outcrops and geographic landmarks in northern Area 133. Outcrops are indicated by the positions of the 17 lithostratigraphic logs. Placement of archaeological sites is after Harris (1997) and Isaac and Isaac (1997).

FxJj 28 ✳ Archaeological site

133-28 ⚡ Lithostratigraphic log

▬ ▬ ▬ Area boundary

133-5: 4°10.431'N, 36°27.825'E   133-6: 4°10.621'N, 36°27.724'E
133-11: 4°10.692'N, 36°27.190'E   133-22: 4°10.589'N, 36°27.342'E
133-26: 4°10.006'N, 36°27.983'E   133-28: 4°10.537'N, 36°27.436'E
133-34: 4°10.437'N, 36°27.708'E

FxJj 26
133-11
FxJj 28
133-22
133-28
FxJj 25
133-6
FxJj 24
133-34
133-5
FxJj 23

133-32
133-26

FxJj 29

FxJj 53
133-51
FxJj 27
133-50

133-47
133-43
133-41, 133-42
133-36
133-37
133-35

N

NORTH STREAM

SOUTH STREAM

road to Derati

300m   500m
1000m

133-32: 4°10.900 N, 36° 26.441'E
133-35: 4°9.013'N, 36°27.644'E
133-36: 4°9.397'N, 36°27.158'E   133-37: 4°9.471'N, 36°27.001'E
133-41: 4°9.453'N, 36°26.932'E   133-42: 4°9.449'N, 36°26.931'E
133-43: 4°9.463'N, 36°26.902'E   133-47: 4°9.579'N, 36°26.631'E
133-50: 4°9.818'N, 36°26.422'E   133-51: 4°9.831'N, 36°26.389'E

Sediments exposed in NA 133 consist of tuffs, mudstones, loosely consolidated quartzo-feldspathic sands and basalt gravels, in addition to conglomerates characterized by basalt clasts in a matrix of calcium carbonate. Typically, the gravels and conglomerates overlie the tuffs, mudstones, and sands. These coarse-grained deposits mantle much of the modern landscape and often form the topmost portions of outcrops. Field examinations and interpretations of all of these sediments were conducted on the outcrops found at the gullies and banks of two northwest-southeast trending ephemeral streams (Fig. 31). Characterizing the sedimentary outcrops involved recording more than 50 lithostratigraphic logs. However, many of these could not be correlated to others because of the discontinuous nature of outcrops and paucity of tuffs. Therefore, only 17 logs are presented in this study (Figs. 31-38) since these best exemplify the diagnostic aspects of the outcrops and/or preserve tuffs important for geochemical analysis and tephrostratigraphic correlation. Ancient depositional environments and paleogeographic settings were reconstructed from detailed sedimentological studies carried out at six key locations. Depositional aspects were defined and interpreted from lithology, grain size, sorting, primary sedimentary structures, bedding morphologies, and vertical-lateral stratigraphic relationships (e.g., Walker, 1984; Reading, 1986; Miall, 1996). Implications from the sedimentary studies were supplemented with paleosol data. The criteria used for the field recognition and interpretation of the ancient soils followed the established guidelines discussed in Mack et al. (1993) and Retallack (2001).

Fig. 32: Representative lithostratigraphic logs documenting sedimentological and other features for outcrops of northern Area 133. Map-view locations for logs are depicted in Fig. 31. Tuff samples for electron-microprobe analyses derive from 133-11 and 133-34 at the north stream locality, and 133-47 and 133-50 from the south stream locality. See discussion in text for descriptions of collection levels.

NORTH STREAM

133-11 · 133-22 · 133-6 · 133-34 · 133-5 · 133-26

tuff sample BS1202

tuff sample BS702

SOUTH STREAM

133-50 · 133-47 · 133-37 · 133-36 · 133-35

tuff sample BS402

tuff sample BS602

(m) 5 · 4 · 3 · 2 · 1 · 0

slickensides

carbonate rhizoliths

carbonate nodules

volcaniclastic

mudstone

cross-stratified gravel/conglomerate

sand ← gravel

gravel
pebble
granule
very coarse
coarse
medium
fine
very fine
silt
clay
sand

Over the past several decades, the separation of glass fractions from tuffs and accompanying analyses for component trace elements has been instrumental in correlating outcrops at disparate geographic locations and refining the Plio-Pleistocene geology of the Turkana Basin and adjacent areas (Cerling and Brown, 1982; Brown and Feibel, 1986; Feibel and Brown, 1993; Feibel et al., 1989; Brown et al., 2006). This is because, during the Plio-Pleistocene, multiple explosive silicic eruptions occurred in northern Kenya and southern Ethiopia, and scattered ash over wide sectors, sometimes as far as the Indian Ocean (Sarna-Wojcicki et al., 1985; WoldeGabriel et al., 1992; Brown et al., 1992). Although the source centers for most of the Plio-Pleistocene ashes are yet to be defined, the composition of the volcanic glass shards potentially represents a unique chemical signature of an erupting magma. Moreover, many of the ashes were widely distributed from pyroclastic, aeolian or aqueous processes, and have distinctive eruptive ages, providing local and regional isochronous stratigraphic markers (Cerling and Brown, 1982; McDougall, 1985; Feibel et al., 1989; Katoh et al., 2000; WoldeGabriel et al., 2005; Brown et al., 2006; McDougall and Brown, 2006). Accordingly, selected samples of glass fractions separated from the tuffs collected from the NA 133 outcrops were subjected to electron microprobe studies. The geochemical results were used to improve the stratigraphy of NA 133 through assessing intra-area correlations and potential correlations with known tuffs of the Turkana Basin and adjacent locations.

4.3. Sedimentological descriptions and interpretations

The sedimentology is described and interpreted below from six key localities. These six provide the most insights to the NA 133 outcrops, and are instrumental for understanding the potential contexts of the surface archaeological occurrences. Each of the localities is named after the lithostratigraphic log that chiefly represents the features of the exposed deposits.

4.3.1. Locality 133-22

Description: Basalt gravels dominate the deposits at locality 133-22 (log 133-22 in Figs. 31, 32). These coarse clastics comprise well-rounded pebbles that have diameters of less than 10 cm and are poorly-moderately sorted by size. The deposits are arranged into 3-5 m long by 1.5 m thick units that have planar cross-stratifications with foresets at ~50 cm thick. Each foreset can be recognized by increases in clast sizes that define foreset boundaries, and from elongated clasts that have long axes arranged parallel to foreset boundaries. Additionally, foreset boundaries are sometimes outlined by carbonate accumulations up to a couple centimeters thick. Basal contacts of the cross-stratified units are sharply erosive and show nearly horizontal contours or concave-up relief of a decimeter or two.

Horizontally stratified sets of massive gravel, 25-50 cm thick, overlie the cross-stratified gravels. This vertical changeover is ether diffuse or at more distinctive contacts marked by an increase in grain size.

Interpretation: Planar cross-stratified gravel suggests the deposition of bars in channels with gravel beds (Eynon and Walker 1974; Boothroyd and Ashley 1975; Gustavson, 1978). They may have been side, transverse, diagonal, or point bars (Allen et al., 1983). A conservative interpretation is the gravel deposits indicate downstream accreting bars with avalanche slip faces (Eynon and Walker 1974; Steel and Thompson, 1983; Rust, 1984).

Sets of horizontally stratified massive gravel on top of the planar cross-stratified gravel are interpreted as indicating vertical aggradation on bar tops (Eynon and Walker 1974). Aggradation probably occurred when bars filled the channels and a shallower flow depth was established.

4.3.2. Locality 133-26

Description: Sediments at this locality (log 133-26 in Figs. 31, 32) consist of horizontal sets of massive gravel or conglomerate, interbedded with sand and siltstones. Cementation of the conglomerates is carbonate, which may form laterally persistent lenticular/tabular beds that are cm's to a few dm's thick. Deposits similar to the gravels and conglomerates at 133-26 are exposed at the sections recorded by logs 133-5, -22, -35, -36, -37, -47, and -50.

Coarse sediments at locality 133-26 include basalt granules, pebbles, cobbles, and small boulders. Most clasts are sub-round to round, and elongate to sub-spherical. These clasts compose 10-100 cm thick sets that extend across the outcrop for distances up to 10 m. Typically, there is little organization to the fabric of each set, but normal or inverse grading occurs. Angular chunks of

carbonate (embedded with basalt clasts), siltstone, and tuff—the size of small boulders and cobbles—are occasionally found among the gravels and conglomerates.

Gravel and conglomerate sets are interstratified with tabular to lens-shaped units of massive sandy siltstones and silty sands. These finer deposits are overprinted with strongly developed but sparse greenish-gray mottles. They also preserve a small/moderate amount of pebble-sized carbonate nodules, and carbonate rhizoliths that are 1-5 cm long by about a centimeter in diameter.

Interpretation: The horizontal sets of massive gravel/conglomerate are interpreted to be the products of high-energy, short-lived flows and bedload deposition. This is based on the large grain sizes, the massive fabrics, and the poor clast organization found in the sets. Flows were probably shallow since individual set thicknesses are up to 100 cm. Moreover, the large angular hunks of siltstone, tuff, and carbonate embedded with basalt clasts imply rapid deposition from a flow of limited duration. Abrasion would have rounded or disintegrated these soft materials if they had long residence times in flows or were readily exposed on the flow surface. The carbonate matrix of the conglomerate likely formed in a shallow vadose zone through infiltration and evaporation of moisture (Mack et al., 2000).

The features overprinted on the sands/siltstones interbedded with the basalt clasts are interpreted to indicate alternating wet-dry conditions. Greenish-gray mottles on these fine-grained sediments reflect reducing conditions in a waterlogged environment. Contrastingly, the carbonate nodules represent dry

episodes and net deficits in effect moisture. These features are considered as evidence of pedogenesis occurring after deposition (Mack et al., 1993). Evidence of pedogenesis and the finer grain sizes suggest the siltstones and sands accumulated in areas with slow rates of clastic input and low-energy flows.

Horizontal sets of massive gravel/conglomerate from NA 133 resemble deposits documented from modern braided channels with gravel beds (Smith 1974; Boothroyd and Ashley 1975; Rust 1975; Miall, 1977). Sedimentary environments may have included channels with longitudinal gravel bars. Such bars can form by flow expansions and have high rates of downstream accretion as compared to vertical aggradation (Leopold and Wolman 1957; Hein and Walker 1977). However, because channel margins are not observable (poor exposure), it is possible that deposition may have resulted from un-channelized sheet flows, like those found in alluvial fan settings (Bull, 1972; Blair, 1987; Stanistreet and McCarthy, 1993; Blair and McPherson, 1994).

Sandy siltstones and silty sands interstratified with the gravel/conglomerate may represent falling-stage and low-flow stage sediments deposited on bar tops (Allen et al., 1983). They are also perhaps indicative of floodplains areas removed from the active channel setting.

4.3.3. Locality 133-43

Description: Exposed at locality 133-43 are massive sets of basalt gravel/conglomerate overlain by carbonaceous mudstone (Fig. 34). This

succession attains an apparent thickness of about 2 m, with the lower ≤30 cm comprising coarse clastics.

Basalt clasts at locality 133-43 mostly consist of granules and pebbles. They are rounded and poorly sorted by size. The lower 20 cm is gravel; vertically however, consolidation gradually improves, which culminates with the upper 10 cm being a carbonate-cemented conglomerate. Overlying the conglomeratic portion are massive mudstones, with the transition between the two occurring over a 1-10 cm thick diffuse contact.

Mudstones measure 120-170 cm thick and show a coarsening-upward trend. Basal levels are composed from a dark brown (10YR 3/3) and very pale brown (10YR 7/3) claystone with a fraction of very fine sand and grayish (5Y 6/1) mottles. This claystone has a thickness of about 50 cm and contains a moderate amount of carbonate rhizoliths. Rhizoliths have vertical, sub-vertical and parallel orientations. At some places in the claystone, they densely intersect to form 5-15 cm thick, mat-like structures. Other areas of the claystone have slickensides, several of which are lined with carbonate. Above this claystone is a pale yellow (2.5YR 7/3) siltstone with fractions of fine through coarse sand. Most of the siltstone is massive, but some coarser portions show parallel laminae. Carbonate rhizoliths like those in the claystone are also present. Overprinted on the contact, or rather marking the boundary between the claystone and siltstone is a horizon of pebble- to cobble-sized carbonate nodules that interlock to form a tabular bed (10-15 cm thick). Many nodules are elongated parallel to bedding, perhaps indicating precipitation near the water table (e.g., Pimentel et al., 1996).

Fig. 33: Key to symbols in figures 34, 37 and 38.
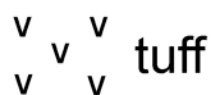
	overburden	v v v v v	tuff
	carbonate rhizoliths		carbonate nodules
	clay		silt
	sand		gravel

Fig. 34: Panel cartoon for locality designated as 133-43. Key to symbols found in Fig. 33. See Fig. 31 for geographic location for logs 133-41, 133-42 and 133-43.
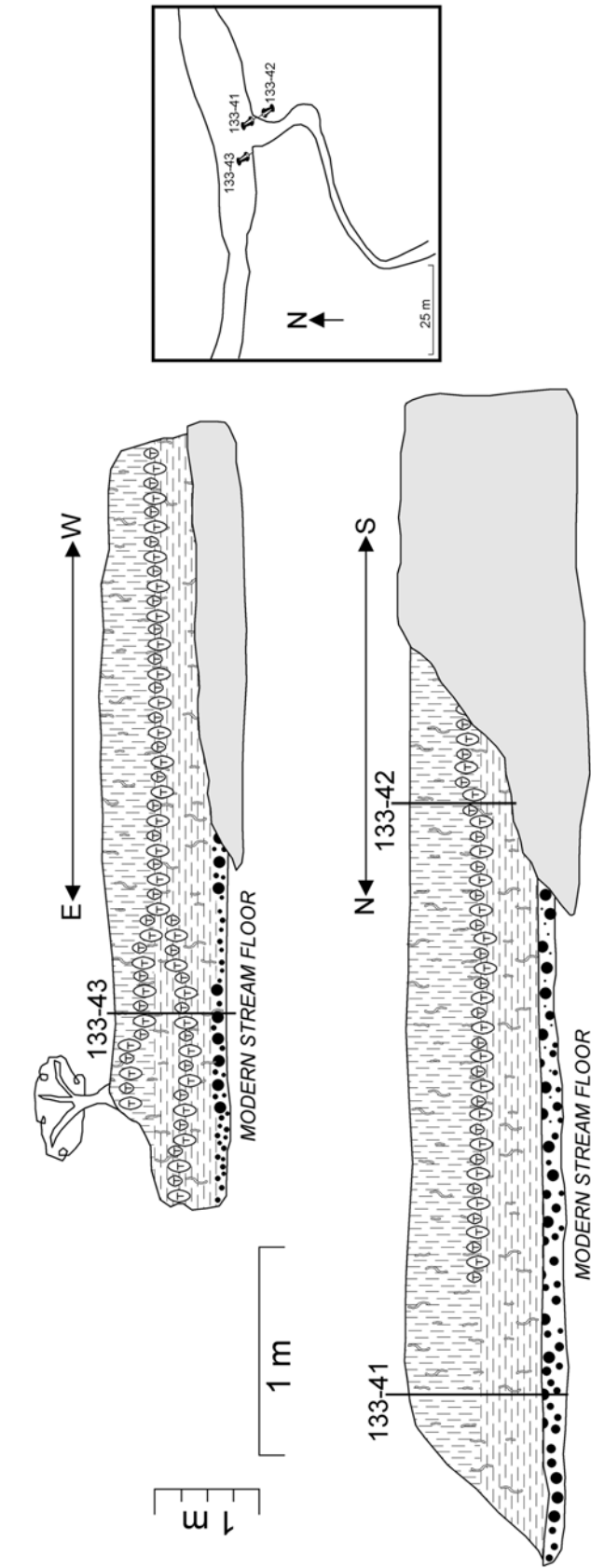
Interpretation: Massive basalt clasts at this locality are interpreted as the result of rapid bedload deposition from high-velocity flows. They likely represent the final stages of high-energy deposition, since the deposits directly above are claystones/siltstones. These finer sediments indicate lower energy environments and probably suspension sedimentation. Slickensides, color mottles and carbonate accumulations overprinted on the mudstones suggest wet-dry moisture changes and pedogenic modification (Mack et al., 1993). Some of the carbonate accumulations may have shallow groundwater origins, such as the ones with rhizoliths arranged into mat-like structures (Mack et al., 2000) and nodules oriented parallel to bedding (Pimentel et al., 1996).

Basalt clasts at 133-43 are generally smaller than the cross-stratified gravel (locality 133-22) and the horizontal sets of massive gravel/conglomerate locally interbedded with sandy-silty fines (locality 133-26). The decreased clast size could be indicative of a comparatively distal depositional setting. Finer clast sizes might have resulted from enhanced abrasive/chemical breakdown of the basalt due to a long transport distance from a volcanic source area (Davies et al., 1978; Frostick and Reid 1980). Alternatively, the smallish clast sizes potentially represent the upper sets of a normally graded succession. Deposition may have been caused by progressively slowing flow velocities of a flood, or shallow flows produced over a vertically accreting bar (Mack and Leeder, 1999). A third prospect is that the entire succession formed from overbank flooding, suspension sedimentation, and pedogenesis in floodplain settings. These settings were

perhaps lateral to high-energy areas predominated by large channel and sheet-flood environments (e.g., Steel, 1974).

4.3.4. Locality 133-28

Description: Deposits at locality 133-28 consist of mudstones erosively overlain by a tuff and pumice complex. This succession extends laterally for over 100 m, from log 133-11 to 133-28 in Figs. 31 and 32. The lower mudstones have an exposed thickness of up to ~2 m, whereas the upper volcaniclastics are about 4 m thick (Figs. 35, 36).

The mudstones vary in thickness at 75-200 cm and begin with pale yellowish orange (10YR 8/6), moderate yellowish brown (10YR 5/4) or grayish orange (10YR 7/4) sandy siltstones that are massive. These fine upward to grayish orange (10YR 7/4) or pale brown (5YR 5/2) siltstones with some laminations. Locally apparent within all of the mudstones are carbonates, which become more numerous and larger up-section. Carbonate forms include vertically and sub-vertically orientated rhizoliths (1-3 cm diameter by 3-15 cm long) and spherical nodules that have diameters of 1-10 cm. At some places the upward increase in carbonate culminates with the formation of a ~20 cm thick horizon of interlocking nodular forms.

All lower mudstones are erosively overlain by a volcaniclastic complex, which has a basal surface with both concave-up shapes (2-3 m of relief) and nearly horizontal contours. A series of smaller internal erosive surfaces subdivide the complex.

Fig. 35: Photo of locality 133-28 (map location in Fig. 31). Note digging tool beneath circled number one for scale (40 cm). Tuff sample for electron-microprobe analysis collected from lens with ripple-drift structures, as indicated by the "X". Circled numbers are major erosive boundary surfaces with concave-up, channel-form contours. Thinner black line above surface number two is a minor erosive surface of limited lateral extent. To the left of photo (northwest) the major surfaces merge into a single surface that can be traced to log 133-11 (map location in Fig. 31), where it also marks a contact between lower sandy silts and upper volcaniclastics (Fig. 32). Fig. 36 is to the immediate right (southeast), just outside the view of this photo.

ripple-drift structures

tuff sample
×—BS202

sandy silts
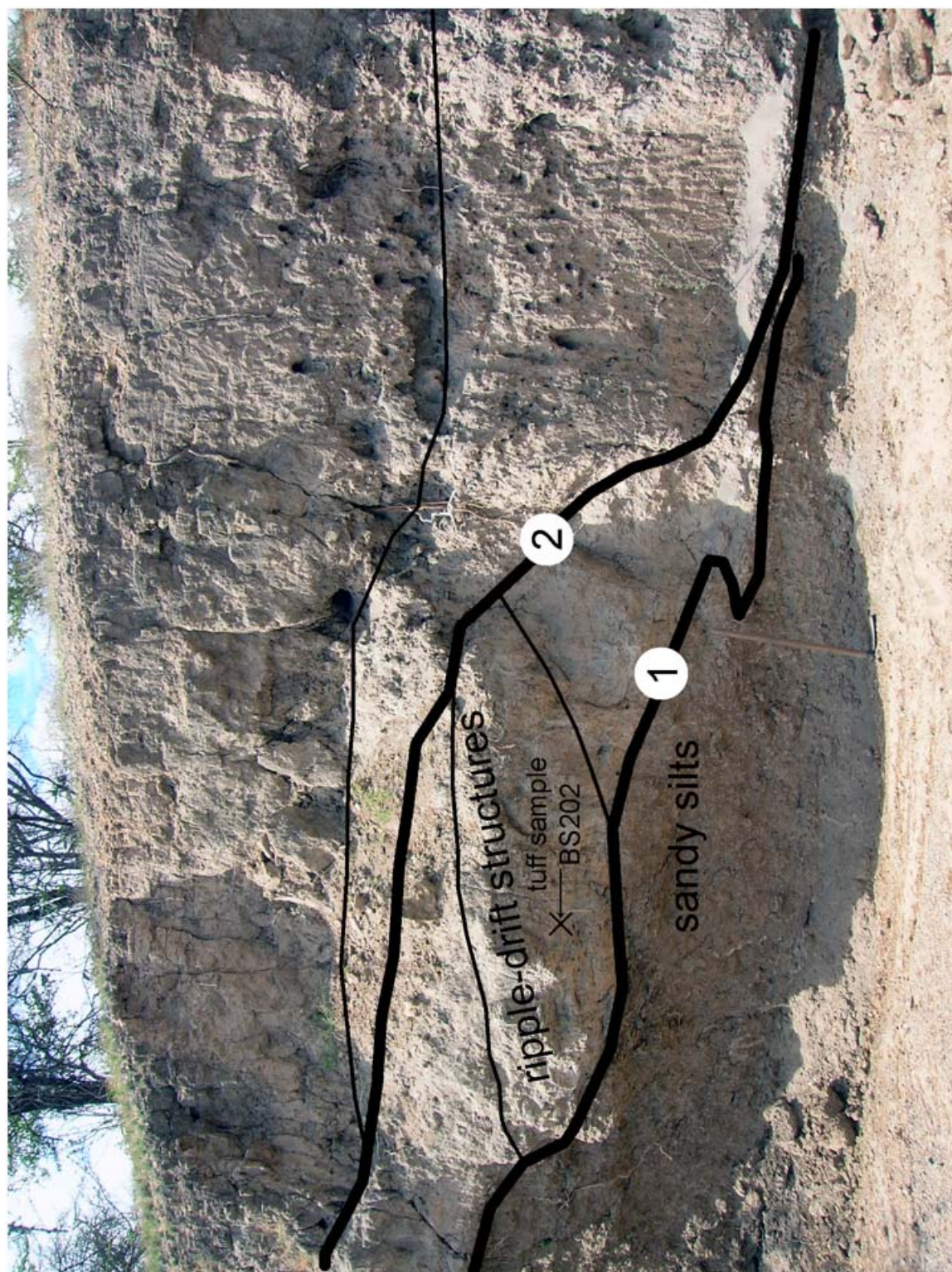
Fig. 36: Alternate photo of locality 133-28, just to the right of log 133-28 (map location in Fig. 31). Note digging tool at base of outcrop for scale (40 cm).   Black lines represent minor erosive surfaces. The second erosive surface from the top in this photo corresponds to the minor erosive surface in Fig. 35. Major erosive surface number two in Fig. 35 dives beneath this outcrop, into the subsurface. Tuff sample for electron-microprobe analysis collected from a level ~1 m up from the base of this outcrop, as indicated by "X".

tuff sample
BS302

planar cross-strata
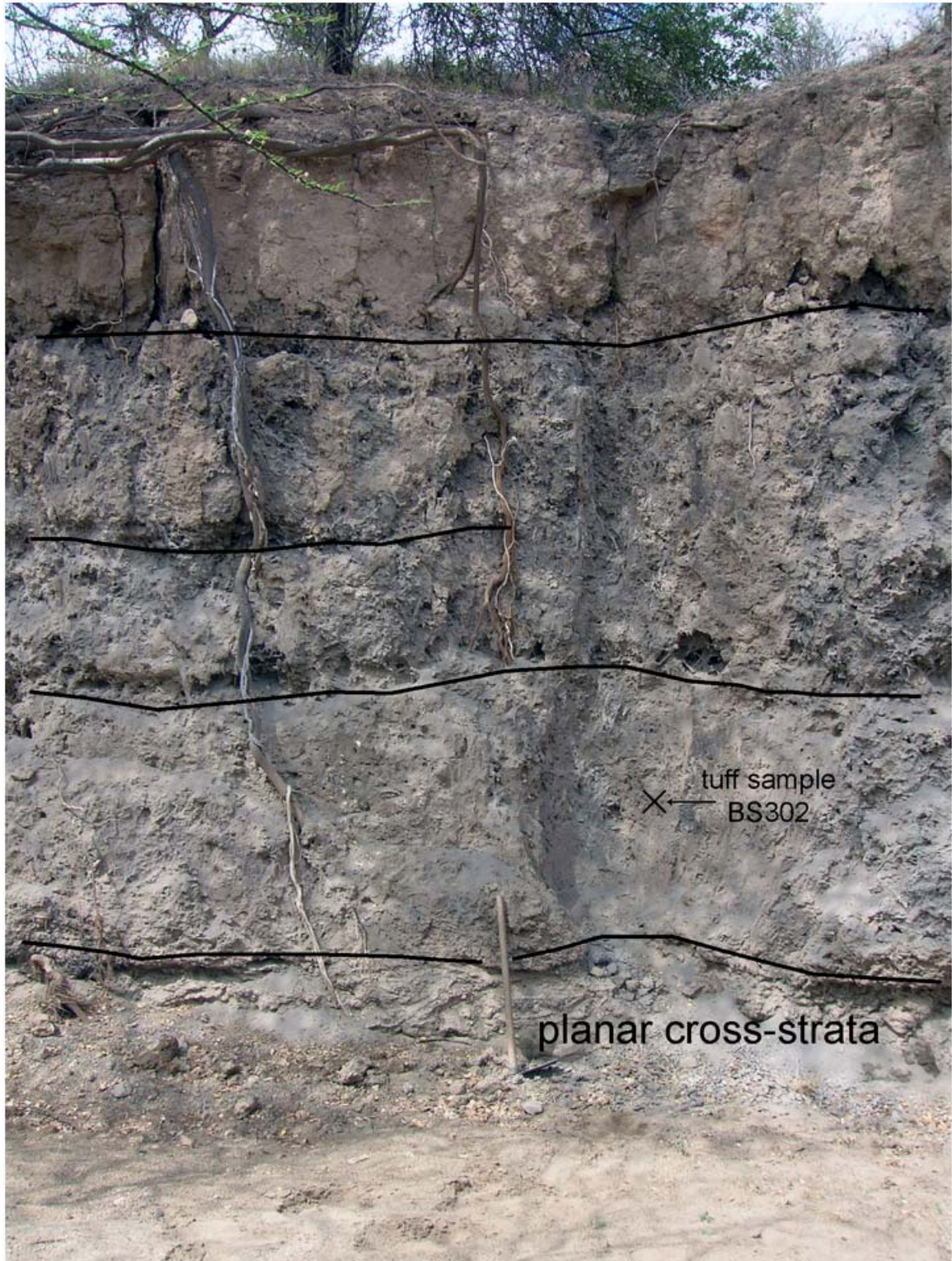
Tuffs of the volcaniclastic complex show several types of fining-upward trends. One is a 60-80 cm thick succession, which extends across exposure for several tens of meters, and is laterally adjacent to 2-3 m of channel-form relief. It is very tabular, and includes a changeover from sand-sized glass shards to silt-sized shards. The sand-sized portion is light gray (N7) or very light gray (N8), whereas the silt-sized one is pinkish gray (5YR 6/1). Both tuffs are largely massive, but also include a fair amount of horizontal laminations, wavy laminations, and thin beds (~3 cm). A sparse abundance of carbonate nodules, having 1-10 cm diameters, are also apparent.

Another fining-upward succession fills about 2-3 m of channel-from relief. It begins with a basal, ~35 cm thick lens of coarse quartzo-feldspathic sand that is planar cross-stratified. Such sands are moderately sorted by size and have angular to sub-angular grains. Compositionally they also include a small fraction of mafic minerals, some very small pebbles or granules of pumice, rounded basalt clasts, and fragments of quartzo-feldspathic minerals. Toward the top of the lens, these predominantly quartzo-feldspathic sands fine to fine/medium tuffaceous sands.

Overlying the sand lens is approximately 250 cm of loosely consolidated light gray (N6) to light olive gray (5Y 6/1) tuff. Glass shards are the size of coarse through fine sand, but larger grains predominate. Granule- to cobble-sized pumice is amply distributed throughout these tuffs. Also incorporated are unarmored clayey balls of mud. Brittle tubules, made from glass shards lightly cemented by carbonate, are also abundantly scattered about the tuffs. This

coarse interval diffusely fines upward into ~75 cm of grayish orange (10YR 7/4) massive tuffs with few pumice clasts. Above these tuffs is approximately 30 cm of similar colored but finer tuffs or tuffaceous silts, which are massive or rarely have laminations.

At one location the volcaniclastic complex includes a lenticular pinkish gray (5YR 8/1) silt-sized tuff. It is situated within the part of the complex displaying channel-from relief. Sediments within this lens-like deposit (35 cm thick by ~1 m long) have some small-scale trough cross-stratification or ripples.

Interpretation: The volcaniclastic complex is interpreted as the product of a channel system, with lateral areas where sheet flows occurred. The basal concave-up relief into finer sediment suggests channel-form geometry and incision. Infilling this concave-up relief are coarse-grained pumices and glass shards, in addition to rip-up clasts of mud, which collectively suggest high-energy flows that excavated channel floors through muddy substrates. Lateral areas with tabular, finer, massive and sometimes laminated tuffs are interpreted as wings that represent overbank sheet flows formed when the main channel flooded (cf., Friend et al., 1979). The compound nature of the complex suggests two instances of basal incision, channel filling, and sheet flooding.

The underlying volcaniclastic-free mudstones could represent a floodplain deposit. However, the fining-upward nature from silty sands to siltstones indicates they may have formed within volcaniclastic-free channels during the final phase of their abandonment. Carbonate nodules and rhizoliths associated with the mudstones suggest pedogenesis after deposition.

The abrupt vertical changeover from volcaniclastic-free mudstones to a channel complex of pumice pebbles/cobbles, coarse glass, and rip-up clasts of mud likely indicates avulsion prompted by a increased sediment supply from explosive volcanism. Conceptual models (Mackey and Bridge, 1995; Heller and Paola, 1996) demonstrate elevated rates of sediment supply can increase rates of avulsion frequency leading to avulsion into "virgin" sites. Episodic explosive volcanism has been documented as an important agent for increasing fluvial sediment supplies in other half-graben settings (e.g., Mack et al., 1996) similar to the Turkana Basin. Therefore, an increased volcaniclastic sediment supply may have raised topographic relief of channels above the floodplain, which led one to avulse into an area where the local gradient was exploitable (Mohrig et al., 2000).

4.3.5. Locality 133-51

Description: Outcrops at this locality are ≥3 m thick and comprise silty sands, sandy siltstones, and sandy-clayey siltstones (Fig. 37). Each of these lithologies typically contains a tuffaceous fraction. Primary sedimentary structures are generally lacking, but some parallel laminations do occur. The deposits are arranged as a series of alternating coarse and fine sets. Sets are 10-100 cm thick and have sheet-like or lenticular cross-sections that laterally extend for at least 10 m. Locality 133-32 (Fig. 38) has deposits similar to but finer than those found at 133-51.

Coarser sets have light yellowish brown (10YR 6/4, 2.5Y 6/3) or light reddish brown (2.5YR 7/3) colors. Constituent sands show angular to sub-

angular grain shapes and coarse-fine grain sizes. They are admixtures of quartz, feldspar, mafic minerals and tephra grains, locally with pumice pebbles.

Finer sets are colored as light reddish brown (2.5YR 6/3, 2.5YR 6/4), brown (10YR 5/3) or light yellowish brown (2.5Y 6/3), and display a fair number of light greenish gray (5GY 7/1) mottles. Other features include few arcuate slickensided fractures, and a low-moderate quantity of carbonate represented by rhizoliths (1 cm diameter, ≤5 cm length) and pebble-sized spherical nodules. Some of these carbonates form interlocking horizons up to a couple of decimeters thick. Rhizoliths in these instances are vertically, sub-vertically and horizontally orientated, and have an overall tabular mat-like structure.

Coarse and fine sets stack to form a series of fining-upward cycles, with each cycle being no more than a meter thick. Upward transitions from coarser to finer sets are diffuse or occur across sharp non-erosive contacts. The changeover from finer to coarser sets is at a nearly horizontal erosive surface, which typically shows 1-5 cm of irregular relief, and some concave-up relief up to 20 cm high and 1 m long. Locally, stacks of individual sets have simple "layer-cake" architecture. Across exposures however, the sets pinch out, bifurcate or crosscut each other, leading to complex stratigraphic relationships.

Interpretation: These deposits may reflect the product of crevasse-splay sedimentation, occurring within the proximal floodplain and/or alluvial ridge of a channel system (cf., Farrell, 1987; Smith et al., 1989; Bristow et al., 1999). Each coarse set is suggested to be a result of the initial phase of an overbank flood. A lack of primary sedimentary structures and the poor sorting of these coarse sets

Fig. 37: Panel cartoon for locality 133-51. See Fig. 31 for map location. Key to symbols in Fig. 33.
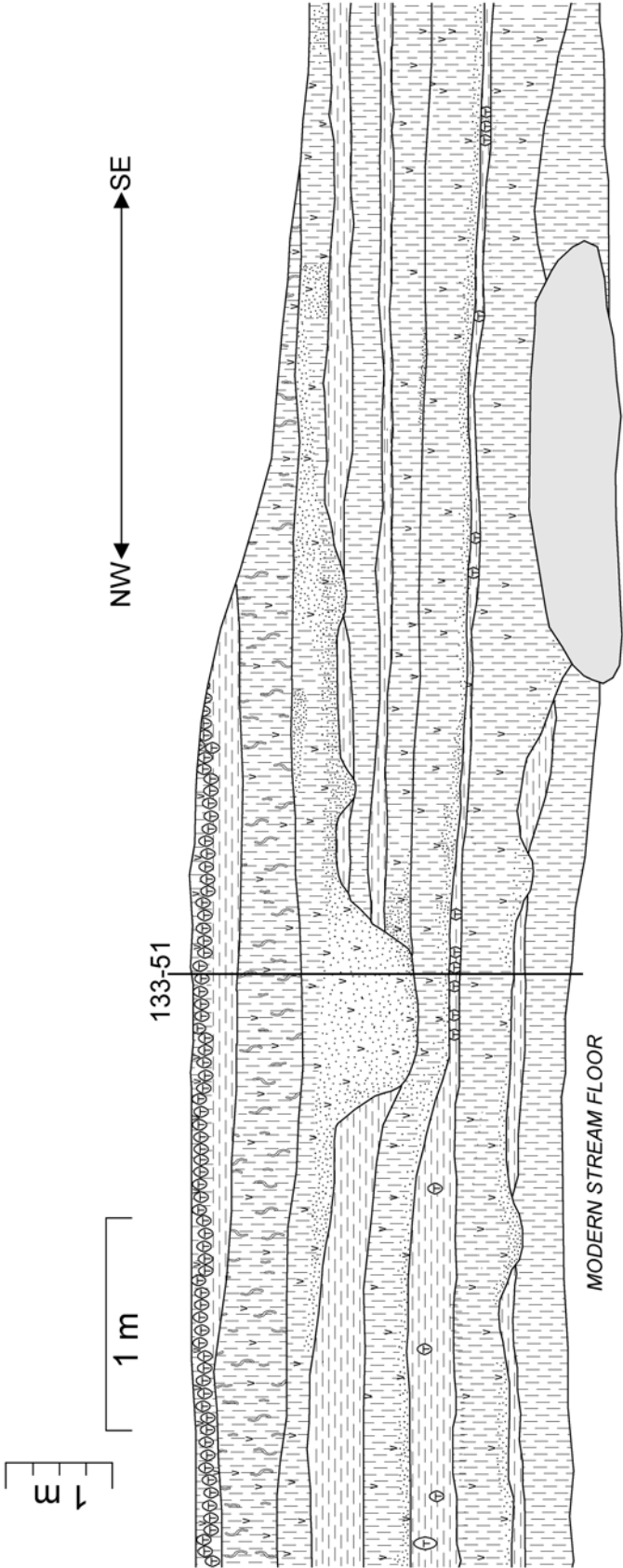
Fig. 38: Panel cartoon for locality 133-32. Map location in Fig. 31. Key to symbols in Fig. 33.
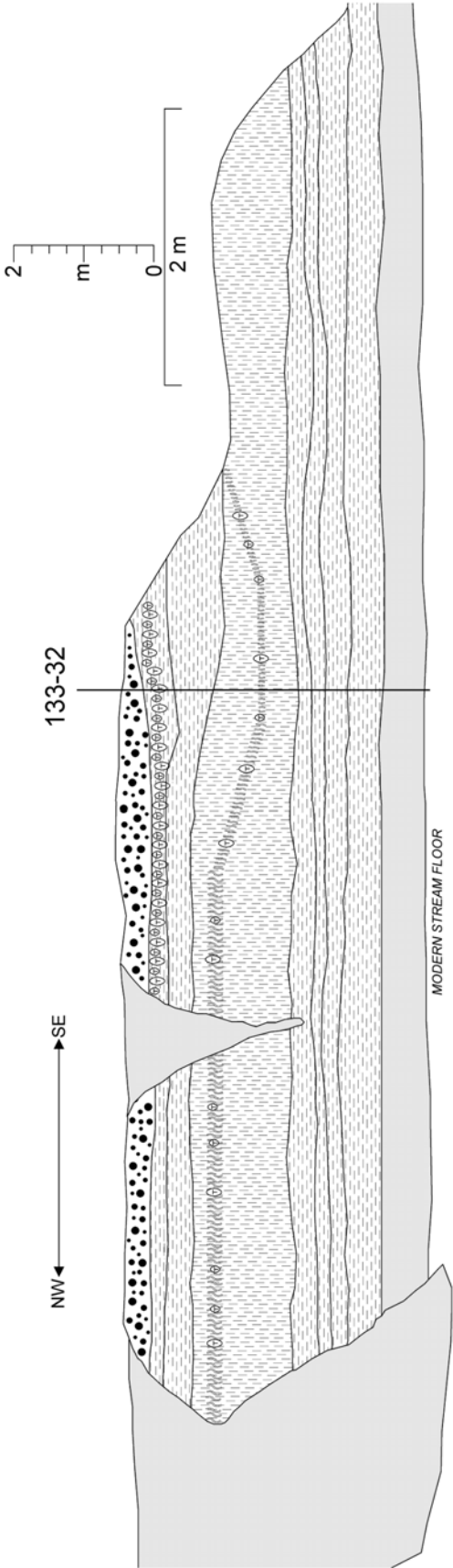
indicate rapid deposition from a sediment-laden flow. The floods were probably shallow, broad and unconfined sheet flows, as inferred from the nearly horizontal basal erosive surfaces, cross-sectional geometries, thicknesses, and laterally extended nature of the sets. Some set bases have coarse sediments filling concave-up erosive relief (ca. 20 cm thick by 1 m long) that is overlain by tabular coarse sediments. This vertical shift indicates flow expansion, and suggests the sheet flows locally had basal channelized portions. Sediments in the concave-up relief also perhaps represent the deposits of a distributary network formed by minor splay channels (Bristow et al., 1999) and/or a central channel developed under waning flow conditions following a sheet-flood event (Fisher et al., 2007).

Finer sediments at locality 133-51 are interpreted as the slack-water sediments of the crevasse splays, deposited sometime after the initial overbank flood surge (possibly late rising-stage to falling-stage deposition). The few overprinted slickensides coupled with the greenish-gray color mottles and carbonates are likely the products of pedogenesis after deposition. Such features might represent poorly developed soils that form in crevasse-splay settings because of a high flood frequency and sedimentation rate (Bown and Kraus, 1987; Kraus, 1987).

Successive crevasse-splay events may account for the stack of fining-upward cycles observed at locality 133-51. Crevasse-splay activity comprises rapid processes and can accumulate complexes of fining-upward cycles as thick as the ones from the study location (≥3 m) in well under 10^2 years (e.g., Smith et al., 1989). A fining-upward cycle from locality 133-51 contains a coarse to fine

couplet that likely indicates flood to slack-water deposition. The smallish thicknesses of the cycles (≤1 m) and the number of cycles (at least three) found at the outcrop suggest a single cycle formed in response to an intra-season flood and/or an annual flood regime (Bristow et al., 1999; Perez-Arlucea and Smith, 1999). It is therefore likely the succession of cycles at locality 133-51 was deposited over a short period, perhaps on the order of 10^0 to 10^1 years.

4.3.6. Locality 133-6

Description: Exposed at this locality are fine-grained mudstones overlain by a tuff that is locally pumiceous. The succession at locality 133-6 (log 133-6 in Figs. 31, 32) has an apparent thickness of 3-5 m and extends laterally for 100's of m. It comprises three parts; in vertical succession these are sandy siltstones, claystones, and tuffs. Upward transitions between the two mudstones are sharp (non-erosive), diffuse, or sometimes marked by a 10-20 cm thick carbonate horizon made from interlocking nodules. The transition from the claystone to the tuff occurs at an erosive surface that is nearly flat lying or irregular with centimeters to a couple of decimeters of relief. Deposits comparably to those at 133-6 are exposed along the section documented by log 133-34 in Figs. 31 and 32.

The lower part of the succession at 133-6 comprises at least 135 cm of light-colored (e.g., 10YR 7/4) siltstones that often include a faction of fine sand. These sediments contain a low-moderate amount of spherical carbonate nodules with diameters of 5-10 cm. Primary sedimentary structures are generally absent,

but some laminations are present, especially within the lower levels of the siltstones.

Massive claystones forming the middle part of the succession are about 160 cm thick. They contain some carbonate nodules (~5 cm diameter) and are overprinted with an abundance of arcuate slickensided fractures that measure 10's of cm long/high. At a few outcrops these slickensides are lined with carbonate sheaths. The claystones are usually a brown color (e.g., 10YR 4/2) and sometimes show grayish color mottles (10G 8/2 or 10GY 7/2).

Light olive gray (5Y 6/1) tuffs comprise the upper meter or so of the succession at locality 133-6. They are massive, laminated or thinly bedded, and contain silt-sized glass shards and granules to small pebbles of pumice. Within these tuffs, there is a moderate amount of small carbonate rhizoliths.

Interpretation: The claystones probably formed by suspension sedimentation and were later modified by pedogenesis. Generous amounts of slickensides overprinted on clays are classic indications of modern (Wilding and Ruben, 1988) and ancient (Mack et al., 1993) vertic soils, which mainly form through the shrinking and swelling of smectite clays. The fine grain sizes and presence of pedogenic features indicate the claystones accumulated in overbank areas that experienced low-energy and infrequent flooding. These areas likely included medial-distal floodplains far from active channels. However, the coarseness of the underlying siltstones and their laminations suggest they may have been deposited during a final phase of channel infilling and abandonment.

Tuff deposits at locality 133-6 are interpreted to have been deposited by sheet-flow or suspension deposition in an overbank setting. The former is more likely since they are coarser than the directly underlying pedogenic claystones and they overlie an erosive surface, both of which indicate an upward increase in flow velocity. This evidence of a change to a higher energy might also indicate deposition occurred from overbank floods that caused sheet flows in a proximal floodplain.

4.4. Tephrostratigraphy

Outcrops of volcaniclastic deposits in NA 133 are 1-4 m thick and represent reworked air-fall sediments ultimately deposited by fluvial/alluvial processes. Exposures of sediment with these characteristics are found in both the northern and southern streams. More laterally continuous volcaniclastics crop out at the northern locality (logs 133-6, -11, -28, and -34 in Fig. 32); whereas, there are isolated occurrences along the southern stream (logs 133-47 and 133-50 in Fig. 32).

The analysis of glass-shard separates using an electron microprobe provides a means for characterizing and correlating the volcaniclastics in NA 133. The data also are a basis for allocating the outcrops to certain (dated) intervals of the Koobi Fora Formation and genetically related formations of northern Kenya and southern Ethiopia. Results of six glass-shard populations, each from a separate tuff sample, are examined and interpreted. Four of these are representative of

tuffs from the northern stream, and two derive from outcrops of the southern stream.

4.4.1. Outcrop descriptions and sample locations

A series of continuous outcrops exposed along the northern stream, and adjacent places, contains several tuffs sampled for this study. Sample BS1202 (backslope 1202) is representative of one of these tuffs. It derives from the basal portion of a 140 cm thick interval of tuff situated upon sandy siltstones with rhizoliths and nodular carbonate (log 133-11, Fig. 32). This tuff contains some carbonate nodules/rhizoliths, and is a massive silt-sized ash with occasional parallel and wavy laminae. Color ranges from light to very light gray (N7 to N8), to pinkish gray (5 YR 6/1).

This sampled tuff (BS1202) extends laterally to the east-southeast (downstream), along the stream's north bank. It can be followed for several hundred meters before it joins with a succession of coarser volcaniclastics with basal channel-form geometry (i.e., log 133-28 in Figs. 31, 32 and 35). A particular tuff of this succession is of limited lateral extent and lenticular in cross-section (25-50 cm thick). It is a pinkish gray (5YR 8/1) silt-sized tuff with ripple-drift structures (Fig. 35). BS202 is a sample taken from the middle part of this lens.

To the right of this lens, some 5 m to the southeast, the succession of tuffs is coarser and consists of a light gray (N6) to light olive gray (5Y 6/1) ash (Fig. 36). BS302 comes from a level about 1 m up from the base of this succession,

from a unit dominated by glass shards the size of medium-coarse (0.5-1 mm) sand.

Further downstream, for ~50 m, the tuff succession is exposed along outcrops situated upon the modern northern floodplain of the stream (log 133-34, Fig. 32). Here, the ash is finer and situated upon claystone strata that show paleosol (vertisol) overprints. BS702 is a sample retrieved from 30 cm above the contact with the claystone. The sampled tuff is light olive gray (5Y 6/1), massive or laminated, and composed of silt-sized material. The exposures of the tuff generally face to the E/SE, and can be traced northward into the outcrops for archaeological sites FxJj 24 and 25 (e.g., log 133-6 in Figs. 31 and 32).

Southern stream outcrops are highly dissected, discontinuous and contain many tuffs laden with sand- or mud-sized terrigenous grains. Two separate outcrops, however, have suitable quantities of silt-sized and larger glass shards. BS402 originates from the more upstream of these locations (i.e., log 133-50 in Figs. 31 and 32). It represents a sample taken from a fine-grained, light gray (2.5Y 7/0) tuff with some carbonate rhizoliths and laminae. The tuff is nearly 65 cm thick, and situated above ~50 cm of pale yellow (2.5Y 7/3) sandy siltstones, but below at least 200 cm of granule-pebble basalt clasts.

BS502 is from a succession (~250 cm thick) of sand- and silt-sized tuff, tuffaceous mudstone, and tuffaceous sand exposed along a medial reach of the southern stream (log 133-47 in Figs. 31 and 32). At least four gross lithological units compose the succession; each is 15-170 cm thick. The sampled interval is the lower 20 cm of the lowermost unit (170 cm thick) exposed. It comprises

coarse-medium glass shards, a fine quartzo-feldspathic sand fraction, and is light gray (2.5Y 7/2). Primary sedimentary structure is generally lacking, but there are some horizontal bedding features and rhizoliths.

4.4.2. Analytical approaches

These six tuff samples are used to assess the stratigraphy of NA 133 (Table 6 and Fig. 39). Laboratory preparations of the samples involved (e.g., Steen-McIntyre, 1977) lightly pulverizing the tuff, sieving for appropriate grains sizes (<60 and >120 mesh), and treating the glass to ultrasonic agitations and baths in distilled water, HNO_3 (10% by volume) and HF (5% by volume) to remove contaminants. Dried glass separates were given to the Earth and Planetary Sciences Department, Rutgers University for mounting in epoxy and analysis by an electron microprobe (JEOL JXA-8600 SuperProbe), running at 15 kV and 15 nA with a rastering beam. For further description of analytical conditions—such as beam angle, spot size, count rate, and standards for calibration—see Mollel (2002).

Weight percentage (wt.%) values of oxides are used to characterize each NA 133 tuff (Table 6). These data are the mainstay for assessing potential intra-area correlations for the tuffs found in NA 133 and correlations with tuffs of the Turkana Basin and adjacent locations (Brown and Feibel, 1985, 1986; Feibel et al, 1989; Feibel and Brown, 1993; Brown et al., 2006). Evaluating the potential correlations for the tuffs from NA 133 is accomplished by: firstly, sorting comparisons that are done with the wt.% of SiO_2, TiO_2, Al_2O_3, Fe_2O_3, MnO, MgO,

Table 6
Tuffs and major elemental oxide data used in the study of Area 133

Locality	Sample	n	SiO$_2$	TiO$_2$	Al$_2$O$_3$	Fe$_2$O$_3$	MnO	MgO	CaO	Na$_2$O	K$_2$O	Total	Reference
	Area 133												
Turkana (NE)	BS202AV	17	74.51	0.17	10.58	3.11	0.10	0.04	0.16	3.63	4.78	97.10	This study
	STDV		1.48	0.03	0.11	0.15	0.05	0.01	0.03	0.29	0.19		
Turkana (NE)	BS302AV	19	73.52	0.18	10.59	3.16	0.10	0.03	0.17	3.86	4.68	96.30	This study
	STDV		2.13	0.03	0.13	0.14	0.04	0.01	0.02	0.27	0.22		
Turkana (NE)	BS402AV	10	71.78	0.24	9.97	3.97	0.13	0.03	0.21	3.48	4.54	94.36	This study
	STDV		1.62	0.08	0.56	0.62	0.06	0.03	0.08	0.47	0.31		
Turkana (NE)	BS502AV	12	71.45	0.12	10.92	1.72	0.10	0.03	0.20	3.27	4.36	92.18	This study
	STDV		2.21	0.03	0.16	0.06	0.05	0.01	0.03	0.22	0.40		
Turkana (NE)	BS702AV	17	73.11	0.19	10.59	3.13	0.09	0.03	0.17	4.02	4.61	95.95	This study
	STDV		0.97	0.05	0.11	0.09	0.04	0.01	0.02	0.23	0.20		
Turkana (NE)	BS1202AV	13	70.91	0.18	10.46	3.05	0.11	0.04	0.16	3.81	4.49	93.20	This study
	STDV		1.30	0.04	0.12	0.10	0.02	0.01	0.02	0.33	0.11		
	Reference population												
Turkana (NW)	K88-3247		74.80	0.25	10.06	4.27	0.13	0.01	0.21	2.13	3.36		Brown et al. (2006)
Konso	Ivory [938-17]		72.65	0.15	11.21	1.32	0.07	0.04	0.22	2.81	4.75		Brown et al. (2006)
Konso	Ivory [9711-65 MP (32)]		74.40	0.15	11.45	1.29	0.06	0.04	0.24	3.29	4.56		Katoh et al. (2000), WoldeGabriel et al. (2005)
Turkana (NW)	Lokapetamoi [K84-2972]		74.81	0.15	11.28	1.27	0.07	0.05	0.24	3.34	4.14		Feibel and Brown (1993), Brown et al. (2006)
Turkana (NW)	Akait [88-3263]		73.54	0.17	10.68	3.10	0.09	0.02	0.20	3.11	4.00		Feibel and Brown (1993), Brown et al. (2006)
Turkana (NW)	K88-3261		73.98	0.17	10.14	3.42	0.10	0.02	0.20	3.33	4.46		Brown et al. (2006)
Omo	ETH314 [ETH86-314 M1]		72.04	0.25	9.94	4.15	0.15	0.05	0.16	1.38	3.19		de Heinzelin (1983), Brown et al. (2006)
Turkana (NE)	KBS [77-17]		70.37	0.16	10.80	3.09	0.12	0.03	0.16	3.23	3.27		Vondra et al. (1971), Brown et al. (2006)
Konso	Turoha [AV 155 analyses]		70.95	0.18	10.31	2.90	0.10	0.03	0.18	3.62	4.18		Brown et al. (2006)
Konso	Turoha [944-57 MP (35)]		70.40	0.17	10.28	2.89	0.10	0.02	0.17	3.83	4.39		Katoh et al. (2000), WoldeGabriel et al. (2005)
Konso	Turoha [944-57 DCP (4)]		71.02	0.18	10.53	2.97	0.10	0.02	0.19	4.44	4.76		Katoh et al. (2000), WoldeGabriel et al. (2005)

Electron microprobe results for the Area 133 tuffs are averages calculated from multiple glass shards (n column) in a purified bulk sample. For example, the SiO$_2$ value for BS202AV is an average compiled from 17 separate glass shards of the same sample. Major element oxides are shown in weight percent. STDV = one standard deviation.

Fig. 39: Tephrochronological correlations between Konso and Turkana formations. Left column—Konso Formation in the Konso Basin (Katoh et al., 2000; Nagaoka et al., 2005; WoldeGabriel et al., 2005). Middle column—Nachukui Formation in the northwest Turkana Basin (Harris et al., 1988; Feibel and Brown, 1993; Brown et al., 2006; McDougall and Brown, 2006). Right column—Koobi Fora Formation in the northeast Turkana Basin (Brown and Feibel, 1986; Feibel et al., 1989; Brown et al., 2006; McDougall and Brown, 2006). Tuff samples for northern Area 133 (this study) of the northeast Turkana Basin to left of Koobi Fora Formation. Sample BS402AV from Area 133 is correlated to the K88-3247 tuff from the Nachukui Formation. BS502AV correlates with the Nachukui Formation's Lokapetamoi Tuff, which is correlative to the Ivory Tuff of the Konso Formation. BS202AV, BS302AV, BS702AV and BS1202AV are correlated with Konso's Turoha Tuff that correlates to the KBS Tuff of the Turkana formations.
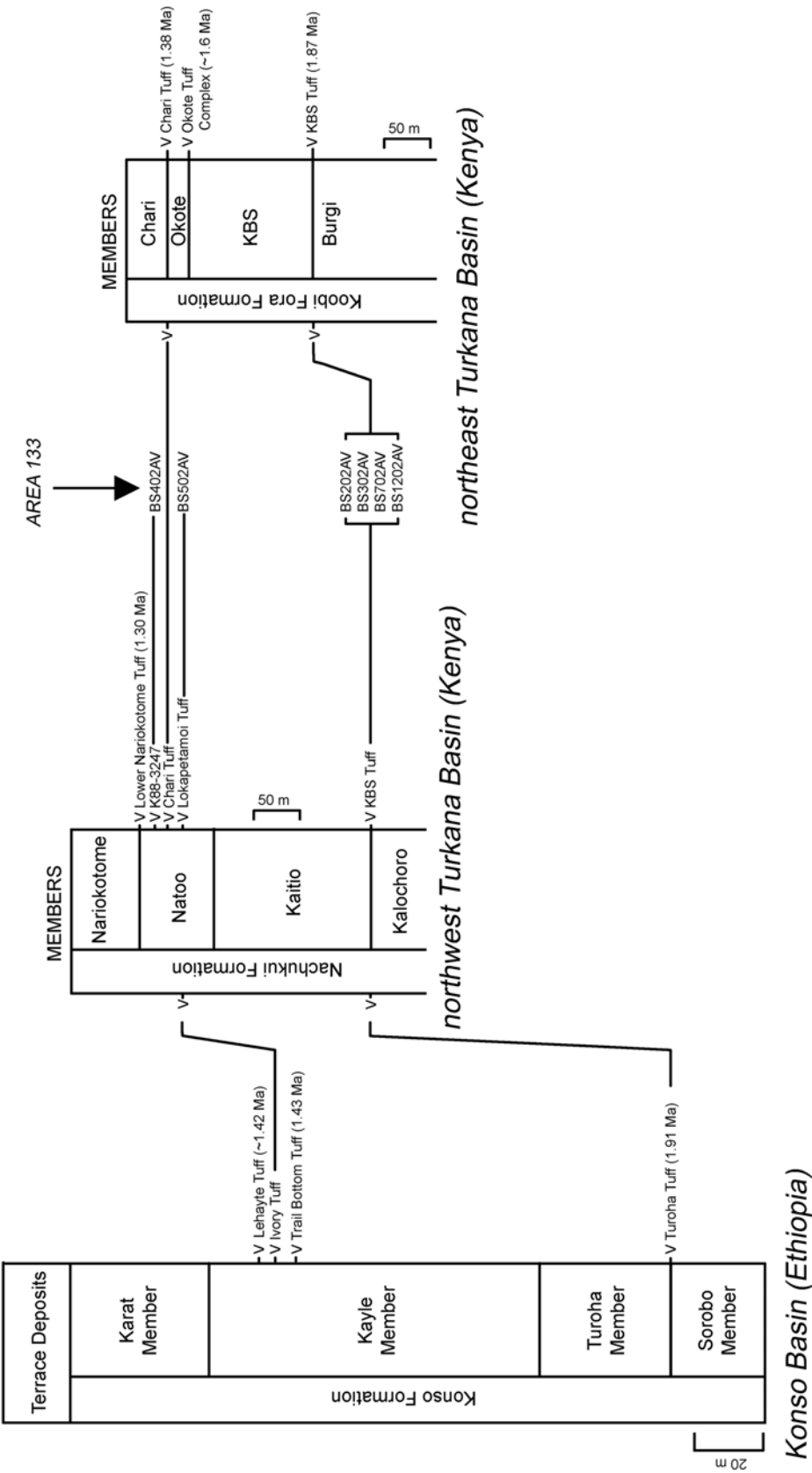
CaO, Na_2O, and K_2O; secondly, using these oxides to calculate mean differences in composition by obtaining a similarity coefficient (SC) score for the NA 133 data and published information (SC=$1/n*(\Sigma(x_1/x_2)$), $x_1 > x_2$ or $x_1 = x_2$, where x_1 and x_2 are the larger and smaller compositions of the oxides; Borchardt et al., 1972); and lastly, visually inspecting bivariate variation diagrams for oxides. The Plio-Pleistocene reference population (Table 6) for out-of-area comparisons includes tuffs of the Koobi Fora Formation and related Plio-Pleistocene Omo Group deposits around the modern Lake Turkana Basin (Brown and Feibel, 1986; Feibel and Brown, 1993; Brown et al., 2006). Additionally, it contains data from the nearby Konso Formation of southern Ethiopia, which has correlates of the Turkana Basin tuffs (Katoh et al., 2000; WoldeGabriel et al., 2005).

Establishing tephrostratigraphic relationships between the NA 133 tuffs and previously defined and interpreted tephra of the Koobi Fora Formation and related deposits (Fig. 39) is confounded by the evolution and eruptive style of parent magma, transport to depocenter, post-depositional alterations, and inter-laboratory analytical biases (Orton, 1996; Feibel, 1999). For these reasons it is often necessary to assess the geochemical identity of a tuff from its outcrop position within a tuff sequence that has a geochemical suite comparable to other well-studied tephrostratigraphic sequences (Brown and Feibel, 1985; Katoh et al., 2000; Brown et al., 2006). It is also usually necessary to evaluate the validity of correlation through multiple types of geochemical indicators and supplementary information from geochronology, biostratigraphy, lithostratigraphy, and outcrop mapping studies (Feibel et al., 1989; WoldeGabriel et al., 2005;

McHenry et al., 2008). Therefore, since each of the examined NA 133 tuffs are not directly stratified by other tuffs at the outcrop, and there is a lack of numerical chronological information, the correlations suggested below are tentative.

4.4.3. Results and interpretations

The six sets of results (i.e., BS202AV = backslope 202 average, BS302AV, BS402AV, BS502, BS702, and BS1202AV) used in this study represent average oxide compositions of the NA 133 tuffs (Table 6). Each average result (of individual nine to 17 member shard populations) samples a ~50 gram split of a tuff collected from outcrops. A shard in these populations is represented by one election microprobe analytical point and its associated oxide results. The number of members (shards) in the total study population is 107. This total population includes six shards with oxide wt.% totals at 86-90%; the remaining 106 have totals at 90-99% (see Appendix 1).

The NA 133 average results are characterized by Al_2O_3 at 9.97-10.92 wt.%, $SiO_2 \geq 70.91$ wt.% and $Na_2O + K_2O \geq 7.63$ wt.% (Fig. 40), collectively indicating (cf., Le Bas et al., 1986; Le Maitre, 1989) rhyolitic volcaniclastics with a general composition that is mildly peralkaline. Comparative diagrams of oxide data display orderly variations in TiO_2, Al_2O_3, Fe_2O_3 and CaO (Fig. 40). Particularly noteworthy are the respective positive and negative linear trends in diagrams that show comparisons of Fe_2O_3 versus TiO_2 and Al_2O_3. The decreasing Al_2O_3 could be a result of progressive crystallization of feldspar minerals (e.g., Wilson, 1993). On the other hand, the observed linearity may not

be indicative of protracted, diachronic changes in magmatic evolution because there are few such consistent orderly tendencies for Fe_2O_3, TiO_2 or Al_2O_3 over large intervals of the Koobi Fora Formation. For example, several penecontemporaneous (~1.4 Ma) tuffs of the upper formation either are strongly peralkaline or have high aluminium, and other tuffs with such compositions are not systematically distributed throughout older (ca. 1.9-1.4 Ma) stratigraphic intervals (Brown and Feibel, 1986). Similar unordered stratigraphic changes can be observed for other oxides and trace elements in these tuffs of the Turkana Basin (Brown et al., 2006). Another possibility is that there are time-sequence trends in magma evolution, but the oxide patterns in the formation are representative of tuffs from several different sources with separate developmental histories.

Samples BS202AV, BS302AV, BS702AV, and BS1202AV derive from a series of tuffs within a set of outcrops from the northern stream locality (logs 133-11, -28 and -34 in Figs. 31, 32, 35 and 36). Thus, continuity exists between the tuffs according to lateral stratigraphy. Moreover, oxide sorting and all SC scores (>0.93) suggest compositional similarities. These four samples are interpreted as a distinctive geochemical subgroup of the NA 133 data, characterized by relatively low CaO, and intermediate TiO_2, Al_2O_3 and Fe_2O_3 wt.% values (Fig. 40). Values of Al_2O_3 range at 10.46-10.59 wt.% and indicate a mildly peralkaline composition. Evidence from examining outcrop patterns, sorting, SC scores, and oxide distribution patterns on variation diagrams indicates the tuff deposits of the northern stream likely represent ash from a similar magma and related eruption.

Fig. 40: Element variation diagrams of selected oxides for tephra samples from the northern Area 133 study location. Data represent the average results (Table 6) of bulk glass analyses derived from electron microprobe trials.
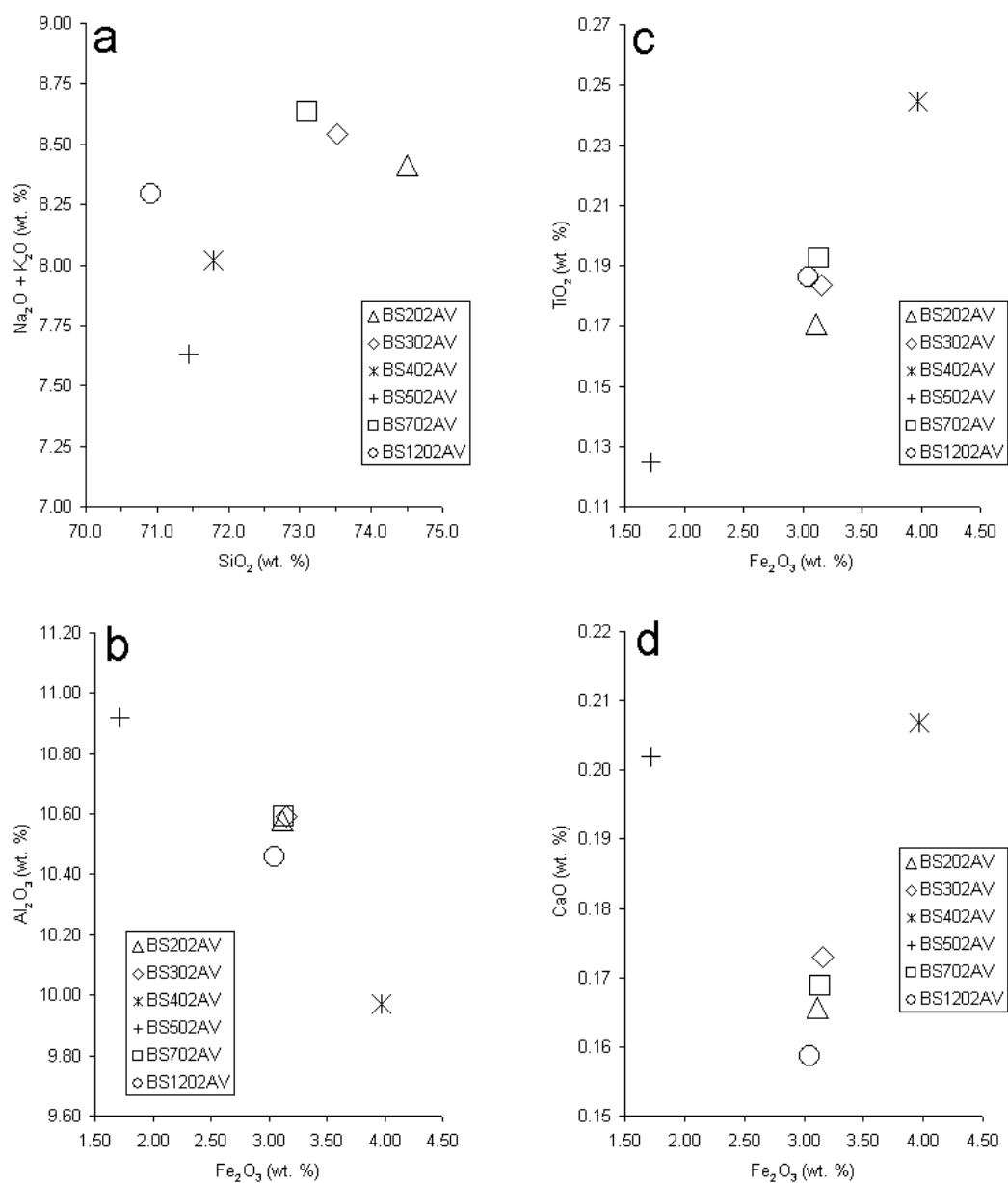
The least peralkaline example from the study area, with an Al_2O_3 wt.% = 10.92, is BS502AV (Fig. 40). It is also remarkable for the lowest TiO_2 (0.12) and Fe_2O_3 (1.72) wt.% values of the sample population (Fig. 40). BS502AV represents a shard population from a tuff that crops outs along middle reaches of the southern stream (log 133-47 in Figs. 31 and 32).

Sample BS402AV derives from an isolated outcrop situated in an upper reach of the southern stream (log 133-50 in Figs. 31 and 32). Its composition is mildly peralkaline (Al_2O_3 wt.% = 9.97), but more peralkaline than any other NA 133 sample (Fig. 40). This sample is also distinguished by having the relatively highest TiO_2 (0.24) and Fe_2O_3 (3.97) wt.% values.

Visual examinations of oxide wt.% (e.g., Table 6) indicate that the NA 133 subgroup formed by BS202AV, BS302AV, BS702AV, and BS1202AV is comparable with reference data for the Turoha Tuff from the Konso Formation (Katoh et al., 2000; WoldeGabriel et al., 2005) and the KBS Tuff, K88-3261 Tuff, and the Akait Tuff from the Turkana Basin (Brown and Feibel, 1986; Feibel and Brown, 1993; Brown et al., 2006). In all cases the highest SC scores (0.92-0.94) are with the Turoha Tuff. SC scores for the other tuffs range from >0.87 to <0.90. As defined by Katoh et al. (2000), the Turoha Tuff is a white to whitish-gray, fine-grained ash with pumice grains less than 1 cm in diameter, and upper and middle portions that are vitric and strongly altered to pinkish white color. Like many of the Konso Formation tuffs, deposition was from air-fall and related processes (Katoh et al., 2000; Nagaoka et al., 2005; WoldeGabriel et al., 2005). Coloration of the Turoha Tuff compares well with those from NA 133, but the

depositional setting is quite different. Furthermore, the small pumices and finer grain sizes are particular points of departure from sample BS302AV of NA 133, which samples a 2-4 m thick volcaniclastic channel complex with sand-sized (coarse to medium) glass, pebble to cobble pumices, and mud rip-up clasts. Katoh et al. (2000) and WoldeGabriel et al. (2005) have argued through geochemical correlations and radiometric-isotopic dates that the Turoha Tuff is a correlate of the KBS Tuff. The KBS Tuff (e.g., Vondra et al., 1971; Cerling and Brown, 1982) is commonly found within a fluvial facies, which is typical for tuffs at Karari outcrops, including those studied here. It is 1-3 m thick, light gray, white to pinkish in color, and composed from fine- to medium-grained ashes that include pumice clasts up to 15 cm in diameter (McDougall, 1985; Brown and Feibel, 1986). Most often, the KBS tuff along the Karari occurs as lens-shaped units surrounded by clayey mudstones (Brown and Feibel, 1991). Facies analyses (White et al., 1981) suggest it was accumulated in floodplain swales, broad and shallow floodbasin distributary streams, and other overbank areas. These lithological and depositional aspects of the KBS Tuff compare well with the NA 133 tuffs, except that at some outcrop locations (e.g., BS302AV) the latter can be substantially coarser and situated within a fluvial channel complex. WoldeGabriel et al. (2005) attribute differences in gross aspects of glass shards, grain sizes, facies and depositional settings between the Turoha and KBS Tuffs to transport and reworking processes, resulting from the fact that Konso tuffs were deposited in settings more proximal to fallout from plinian eruptions in the central Main Ethiopian Rift, and the Koobi Fora Formation and other Turkana

Basin tuffs were accumulated by aqueous processes in more distal settings. Brown et al. (2006) and McDougall and Brown (2006) generally concur that the Turoha and KBS Tuffs are correlates. But these authors point out that, even though the ages 1.91±0.03 Ma (Turoha; Katoh et al., 2000) and 1.87±0.02 Ma (KBS; McDougall and Brown, 2006) agree well, the iron and aluminum contents of the Turoha Tuff are distinctly lower than those of the KBS Tuff. Al_2O_3 values for the four NA 133 samples (10.46, 10.58, 10.59 and 10.59 wt.%) are constrained by those of the Turoha and KBS Tuffs (10.31 and 10.80 wt.%, respectively) (Table 6). Additionally, they lack the low amount of this oxide described for the Turoha Tuff. The accompanying Fe_2O_3 range (3.05-3.16 wt.%) for the NA 133 data is not concordant with the low value of the Turoha Tuff (2.90 wt.%), but it clusters around the value of the KBS Tuff (3.09 wt.%) (Table 6). However, iron and aluminum composition are evidently not rigorous measures for the KBS-Turoha Tuff correlation, as implied by the work that has established the correlation between the two. Therefore, despite the higher iron and aluminum wt.% for the four NA 133 samples (BS202AV, BS302AV, BS702AV, and BS1202AV), they are considered to be correlated best with the Turoha Tuff on the basis of high SC scores (0.92-0.94). The data suggest the four NA 133 tuffs can be allocated to a stratigraphic position within the framework of the Konso Formation/Koobi Fora Formation that dates to about 1.91-1.87 Ma. In the Koobi Fora Formation, this would be the uppermost portion of the Burgi Member and/or the lowermost portion of the KBS Member, since the KBS Tuff defines the base of the KBS Member (Fig. 39).

Inspection of wt.% values (Table 6) suggests sample BS502AV compares best with the Ivory and Turoha Tuffs of the Konso Formation (Katoh et al., 2000), and the Lokapetamoi Tuff of the Turkana Basin sequences (Feibel and Brown, 1993). WoldeGabriel et al. (2005) correlate the Lokapetamoi to the Ivory. As discussed previously, they also correlate the KBS Tuff from the Koobi Fora Formation (Brown and Feibel, 1986) to the Turoha Tuff. The best comparisons from SC score include: 0.87 = Ivory Tuff (sample 938-17; Brown et al., 2006), 0.87 = Ivory Tuff (sample 97-65MP(32); WoldeGrabriel et al., 2005), 0.86 = Turoha Tuff (average of 155 analyses; Brown et al., 2006), and 0.86 = Lokapetamoi Tuff (sample K84-2972; Brown et al., 2006). The Ivory Tuff is a whitish and well- laminated unit stratified between grayish mudstones, which fine upward from thin sands overlying the Trail Bottom Tuff (Katoh et al., 2000; Nagaoka et al., 2005). Above this level is the Lehayte Tuff that, in conjunction with the dates of the Trail Bottom Tuff, constrain the age of the Ivory Tuff to approximately 1.43-1.41 Ma (Katoh et al., 2000; WoldeGabriel et al., 2005; Nagaoka et al., 2005). At its type section in the Turkana Basin, the Lokapetamoi is about 1 m thick and locally includes accumulations of mollusks at its base (Feibel and Brown, 1993). The Lokapetamoi Tuff is dated between 1.48 and 1.38 Ma (probably ~1.42 Ma due to its correlation with the Ivory Tuff) and allocated to an interval that correlates with the upper Okote Member, Koobi Fora Formation (Brown and Feibel, 1986; Feibel and Brown, 1993; Brown et al., 2006; McDougall and Brown, 2006). The Turoha Tuff and its correlate the KBS Tuff date to 1.91-1.87 Ma (Katoh et al., 2000; McDougall and Brown, 2006). It is least

likely, however, that the Turoha Tuff is linked with sample BS502AV, because this sample has a lower wt.% value for TiO_2 (0.12) and substantially less Fe_2O_3 (1.72) (Table 6). Evidently, these low oxide amounts are also particularly characteristic—especially the low iron—of the Lokapetamoi and Ivory Tuffs (Table 6) and not a common feature of other tuffs in the Plio-Pleistocene sequences (WoldeGabriel et al., 2005; Brown et al., 2006). Another possibility is that BS502AV matches with tuffs formally designated as the White Tuff (Feibel et al., 1989; Brown et al., 2006), which also has low Fe_2O_3 (1.81 wt.%) content. But the two variants of the White Tuff have sufficiently low TiO_2, MnO and MgO, in addition to poor SC scores (0.72, 0.78), to not warrant a correlation with BS502AV. Thus, BS502AV is correlated with the Ivory (=Lokapetamoi) Tuff on the basis of SC scores (0.87) and a characteristic glass shard chemistry that is unusual within the tephra units of the stratigraphic sequences from Konso and Turkana (WoldeGrabriel et al., 2005). Accordingly, the tuff from which this sample derives is allocated to an upper part of the Okote Member, Koobi Fora Formation, and roughly dates at 1.5-1.4 Ma (Fig. 39).

On the basis of similar oxide wt.% values, sample BS402AV consistently sorts with about a dozen tuffs from the reference population (e.g., Fig. 41) and matches fairly with these according to SC scores (range of about 0.80 to 0.87). Despite this, there are very good correspondences between BS402AV and tuffs K88-3247 and ETH86-314 M1 when selected oxides are compared (Table 6). These three are distinguished from others in the reference population by intermediate wt.% values for TiO_2 (0.24-0.25), Al_2O_3 (9.94-10.06), Fe_2O_3 (3.97-

Fig. 41: Element variation diagrams of selected oxides for sample BS402AV (asterisk-shaped symbol) from the northern Area 133 study location. Data represent the average results (Table 6) of bulk glass analyses derived from electron microprobe trials. Black diamonds in diagrams are data for known tuffs of the Konso and Turkana Basin formations (WoldeGabriel et al., 2005; Brown et al., 2006). Open circle and open diamond symbols represent tuffs K88-3247 and ETH86-314 M1, respectively (Brown et al., 2006). Oxide correspondences for BS402AV and K88-3247, especially for MnO (Fig. 41b) and CaO (Fig. 41d), are interpreted as evidence for a correlation between the two.
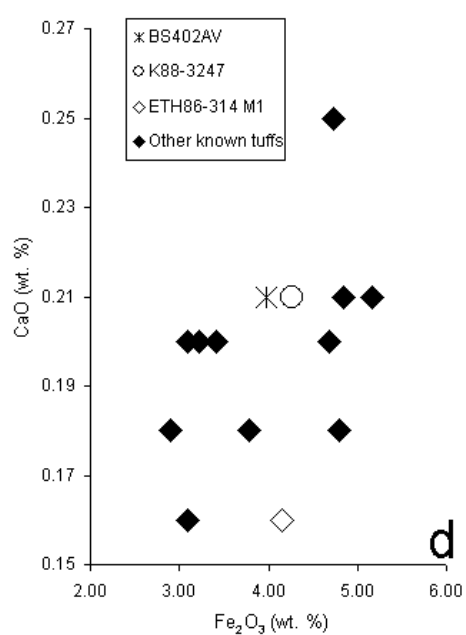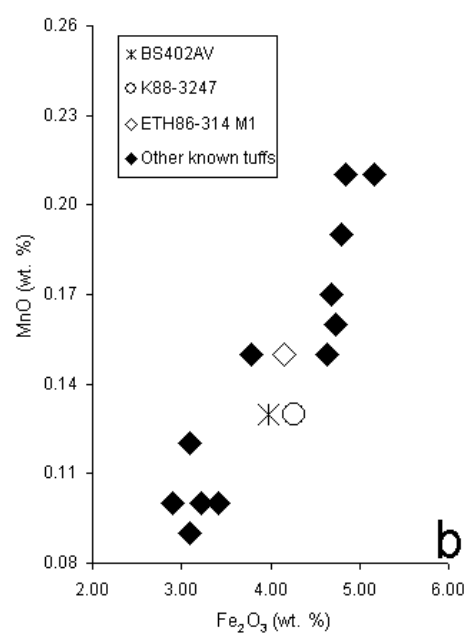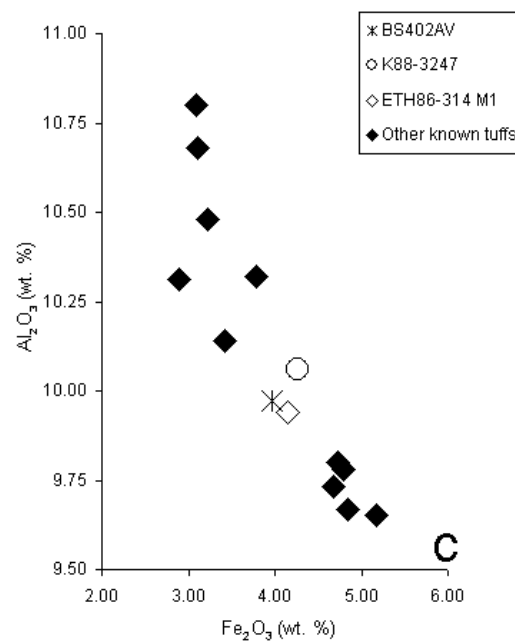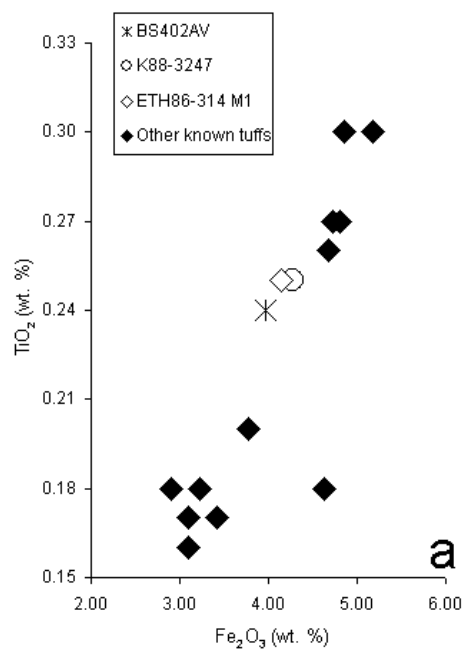
4.27), and MnO (0.13-0.15) (Fig. 41).   Brown et al. (2006) indicate ETH86-314 has a tri-modal shard composition and its principle mode, ETH86-314 M1, is an equivalent to the ETH45(=J-3) Tuff of the Omo-Turkana Basin sequences. These authors estimate a depositional age of around 1.65-1.60 Ma for ETH 45(=J-3)/ETH86-314 M1 and place it at a stratigraphic position that corresponds to the uppermost part of the KBS Member, Koobi Fora Formation (e.g., Brown and Feibel, 1986).   On the other hand, K88-3247 is evidently representative of a tuff that is only known from the Lokapetamoi South locality of the western Turkana Basin (Brown et al., 2006).   A better similarity is observed between BS402AV and K88-3247 because of the low CaO (0.16 wt.%) for ETH86-314 M1, which is not characteristic of the others (i.e., both have 0.21 wt.%) (Fig. 41).   On this basis the two are more likely to be correlates and interpreted as such.   Tuff K88-3247 is positioned above the Chari Tuff but below the Lower Nariokotome Tuff (Brown et al., 2006).   These tuffs are respectively dated to about 1.38 Ma and 1.30 Ma, and correlate to a lower interval of the Chari Member, Koobi Fora Formation (Brown and Feibel, 1986; Brown et al., 2006; McDougall and Brown, 2006).   BS402AV is therefore assigned to this interval (Fig. 39).

5. Paleogeographic and stratigraphic contexts of the hominin remains

The geological contexts of hominin remains from Areas 130 and 133 are described below. The paleoanthropological materials from Area 130 represent *in-situ* finds that were excavated from the subsurface (Harris et al., 1997; Isaac and Behrensmeyer, 1997). Archaeological sites from Area 133 are all unexcavated surface occurrences of stone stools (Harris, 1997); therefore, only potential contexts can be discussed. To ensure the best integration with this study's geological information, each of the archaeological sites and fossil localities was revisited in the field. Given in Appendix 2 is a complete list of the geographic locations and GPS provenances for the hominin remains.

5.1. Fluvial contexts of the Area 130 hominin remains

Previous work indicates that the Area 130 hominin remains accumulated within sediments deposited by braided and meandering channels (e.g., Burggraf et al., 1981; Isaac and Behrensmeyer, 1997). The results of this study suggest these fluvial styles were mutually exclusive aspects of the Area 130 paleogeography. However, a majority of the remains derive from stratigraphic levels of the upper KBS/lower Okote members, near which there is a vertical changeover between the deposits of these river types.

Braided-channel deposits contain stone-tool sites FxJj 11 and FxJj 38, in addition to fossil hominins KNM-ER 1805, and KNM-ER 1806 (Fig. 42). FxJj 38, KNM-ER 1805, and KNM-ER 1806 are situated within coarse channel fills (Harris et al., 1997; Isaac and Behrensmeyer, 1997). These deposits accumulated

Fig. 42: Landscape-scale paleogeography of Area 130 showing the situations of archaeological sites FxJj 11, FxJj 38 and hominin fossils KNM-ER 1805 and KNM-ER 1806 in relation to facets of the braided-river system represented by coarse lithosome I (bars and channel segments) and fine lithosomes I_2 and n_2 (fine-grained infills of channel segments). Although the floral types are accurate (e.g., Quinn et al., 2007), the density and spatial distribution of paleo-vegetation is schematic. Figure is after Miall's (1996) model of a gravelly-sandy braided river.

PALEO-VEGETATION (after Quinn et al., 2007)

Savanna Woodland

Thicket and Scrub

Low Tree-Scrub Savanna

longitudinal bars

fine-grained infills of
channel segments

KNM-ER 1805

KNM-ER 1806

FxJj 38

FxJj 11

LITHOLOGY

gravel

mud

sand

tuff
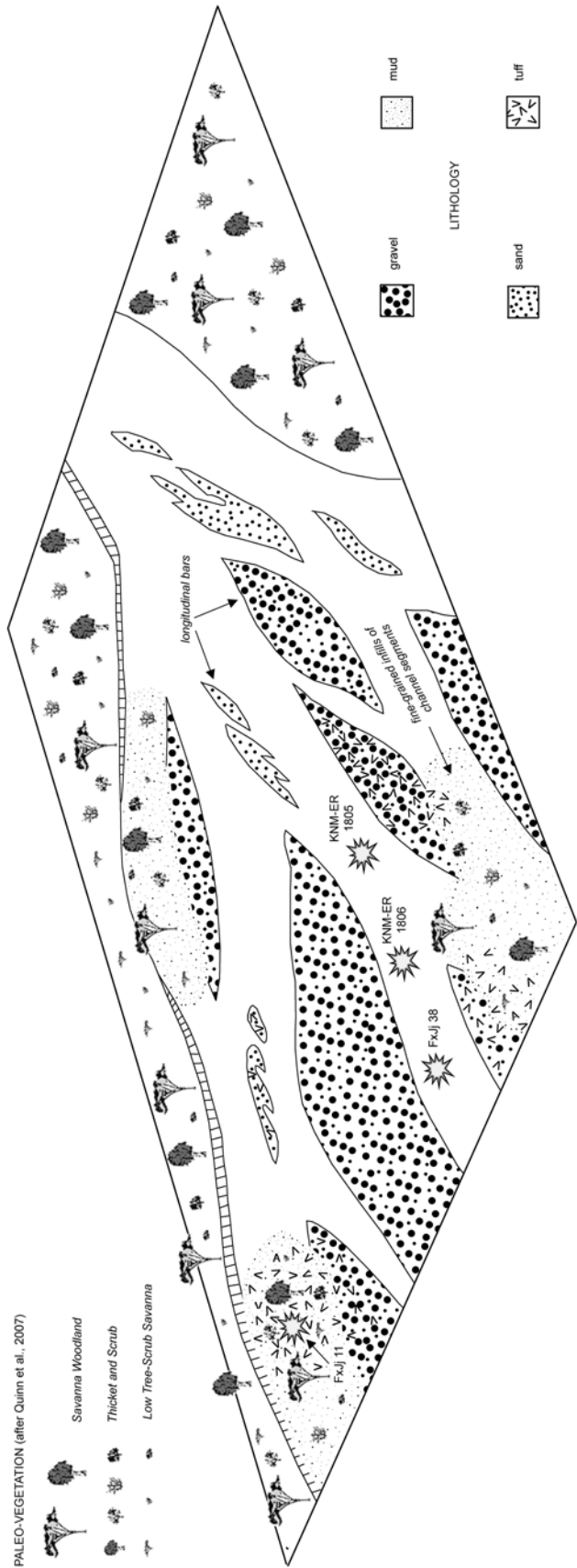
within channel segments that were lateral to a large mid-channel bar complex. FxJj 11 derives from a lower-energy sedimentary context and is preserved within a succession largely consisting of mudstones (Kaufulu, 1983; Harris et al., 1997). The mudstones were deposited within channel segments during a phase of fine-grained infilling and abandonment for the braided river. Following channel abandonment, or coinciding with a later stage of infilling, soils developed upon the mudstones (type-III paleosol in Figs. 18, 21). These soils formed over a timeframe on the order of 10^3-10^5 years, indicating paleolandscapes of Area 130 experienced a period of low aggradation of equal duration.

Archaeological sites FxJj 16, FxJj 17, FxJj 18 complex, and FxJj 19 derive from the sediments of the same meandering channel and floodplain depositional system (Fig. 43). Within this system, stone tools were deposited on the floor of the channel as lags and within thalwegs (FxJj 16 and 19; e.g., Kaufulu, 1983), accumulated with the deposits of channel bars and banks (FxJj 18 GL, GU and NS; e.g., Isaac and Behrensmeyer, 1997), and preserved in tuffaceous channel fills (FxJj 18 IH; e.g., Harris et al., 1997). Overbank floods resulted in the deposition of crevasse splays in proximal-floodplain areas. Crevasse-splay deposition buried archaeological materials accumulated on these proximal floodplains (FxJj 17; e.g., Burggraf et al., 1981). Floodplain deposition alternated with brief periods of soil formation, lasting for times on the order of 10^0 to 10^2 years (type-I paleosol in Figs. 18, 19). Eventually, the channel was infilled and abandoned, and floodplain aggradation dominated the paleolandscape. This further preserved the sites in the geological record.

Fig. 43: Landscape-scale paleogeography of Area 130 showing the situations of archaeological sites FxJj 16, 17, 18 complex, and 19 in relation to facets of the meandering channel and proximal floodplains respectively represented by coarse lithosome m (bars and channel) and fine lithofacies association LA5a (crevasse splay and adjacent overbank area). Although the floral types are accurate (e.g., Quinn et al., 2007), the density and spatial distribution of paleo-vegetation is schematic.   Figure is after Miall's (1996) model of a sandy-gravelly meandering river.

PALEO-VEGETATION (after Quinn et al., 2007)

Savanna Woodland

Thicket and Scrub

Low Tree-Scrub Savanna

LITHOLOGY

gravel

sand

mud

tuff

longitudinal bar / channel lag

lateral bar

crevasse splay

FxJj 19

FxJj 16

FxJj 18 NS

FxJj 18 IH

FxJj 18 GL

FxJj 18 GU

FxJj 17
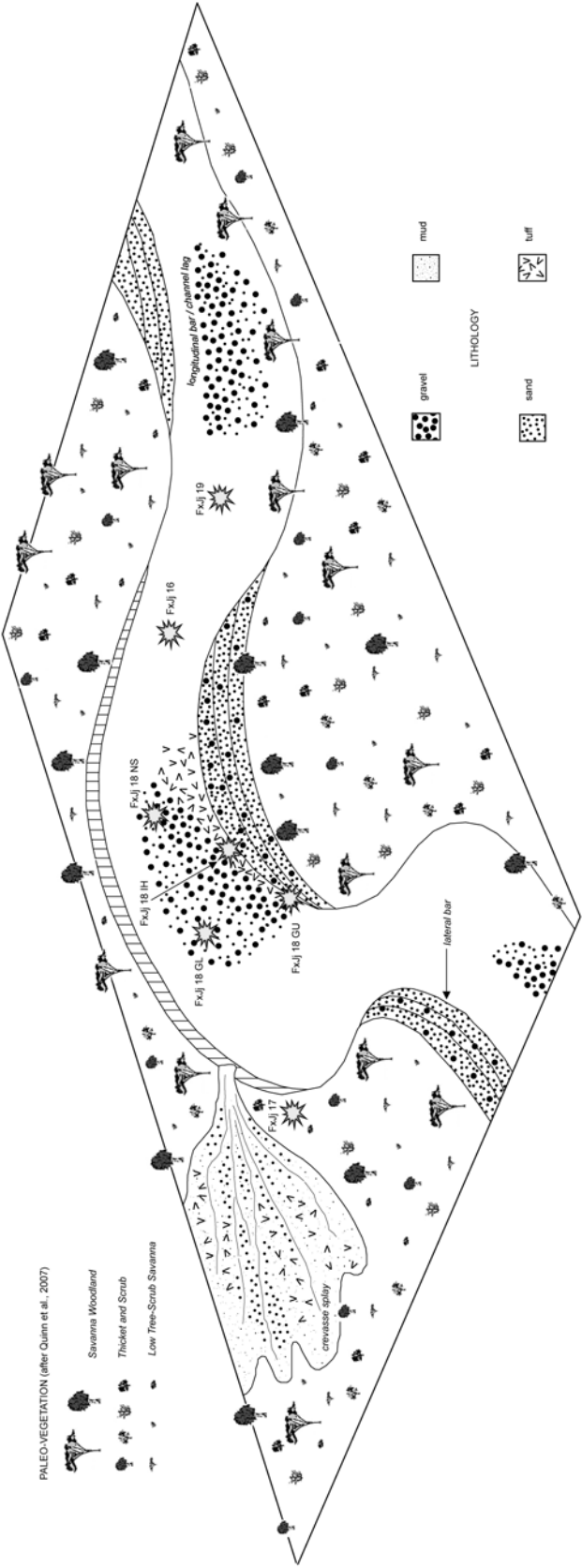
5.2. Potential contexts of the Area 133 surface archaeology

Along the northern stream in northern Area 133, four surface archaeological sites (i.e., FxJj 24, FxJj 25, FxJj 26, and FxJj 27) are reported from a series of small tributaries that drain from N/NW to S/SE (Harris, 1997). Two of these sites, FxJj 24 and FxJj 25, are closely spaced on the modern landscape and found along the same tributary (Fig. 31). The purported location of FxJj 24 is on the eastern bank of the tributary. It is adjacent to an uplifted set of outcrops with ample exposure facing the northwest and west. Within these outcrops is a ~5 m thick sedimentary succession (log 133-5 in Figs. 31 and 32) consisting of floodbasin claystones with vertisols, which are overlain by gravels and conglomerates. FxJj 25 is located about 500 m upstream (NW) from FxJj 24 and on the opposite bank of the tributary. Outcrops in this area rise to about 3 m from the tributary's floor and generally face to the northeast. The sedimentary succession here is like the one adjacent to FxJj 25, except that above the floodbasin claystones with vertisols is the Turoha(=KBS) Tuff (log 133-6 in Figs. 31 and 32) instead of gravel/conglomerate. As for FxJj 26 and FxJj 27, it is difficult to assess their potential sedimentary and stratigraphic contexts. Their respective tributaries provide virtually no exposure of sediments that can be confidently attributed to the Koobi Fora Formation. Beginning about 200 m south of the sites, however, tuffs sporadically crop out along the tributaries' banks. These are perhaps the Turoha(=KBS) Tuff.

Adjacent to the southern stream of northern Area 133, three surface archeological sites are known (FxJj 27, FxJj 29, and FxJj 53 in Fig. 31) (Harris,

1997). Outcrop relief at this stream is overall more subdued and discontinuous as compared to the northern stream. Good exposures of sediment are found adjacent to surface site FxJj 53, however. Small and rounded, badland-like hills compose the topography here, and the exposed sections of sediment reach thicknesses of about 4 m. The sections contain interbedded sands, siltstones and tuffs (Fig. 37), interpreted as proximal floodplain deposits. Some units of these floodplain deposits can be traced toward the direction of surface site FxJj 27. Most of the topography surrounding this other site appears to be a result of denuding Plio-Pleistocene sediment. But the local relief is very subtle and hampers the description and interpretation of the sediments. In fact, most of the landscape near FxJj 27 is flat and the modern ephemeral streams have incised through the basin fill for depths of no more than 50 cm. Outcrop relief is no better around surface site FxJj 29; and there are no lateral continuities with well-exposed sedimentary sections in the vicinity.

Based on these comparisons between the reported geographic locations of surface sites and the collected geological data, some inferences can be made about potential subsurface archaeological occurrences. If indeed the surface sites are representative of *in-situ* materials, then FxJj 24 and FxJj 25 are the best possibilities for recovering artifacts with good chronostratigraphic provenance. Ample exposure of the Turoha(=KBS) Tuff will permit for sound stratigraphic placement of recovered materials relative to the level of the upper Burgi/lower KBS Member and allow for comparisons to other sites dating to ~1.9 Ma. At the southern stream locality, the best prospect is FxJj 53. Yet, tuffs do not crop out

at the site, and the allocation of artifacts to a chronostratigraphic level would be based on the assumption that the surrounding floodplain deposits derive from the upper Okote/lower Chari Member (~1.4 Ma).

6. Paleogeographic summary for the north-central Karari Escarpment

Studied deposits of the north-central Karari Escarpment are exposed along NE/SW trending outcrops in Area 130 (Fig. 8) and a series of NW/SE trending outcrops in northern Area 133 (Fig. 31). Mapping and tephrostratigraphic evidence (e.g., Figs. 9 and 39) indicate these deposits of the Koobi Fora Formation collectively reflect portions of an interval that spans the upper Burgi to lower Chari members. However, whereas the examined sedimentary successions of Area 130 allocate to the upper Burgi through lower Okote members, successions in northern Area 133 are representative of the upper Burgi/lower KBS members and the upper Okote/lower Chari members (Fig. 44). By integrating these stratigraphic interpretations with the results of sedimentological, paleosol and fluvial architectural studies from Areas 130 and 133, through-time spatial changes in the paleogeography of the north-central Karari can be assessed (Figs. 45-50).

6.1. Upper Burgi to lower KBS members

Mapping of the upper Burgi to lower KBS members of the north-central Karari reveals mudstone deposits (e.g., LA5b in Fig. 22 and log 133-6 in Fig. 32) indicative of a widespread floodbasin that covered an area of at least 8 km^2 (Fig. 45). The floodbasin mainly accumulated clayey alluvium, which provided a substrate for soils to develop in places with low clastic and water input. These soils (vertisols) suggest a low-lying topography and seasonal contrasts in moisture, probably due to prevailing rainfall and/or flood regimes.

Fig. 44: Synthetic lithostratigraphic scheme for the studied areas, with positions of archaeological and fossil sites.

Koobi Fora Formation
(Brown and Feibel, 1986, 1991;
McDougall and Brown, 2006)

Area 130 composite
reference section

Area 133 composite
reference section
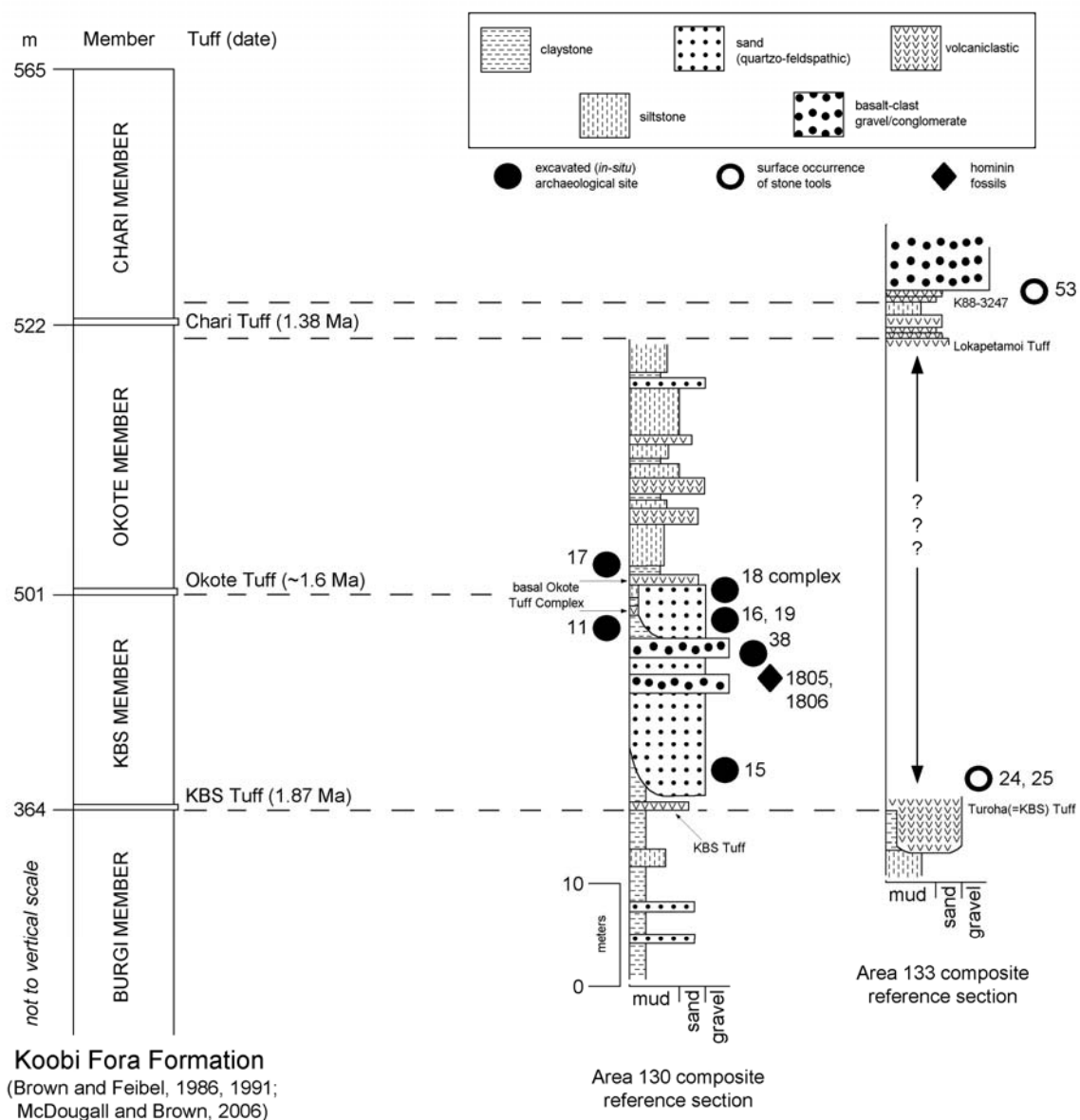
Fig. 45: Paleogeographic cartoon of the north-central Karari Escarpment during the deposition of sediments from the upper Burgi to lower KBS members. The landscape mainly consisted of floodbasins (brown area) and vertisols (type-II paleosols). Locally, a volcaniclastic channel complex (yellow area) was present. Numbered dots are surface occurrences of stone-tool artifacts that might be indicative of *in-situ* archaeological sites from the upper Burgi/lower KBS members. Modern ephemeral streams (thin black lines) and the road (double black line) included for reference.

type-II paleosol

N

1 km
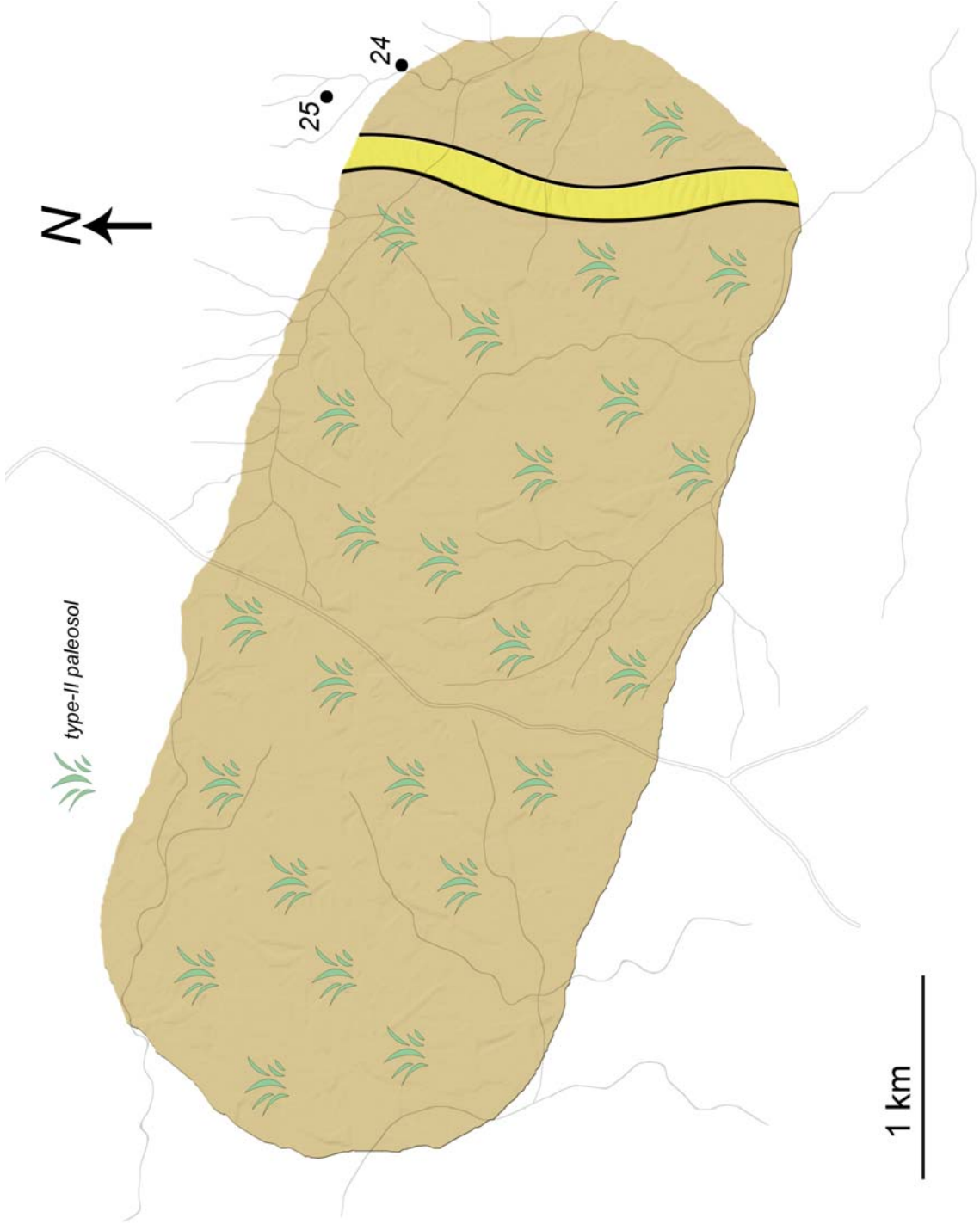
Fine-grained aggradation and pedogenesis was locally arrested in the north/east part of the floodbasin by the influx of coarse volcaniclastics, represented by the deposition of the Turoha(=KBS) Tuff in a channel complex (Figs. 35, 36). The channel delivered ample amounts of pumice and ash to the northern Karari from extra-basin sources, which received reworked and/or primary fallout from erupting volcanoes in the Main Ethiopian Rift (e.g., Brown, 1972). This channel flowed along a generally N/S axis and was ~3 m deep. Size sorting of the volcaniclastics and geochemical data suggest the majority of the sediment derived from the same eruption and accumulated rapidly, perhaps over days or weeks (cf., Mack et al., 1996). The channel complex comprises superimposed basal erosive surfaces and multiple tabular storeys, indicating successive episodes of sediment influx, causing the channel to incise, widen and infill.

White et al. (1981) interpreted lenticular and sheet-like units of sand/tuff locally interstratified with the floodbasin claystones (e.g., LA5b in Figs. 20c, 22) as deposits accumulated through aqueous or aeolian processes within ridge-and-swale topography. An alternate possibility suggested here is they represent deposition on crevasse splays (e.g., Perez-Arlucea and Smith, 1999) that possibly emanated from the channel, or a derivative of it, to the north/east. These splays are thought to have episodically or perhaps periodically inundated the floodbasins when the active channel flooded and spilled over its banks. However, considering the deposits are overwhelming composed of pedogenic-modified claystone, sediment and water delivery from crevassing was likely a

rare event, and the floodbasin landscape was rather dry and occupied by vertic soils. Such a situation suggests crevassing only occurred when overbank floods were exceptionally large, like during the wettest season of an annual rainfall regime, and/or channels were transient temporal-spatial components of the floodbasin landscape.

6.2. Middle-upper KBS Member

Deposits of the middle-upper KBS Member crop out in Area 130. They are represented by coarse lithosomes j_2 and l, in addition to fine lithosomes j_3, l_2, and n_2 (Figs. 11, 26 and 27). Concave-up, channel-form basal surfaces, lithofacies, and cross-sectional geometries indicate the coarse lithosomes are channel bodies with NW/SE trending axes. Considering this and the lateral extents of the lithosomes being at least 2 km, it seems reasonable to assume the channels extended to the east or southeast into paleo-Area 133.

Basal contours on lithosome j_2 suggest channels initially generated a series of incisions up to about 8 m deep into the previous floodbasin landscape (Fig. 46). Channels progressively broadened and shallowed, however, as they infilled. This led the development of unconfined flows and/or flows confined by channel banks with low relief (Fig. 47). The expanded flow also decreased transport potentials and, consequently, caused further channel infilling through the aggradation of fine-grained sediments. Over time, deposition became increasing limited, which culminated with the formation of a calcic soil through a period of at least 1,000 years.

Fig. 46: Paleogeographic cartoon of the north-central Karari Escarpment during an initial episode of deposition for sediments from the middle-upper KBS Member. Depicted is a complex of channels (yellow area) incised through the previous floodbasin landscape from Fig. 45. Numbered dot is archaeological site FxJj 15. Modern ephemeral streams (thin black lines) and the road (double black line) included for reference.
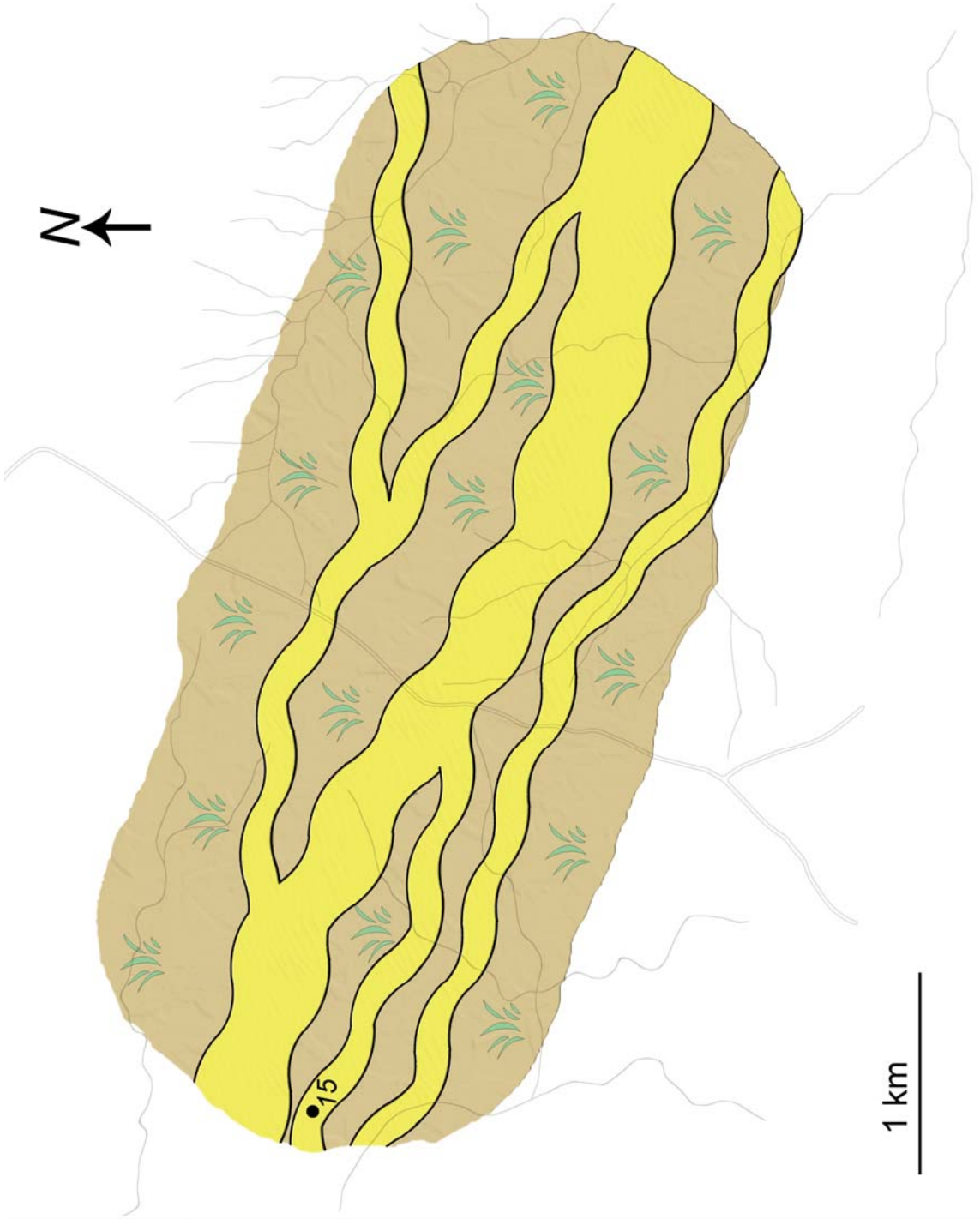
Fig. 47: Paleogeographic cartoon of the north-central Karari Escarpment during a second episode of deposition for sediments from the middle-upper KBS Member. Expansive yellow area represents sandy deposits accumulated by sheet-flow processes. Brown represents areas of the landscape where very-mature calcic soils (type-III paleosols) developed upon fine-grained deposits aggraded within abandoned channel segments. This scene is transitional from the channel-complex paleogeography depicted in Fig. 46. Modern ephemeral streams (thin black lines) and the road (double black line) included for reference.

type-III paleosol

N

1 km
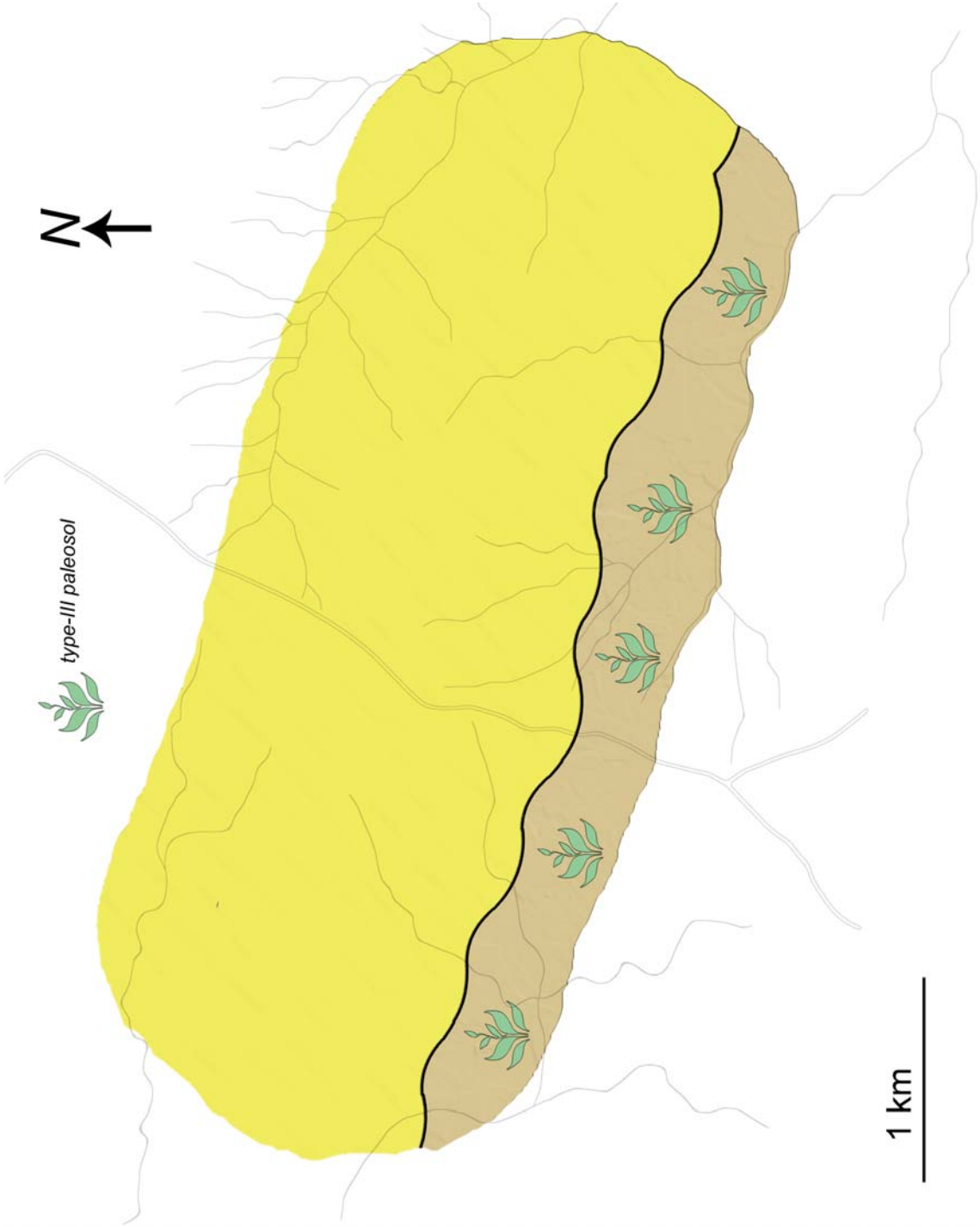
Pedogenesis discontinued with an incursion of coarse clastics delivered from a braided-channel system (Fig. 48) represented by lithosome l. Early influxes of water and sediment seem to have been distributed across a network of shallow channels, partitioned by low-relief bars, before organizing into a system with a large, mid-channel bar complex. As the bar complex grew and blocked entrances, channels were infilled with mud and eventually abandoned (Fig. 49). Calcic soils once again formed on the landscape, and aggradation was limited for at least a few thousand years.

6.3. Upper KBS to lower Okote members

Identified sediments of the upper KBS to lower Okote members crop out in Area 130. They consist of interbedded sands, tuffs, and mudstones (LA5a in Figs. 19, 22 and 25) as well as coarse lithosome m (Figs. 11 and 29). Collectively, these sediments reflect deposition from a meandering channel and associated proximal floodplains (Fig. 50). Orientations of the preserved channel margins suggest a roughly NW/SE paleo-flow axis.

A return of fluvial accumulation to the northern Karari, after limited aggradation on the order of 10^3-10^5 years, is represented by this channel-floodplain system. Since significant deposition did not occur prior to the arrival of the fluvial system, landscapes of the northern Karari may have been topographic lows relative to other nearby areas. As a consequence, the meandering channel avulsed into this setting perhaps because of the exploitable gradient and low rate of aggradation (cf., Mohrig et al., 2000; Slingerland and Smith, 2004). The calcic

Fig. 48: Paleogeographic cartoon of the north-central Karari Escarpment during a third episode of deposition for sediments from the middle-upper KBS Member. Depicted is a braided-channel system developed after the previous landscape from Fig. 47. Numbered dots refer to fossil hominins (KNM-ER 1805 & KNM-ER 1806) and archaeological site (FxJj 38) situated within a channel segment. Modern ephemeral streams (thin black lines) and the road (double black line) included for reference.

N

braid (gravel) bar

38 1806 1805

1 km
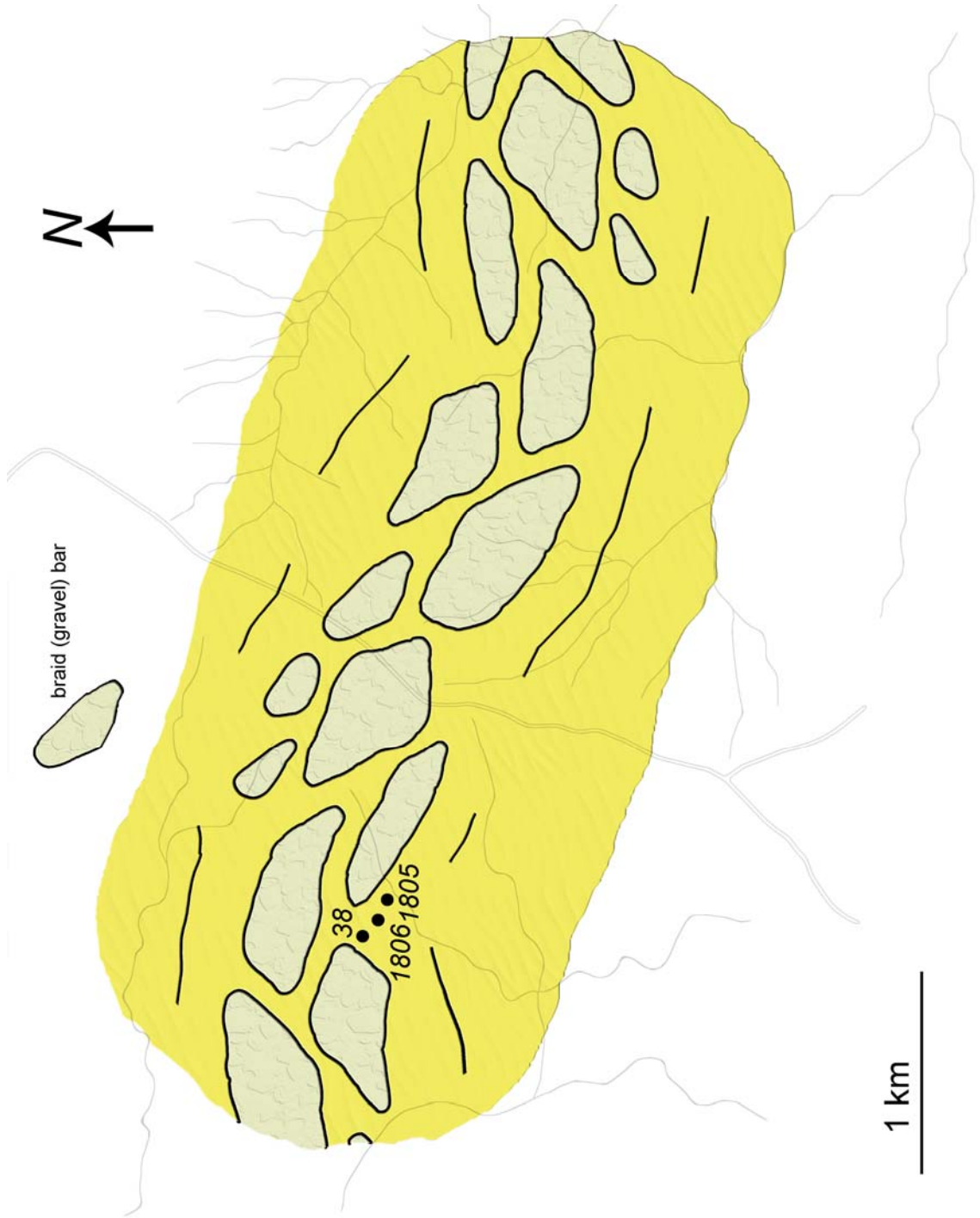
Fig. 49: Paleogeographic cartoon of the northern Karari Escarpment during a fourth episode of deposition for sediments from the middle-upper KBS Member. Expansive brown represents areas of the landscape where very-mature calcic soils (type-III paleosols) developed upon fine-grained deposits accumulated within abandoned channel segments and overbank settings. This scene is transitional from the braided-channel paleogeography depicted in Fig. 48. Numbered dot is archeological site FxJj 11. Modern ephemeral streams (thin black lines) and the road (double black line) included for reference.

type-III paleosol

1 km
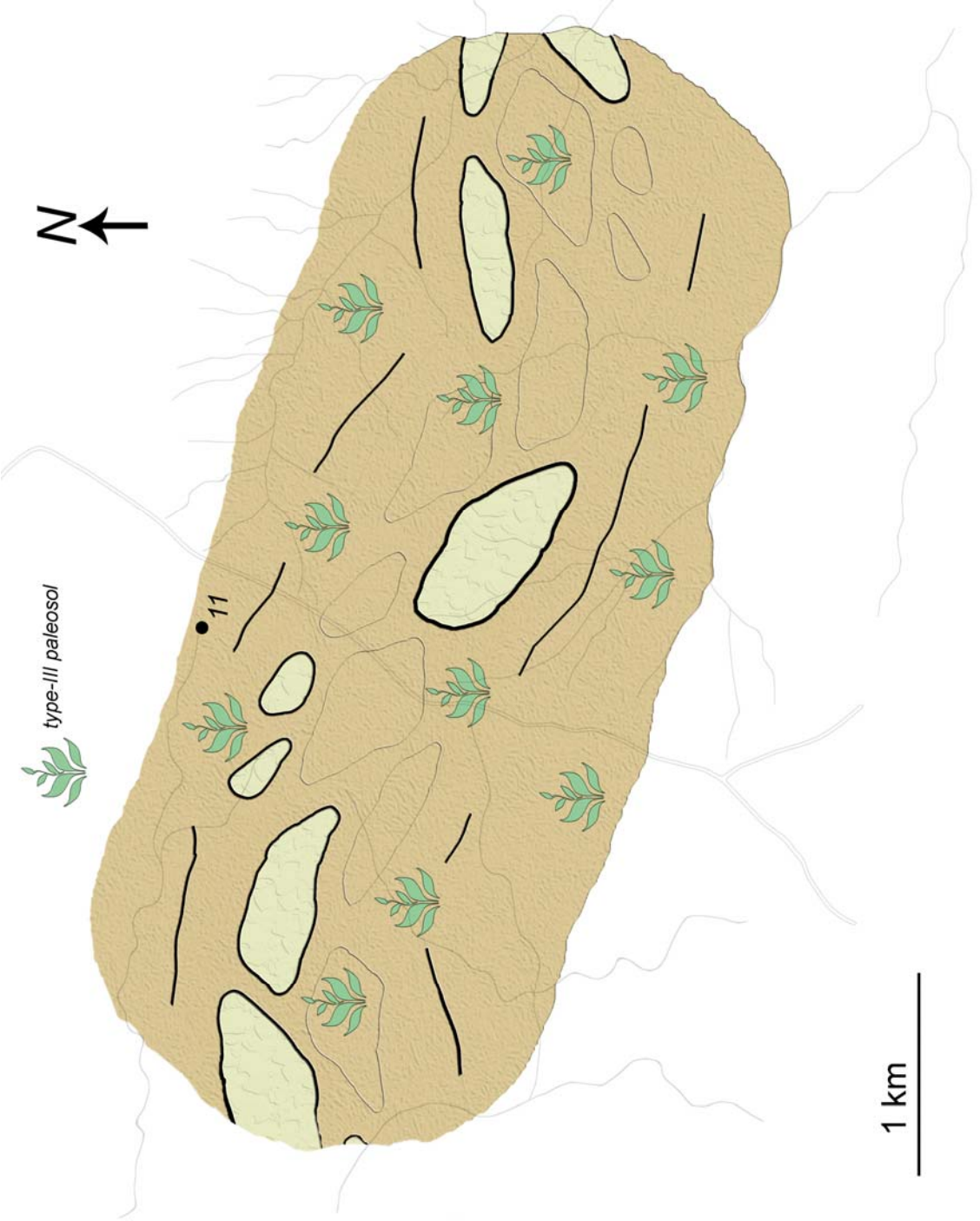
Fig. 50: Paleogeographic cartoon of the northern Karari Escarpment during the deposition of sediments from the upper KBS/lower Okote members. Expansive yellow area represents sandy deposits accumulated by a meandering channel. Brown represents areas where immature soils (type-I paleosols) developed upon fine-grained deposits that were aggraded in overbank settings. Fan-shaped yellow areas are crevasse splays, with associated distributary channels indicated by sinuous black lines. Numbered dots refer to archaeological sites FxJj 16, 17, 18 complex, and 19. Modern ephemeral streams (thin black lines) and the road (double black line) included for reference.

type-I paleosol

1 km
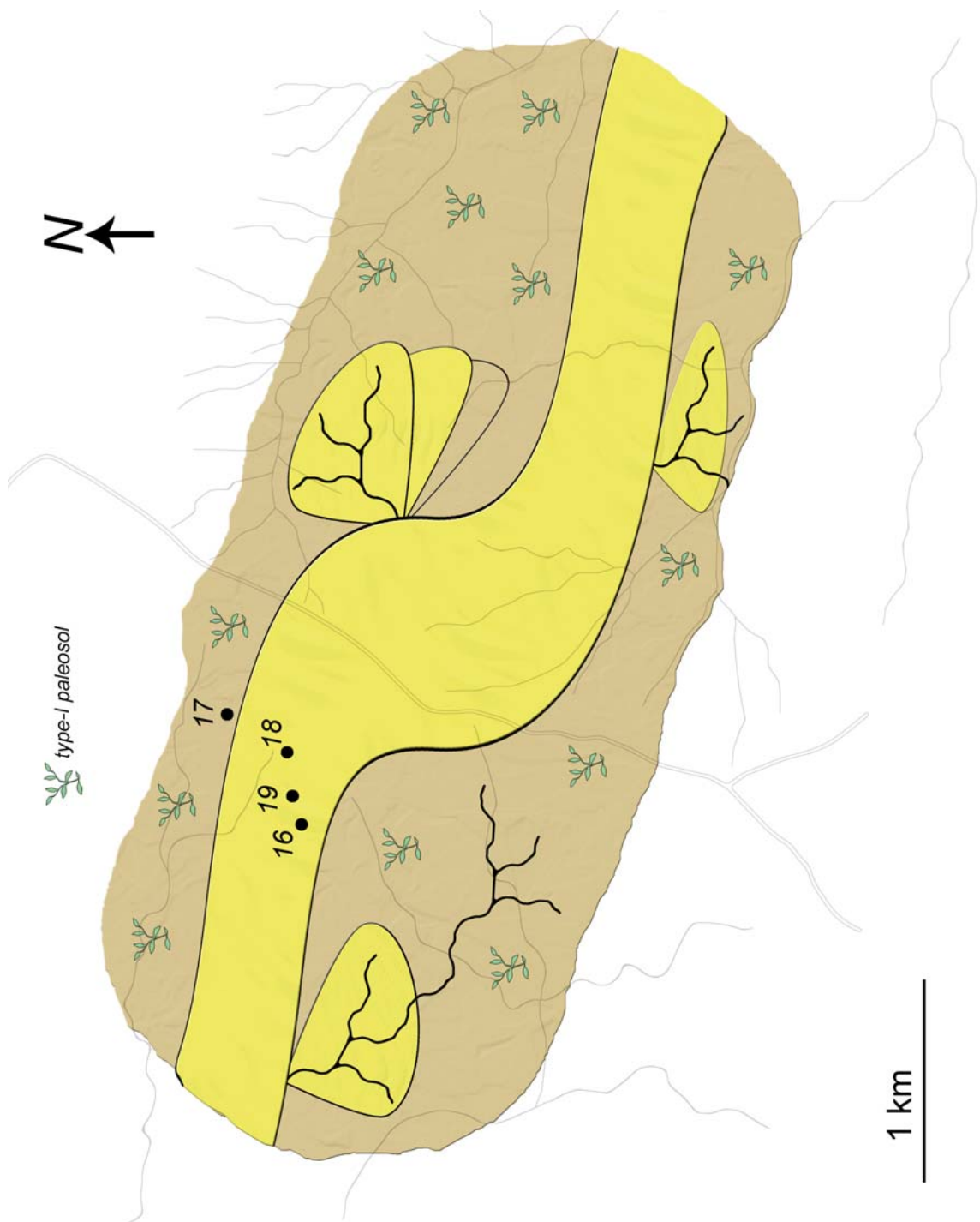
soil (e.g., Fig. 49) that had been previously forming on a slowly aggrading landscape was buried and its pedogenic development was stopped. The meandering channel was erosive, but only incised through the paleosol and older braided-channel deposits for a couple of meters. Adjacent proximal floodplains were wet, but not annually, and aggraded largely through crevasse-splay deposition. Soils developing on the muddier crevasse-splay sediments were poorly drained and formed over a timeframe on the order of 10^0-10^2 years.

6.4. Upper Okote to lower Chari members

The overbank style of sedimentation common to the upper KBS to lower Okote members (Fig. 50) also accumulated the deposits in Area 133 from the upper Okote to lower Chari members. These deposits (see logs 133-32, -47, -50 and -51 in Figs. 31, 32, 37 and 38) consist of fining-upward cycles that represent crevassing at an alluvial ridge, followed by episodes of levee/splay deposition on the adjacent floodplain. Initial deposition was from sheet flows produced by seasonal/annual overbank floods of a channel, which was active at some nearby location. The sheet-flow sediments are commonly massive, coarse and poorly sorted by grain size, possibly resulting from the deposition of extremely concentrated suspension clouds that hamper the formation of normal bedforms (Perez-Arlucea and Smith, 1999; Perez-Arlucea et al., 2000). Under waning flood conditions, low-energy flows were progressively established, ultimately resulting in the fallout of finer grains from quiescent and probably pooled waters. Fine-grained mudstones accumulated by these processes have calcareous

concretions, rhizoliths, and greenish-gray mottles. These features, and otherwise massive fabrics of the mudstones, suggest bioturbation and pedogenesis after deposition.

7. External controls on sedimentation and paleogeography

   7.1. Tectonic setting

The flexural margin of the northeast Turkana Basin is a broad, gently sloping setting. It is composed of a series of titled blocks, developed from antithetic and synthetic faults with small throws (Frostick, 1997). This structure dissects the margin with a number of localized depocenters and topographic highs that influence depositional gradients. However, regional gradients determined by basin-margin to basin-axis depositional slopes were probably also important influences on the Plio-Pleistocene development of northern Karari fluvial systems. Progressive basin margin uplift and axial subsidence due to continued rifting (Gawthorpe and Leeder, 2000) likely positioned the northeast margin of the basin as a highland to some extent. Presumably, this facilitated the transport of sediment and water toward basinward depocenters.

Potential evidence for the tectonic setting influencing sedimentation may come from the basal concave-up surfaces of the coarse lithosomes in Area 130 (Fig. 11) and the volcaniclastic body in Area 133 (Fig. 35). These indicate channel axes were orientated NW/SE and N/S respectively, and thus suggest paleo-flow directions were roughly oblique to each other. A N/S direction is parallel to the overall trend of the basin margin but normal to the Suregei Cuesta (Fig. 3). The NW/SE axis is largely orthogonal to most modern topographic and structural edifices, but inline with the intra-basin low between the Kokoi and Suregei (Fig. 3). There is little doubt, however, these promontories were lower lying (if not absent) during the Plio-Pleistocene. More evidence is therefore

needed to determine if the perceived paleo-flow directions for the channels derive from local conditions or larger-scale controls related to the tectonic setting.

7.2. Base (lake) level

Approximately 25 m of sediment accumulated during the ~300,000 years represented the examined stratigraphic interval of Area 130 (Fig. 9), yielding an aggradation rate of around 8 cm/ka (uncorrected for compaction/hiatuses). Utilizing this sediment accumulation rate and measuring the thickness (10 m) of coarse lithosome j_2 (Fig. 11), an approximate age of 1.8 Ma is determined for the appearance of fluvial channels in the Area 130 section. This age is coeval with a phase of high lake-level variability in northeastern basin (Fig. 6) that is well documented from contemporaneous lake-margin strata of the KBS Member (Brown and Feibel, 1991; Feibel et al., 1991). The arrival of fluvial systems to the northern Karari at nearly the same time as the lake variability may indicate the depositional histories of coarse lithosome j_2 and coarse lithosome l are linked with purported (Lepre et al., 2007) climate-related regressions in lake level of the lower-middle KBS Member. Correlating coarse lithosome m with lake-level changes in the axial basin is more difficult, however, due to poor age control and the high concentration of lake-level cycles in the upper KBS/lower Okote members.

Basal concave-up relief on the j_2 lithosome measures some 8 m (Fig. 26) and resembles that of an incised valley formed due to a fall in base (lake) level (e.g., Shanley and McCabe, 1994). Coarse lithosome l, on the other hand, is less

incised but has a more horizontal basal morphology (Fig. 27). The differences between the two are difficult to explain if they did indeed result for similar processes of lake-level fall. For example, deep valley incision is expected when there is a pronounced difference in the slope gradient of the fluvial plain and the lake margin (Shanley and McCabe, 1994). However, a planar erosive geometry is predicted to form in basin margins during base-level fall and early rise, because these settings are purported to have shallow gradients and low accommodation that inhibit valley incision (Allen and Fielding, 2007).

7.3. Climate

During the Plio-Pleistocene, Sub-Saharan African climate north of the equator was strongly modulated by monsoonal precipitation variations but experienced heightened aridity centered near 1.7 Ma (deMenocal, 2004). This event manifested in East Africa as a changeover from the dominance of C3 plants and trees to C4 grasses occurring at 1.8-1.7 Ma (Cerling, 1992; Wynn, 2004; Quinn et al., 2007). A reduction in woodland cover may have increased runoff and regolith production in the source-area catchments for the northern Karari fluvial systems, leading to enhanced detrital supply (Leeder et al., 1996; Leeder et al., 1998). The more laterally extensive, coarse lithosomes in the lower part of the Area 130 section (Fig. 11) are suggestive of higher sediment-transport capacity and larger channels, which may have arisen as a result of these changing climatic and floral conditions.

Paleosols and vertebrate faunas in the Koobi Fora Formation indicate a semi-arid setting with seasonal contrasts in rainfall (Feibel et al., 1991). Calcic concretions in all of the paleosol types (Fig. 18) formed in dry environments, probably receiving less than 1000 mm of annual precipitation (cf., Retallack, 2001). Vertic features of the paleosols, like wedge-shaped peds and slickensides (Fig. 20) signify seasonal wet/dry phases of an annual climate regime (Gustavson, 1991). The crevasse-splay deposits (Figs. 19, 37) reflect overbank floods likely related to seasonal precipitation variations. Overall, it appears the northern Karari was a dry area periodically emolliated by the rainy phases of the East African monsoon.

7.4. Volcanism

An important control on fluvial sedimentation processes of the northern Karari appears to have been extra-basin volcanism occurring at/near source areas for sediment supplies. Volcaniclastics of the Koobi Fora Formation reflect eruptions related to stages of uplift and extension of the East African Rift System north of the Turkana Basin (Brown, 1972; WoldeGabriel et al., 2005). Evidence of this extra-basin activity comprises the reworked tuffs and pumices accumulated within the fluvial settings of the northern Karari (Brown and Feibel, 1985, 1986, 1991; Brown et al., 2006). This influx of fine-grained volcaniclastic material is thought to have contributed to the formation of coarse lithosome m of the upper KBS/lower Okote members (Fig. 11), in addition to crevasse-splay deposits of the upper KBS/lower Okote members (Figs. 19, 25) and of the upper Okote/lower

Chari members (Fig. 37). In particular, the increased mud-to-sand proportion and channel isolation within fine-grained strata observed for the upper KBS/lower Okote members is interpreted as an outcome of interrelated factors. Initially, the carrying capacity of the channel diminished as the clastic load rapidly enlarged in response to the delivery of copious amounts of unconsolidated, volcanic detritus. This increased the frequency of overbank floods and promoted deposition on crevasse splays within rapidly aggrading proximal floodplains. The high aggradation rate limited the maturation of soils, accounting for the poorly developed paleosols overprinted on the crevasse-splay deposits (Fig. 19).

Also of importance is the Turoha(=KBS) Tuff identified in a volcaniclastic channel deposit from northern Area 133. A number of intrinsic and external factors can contribute to the formation of such deposits (sedimentation rate, grain size, slope, subsidence, climate, etc.; Smith, 1991). Yet, detailed studies (Mack et al., 1996) suggest at the outset they may form in two ways. One is by pyroclastic eruptions that instantaneously inject material downriver by means of a catastrophic surge. Another is when the material rapidly moves downstream after it has burst from a channel obstruction.

8. Summary and conclusions

Detailed sedimentological, paleosol and stratigraphic studies have been carried out in Areas 130 and 133 of Koobi Fora in order to improve the understanding of fluvial systems from the north-central Karari Escarpment and refine the paleogeographic and chronological context of hominin remains from the Koobi Fora Formation. The lower Burgi/upper KBS members, as exposed along the north-central Karari, represent an expansive floodbasin, where vertisols developed over periods lasting 10^2 to 10^3 years. Closer to the basin margin (Area 133), the Turoha(=KBS) Tuff accumulated within a multi-storied channel that incised through the floodbasin landscape along a N/S axis.

Examined deposits of the middle KBS to lower Okote members exposed in Area 130 attain a thickness of >20 m. Based on lithosomes, stacking patterns and paleosols, three separate fluvial deposition systems have been distinguished—two from the middle-upper KBS Member and one from the upper KBS/lower Okote members. Channel axes for all three systems were situated along a roughly NW/SE direction. A first system is recognized from a 10 m thick coarse lithosome overlain by a 5 m thick fine lithosome. The coarse lithosome is incised into floodbasin strata for up to 8 m and a composite of multiple channel fills of varying thicknesses and widths. The fine lithosome reflects aggradation on bar tops, within abandoned channel segments, and at overbank settings. It is largely a claystone deposit overprinted with thick (up to 2 m) calcic paleosols. These ancient soils signify periods of limited aggradation that lasted on the order of 10^3 to 10^5 years. The second system is defined from one coarse lithosome

overlain by two fine lithosomes, collectively reaching a thickness of 5 m. Cross-sectional geometries, lithofacies, and stratigraphic relationships with the fine lithosomes suggest the coarse lithosome is indicative of channel and bar deposits of a braided-river system. Fine lithosomes are remarkable similar to the one from the first system and characterized by comparable depositional processes, environments, and paleosols. Deposits of the third system accumulated after a period of low aggradation lasting for at least 1,000 years. They consists of a ~5 m thick meandering channel lithosome situated within a thick succession of proximal floodplain strata that was mainly accumulated by deposition on crevasse splays. Immature soils overprinted on the crevasse-splay strata developed over periods of 10^0 to 10^2 years.

Along a series of discontinuous exposures in northern Area 133, thin (1-3 m) successions of the upper Okote/lower Chari members crop out. The successions consist of multiple fining-upward cycles of interstratified tuffs, mudstones, and sands that accumulated within proximal-floodplain environments. These depositional patterns suggest that the fluvial trends of the lower Okote Member (ca. 1.6-1.5 Ma) may have continued until at least ~1.4 Ma on the north-central Karari.

Previously excavated archaeological sites and two hominin localities from Area 130 have been placed within environments of the reconstructed fluvial systems. Archaeological site FxJj 11, site FxJj 38, and fossil hominins KNM-ER 1805 and KNM-ER 1806 derived from deposits of the braided-river system of the middle-upper KBS Member. Archaeological sites FxJj 16, FxJj 17, FxJj 18

complex, and FxJj 19 were preserved within the sediments of the meandering channel and floodplain system of the upper KBS/lower Okote members. Paleosol evidence suggests that prior to the arrival of this system, and after the infilling/abandonment of the braided river, the paleolandscape in Area 130 experienced low aggradation for period lasting on the order of 10^3 to 10^5 years. This suggests the upper KBS/lower Okote sites are at least ~1000 years younger than the sites from the middle-upper KBS Member.

The stratigraphic data from northern Area 133 highlight its unexploited nature and potential importance. In particular, surface archaeological occurrences of stone tools may represent indications of *in-situ* sites from the upper Burgi/lower KBS members and the upper Okote/lower Chari members. As compared with other intervals of the Koobi Fora Formation, a relatively small number of stone tool assemblages have been collected from these chronostratigraphic levels (Rogers et al., 1994; Isaac and Behrensmeyer, 1997; Harris et al., 1997). The research presented in this dissertation thus provides a geological framework for increasing the archaeological sample size from relatively old and young stratigraphic intervals of the formation. Future excavation studies in northern Area 133 may help to further document and interpret long-term trends in Plio-Pleistocene hominin behavior within the Turkana Basin (e.g., Rogers et al., 1994; Roche et al., 2003).

Lastly, it appears that a most pervasive extrinsic control on the northern Karari fluvial systems was the climate regime. This paleoclimate involved seasonal wet and dry periods in an otherwise semi-arid setting. Such short-term

changes affected the way soil developed, influenced channel crevassing and thus overbank deposition, and probably elicited a flashy discharge for some channels. Nonetheless, sediment-supply effects from extra-basin volcanic events were also important, as volcaniclastic influxes not only added to the quantity and variability of sedimentary loads but likely also increased rates of overbank aggradation and avulsion frequency. Other factors controlling the observed sedimentary and stratigraphic patterns may have been lake-level shifts and/or heightened aridity at 1.8-1.7 Ma.

APPENDIX 1: raw data of electron microprobe results for major element oxides

(wt.%) of individual glass shards from bulk samples of northern Area 133 tuffs

Sample	Shard	SiO_2	TiO_2	Al_2O_3	FeO	MnO	MgO	CaO	Na_2O	K_2O	Cl
BS202AV	317	74.84	0.15	10.61	2.81	0.02	0.05	0.19	3.66	4.74	0.22
	318	73.17	0.13	10.29	2.69	0.09	0.04	0.17	3.28	4.56	0.28
	319	73.24	0.18	10.58	2.66	0.07	0.05	0.22	3.65	4.68	0.25
	320	75.31	0.21	10.54	3.05	0.13	0.05	0.14	4.09	4.50	0.28
	321	75.63	0.18	10.65	2.69	0.18	0.03	0.16	3.57	4.85	0.21
	322	73.69	0.14	10.68	2.73	0.13	0.05	0.08	3.65	4.88	0.21
	323	74.45	0.15	10.64	2.69	0.12	0.03	0.17	3.90	4.84	0.22
	324	71.98	0.18	10.54	2.71	0.15	0.04	0.21	3.39	4.60	0.23
	325	71.11	0.21	10.49	3.05	0.15	0.03	0.16	4.09	4.72	0.21
	326	75.72	0.18	10.71	2.93	0.12	0.04	0.14	4.06	4.75	0.21
	328	76.60	0.18	10.53	2.86	0.02	0.06	0.15	3.53	5.06	0.19
	329	74.81	0.18	10.59	2.71	0.13	0.07	0.19	3.44	4.80	0.22
	330	74.61	0.19	10.64	2.97	0.06	0.04	0.17	3.70	5.20	0.20
	331	74.80	0.20	10.55	2.67	0.10	0.04	0.16	3.59	4.53	0.21
	332	75.98	0.16	10.55	2.81	0.15	0.04	0.17	3.14	4.94	0.20
	333	74.59	0.11	10.46	2.66	0.09	0.03	0.14	3.22	4.76	0.22
	334	76.16	0.18	10.80	2.95	0.04	0.04	0.18	3.73	4.92	0.18
BS302AV	335	74.07	0.25	10.53	2.69	0.11	0.03	0.18	3.52	4.78	0.21
	336	72.39	0.17	10.53	2.89	0.13	0.05	0.18	4.03	4.40	0.16
	337	70.33	0.13	10.52	2.99	0.12	0.03	0.16	3.46	4.41	0.19
	338	72.77	0.21	10.59	2.79	0.08	0.02	0.15	3.80	4.47	0.21
	339	74.68	0.23	10.62	2.84	0.05	0.03	0.18	3.99	4.69	0.20
	340	75.73	0.14	10.69	2.85	0.06	0.04	0.15	3.44	4.85	0.34
	341	74.92	0.18	10.72	2.98	0.14	0.05	0.19	3.35	4.93	0.16
	342	70.03	0.18	10.50	2.94	0.09	0.01	0.13	4.00	4.44	0.22
	343	70.09	0.18	10.35	2.84	0.05	0.03	0.17	3.58	4.49	0.18
	344	72.44	0.17	10.59	2.95	0.14	0.03	0.20	4.13	4.81	0.24
	345	76.27	0.16	10.80	2.72	0.09	0.03	0.24	4.04	4.80	0.20
	346	73.73	0.12	10.67	2.79	0.13	0.04	0.18	4.03	4.84	0.19
	347	71.04	0.15	10.39	2.66	0.18	0.04	0.16	3.55	4.54	0.27
	348	72.80	0.25	10.48	2.65	0.16	0.03	0.17	4.03	4.46	0.18
	349	72.58	0.19	10.43	2.58	0.07	0.04	0.16	4.13	4.49	0.30
	350	75.01	0.19	10.63	2.89	0.09	0.04	0.17	4.20	4.93	0.24
	351	76.00	0.23	10.77	3.04	0.10	0.04	0.16	3.96	5.17	0.24
	352	75.52	0.19	10.62	3.00	0.06	0.04	0.20	4.12	4.70	0.20
	353	76.47	0.16	10.79	2.86	0.11	0.04	0.16	3.92	4.79	0.22

Sample	Shard	SiO_2	TiO_2	Al_2O_3	FeO	MnO	MgO	CaO	Na_2O	K_2O	Cl
BS402AV	354	70.35	0.36	10.83	2.93	0.14	0.11	0.40	3.86	4.83	0.06
	355	71.43	0.39	11.19	2.96	0.20	0.11	0.36	4.19	4.33	0.10
	356	72.60	0.32	9.29	4.85	0.25	0.00	0.20	3.70	4.59	0.07
	358	72.84	0.18	9.62	3.51	0.07	0.01	0.15	3.73	4.68	0.18
	359	72.25	0.24	9.67	3.67	0.08	0.01	0.11	3.56	4.77	0.19
	362	70.59	0.19	9.63	3.71	0.11	0.04	0.13	3.44	4.63	0.12
	364	69.31	0.15	9.58	3.75	0.14	0.00	0.17	3.49	4.55	0.19
	366	74.95	0.22	10.48	2.75	0.06	0.03	0.28	3.12	4.83	0.11
	369	73.20	0.15	9.86	3.68	0.14	0.00	0.16	2.39	3.74	0.20
	371	70.29	0.23	9.58	3.89	0.13	0.02	0.11	3.31	4.47	0.15
BS502AV	372	73.95	0.12	10.95	1.51	0.10	0.03	0.23	2.89	4.49	0.13
	373	70.06	0.11	10.82	1.54	0.12	0.02	0.25	3.41	4.53	0.17
	375	75.02	0.13	11.07	1.62	0.18	0.04	0.22	3.03	4.85	0.14
	376	71.69	0.07	11.00	1.50	0.13	0.03	0.16	3.30	4.56	0.10
	377	71.35	0.13	10.93	1.49	0.04	0.03	0.21	3.60	4.30	0.14
	378	69.27	0.13	10.87	1.47	0.14	0.03	0.21	3.13	3.43	0.17
	379	72.02	0.10	11.02	1.53	0.09	0.04	0.20	3.20	4.51	0.18
	380	73.66	0.11	11.24	1.64	0.10	0.05	0.26	3.74	4.63	0.16
	381	74.11	0.11	10.96	1.54	0.05	0.04	0.19	3.09	4.62	0.16
	382	69.30	0.14	10.70	1.53	0.02	0.04	0.16	3.41	3.80	0.12
	383	68.60	0.20	10.80	1.61	0.13	0.03	0.17	3.41	4.53	0.12
	385	68.35	0.14	10.65	1.58	0.07	0.03	0.17	3.04	4.09	0.16
BS702AV	387	71.82	0.16	10.60	2.82	0.10	0.03	0.19	3.76	4.63	0.18
	388	73.91	0.24	10.50	2.77	0.08	0.03	0.18	3.58	4.88	0.23
	389	74.52	0.16	10.64	2.94	0.09	0.05	0.15	4.28	4.77	0.23
	390	74.19	0.21	10.75	2.74	0.11	0.05	0.17	4.05	4.68	0.25
	391	72.65	0.24	10.55	2.74	0.09	0.02	0.19	3.66	4.44	0.21
	392	74.19	0.16	10.67	2.79	0.08	0.03	0.17	3.92	4.95	0.20
	393	72.72	0.20	10.51	2.93	0.08	0.04	0.15	3.75	4.66	0.23
	394	72.94	0.13	10.69	3.00	0.00	0.02	0.14	4.31	4.62	0.20
	395	73.34	0.10	10.65	2.77	0.18	0.02	0.18	4.13	4.58	0.18
	396	73.35	0.24	10.72	2.81	0.13	0.04	0.16	4.13	4.62	0.20
	397	73.14	0.17	10.70	2.89	0.02	0.02	0.18	4.40	4.60	0.23
	398	70.40	0.13	10.36	2.72	0.07	0.04	0.16	3.85	4.07	0.25
	399	72.88	0.20	10.50	2.83	0.11	0.03	0.20	4.07	4.62	0.26
	400	74.03	0.25	10.62	2.76	0.09	0.05	0.16	4.25	4.59	0.19
	401	73.03	0.21	10.48	2.74	0.13	0.04	0.14	4.00	4.53	0.19
	402	73.72	0.23	10.62	2.92	0.08	0.05	0.20	4.18	4.79	0.23
	403	72.02	0.23	10.47	2.77	0.13	0.03	0.16	4.02	4.40	0.25

Sample	Shard	SiO_2	TiO_2	Al_2O_3	FeO	MnO	MgO	CaO	Na_2O	K_2O	Cl
BS1202AV	404	73.07	0.19	10.59	2.74	0.06	0.04	0.16	4.04	4.38	0.16
	405	72.17	0.17	10.63	2.67	0.12	0.04	0.14	3.37	4.40	0.21
	406	70.61	0.15	10.35	2.72	0.16	0.03	0.19	4.09	4.32	0.16
	407	71.24	0.20	10.41	2.78	0.14	0.03	0.19	4.01	4.50	0.18
	408	70.87	0.23	10.42	2.72	0.10	0.05	0.15	4.12	4.71	0.26
	409	69.89	0.22	10.39	2.75	0.10	0.04	0.16	4.38	4.45	0.25
	410	67.49	0.25	10.22	2.66	0.11	0.03	0.15	3.72	4.43	0.26
	411	71.61	0.14	10.55	2.77	0.07	0.05	0.18	3.47	4.43	0.23
	412	71.70	0.19	10.52	2.61	0.13	0.03	0.16	3.76	4.56	0.19
	413	69.24	0.20	10.32	2.79	0.12	0.04	0.12	3.79	4.48	0.22
	414	71.67	0.18	10.59	2.99	0.09	0.02	0.18	4.02	4.70	0.22
	416	70.24	0.19	10.46	2.74	0.09	0.05	0.15	3.48	4.46	0.20
	417	71.97	0.09	10.55	2.73	0.11	0.05	0.14	3.28	4.49	0.22

APPENDIX 2: geographic provenance for hominin remains and studied outcrops

Area	Place	GPS Coordinates	
105	FxJj 1	4° 4.320'N	36° 21.840'E
105	FxJj 3	4° 3.701'N	36° 21.997'E
118	FxJj 10	4° 5.004'N	36° 22.773'E
130	CJL04-130-1 (top)	4° 11.110'N	36° 26.262'E
130	CJL04-130-2z (base)	4° 11.155'N	36° 26.044'E
130	CJL04-130-12 (top)	4° 10.900'N	36° 26.035'E
130	CJL04-130-22 (top)	4° 10.809'N	36° 25.801'E
130	CJL04-130-16 (top)	4° 10.748'N	36° 25.636'E
130	CJL04-130-97 (top)	4° 10.674'N	36° 25.450'E
130	FxJj 11	4° 11.126'N	36° 26.186'E
130	FxJj 15	4° 10.868'N	36° 25.537'E
130	FxJj 16	4° 10.746'N	36° 25.616'E
130	FxJj 17	4° 10.985'N	36° 25.976'E
130	FxJj 18	4° 10.847'N	36° 25.937'E
130	FxJj 19	4° 10.763'N	36° 25.671'E
130	FxJj 38	4° 10.545'N	36° 25.460'E
130	KNM-ER 1805	4° 10.538'N	36° 25.505'E
130	KNM-ER 1806	4° 10.553'N	36° 25.495'E
131	FxJj 20	4° 9.150'N	36° 24.937'E
133	CJL01-133-5	4° 10.431'N	36° 27.825'E
133	CJL01-133-6	4° 10.621'N	36° 27.724'E
133	CJL01-133-11	4° 10.692'N	36° 27.190'E
133	CJL01-133-22	4° 10.589'N	36° 27.342'E
133	CJL01-133-26	4° 10.006'N	36° 27.983'E
133	CJL01-133-28	4° 10.537'N	36° 27.436'E
133	CJL01-133-32	4° 10.009'N	36° 26.441'E
133	CJL01-133-34	4° 10.437'N	36° 27.708'E
133	CJL01-133-35	4° 9.013'N	36° 27.644'E
133	CJL01-133-36	4° 9.397'N	36° 27.158'E
133	CJL01-133-37	4° 9.471'N	36° 27.001'E
133	CJL01-133-41	4° 9.453'N	36° 26.932'E
133	CJL01-133-42	4° 9.449'N	36° 26.931'E
133	CJL01-133-43	4° 9.463'N	36° 26.902'E
133	CJL01-133-47	4° 9.579'N	36° 26.631'E
133	CJL01-133-50	4° 9.818'N	36° 26.422'E
133	CJL01-133-51	4° 9.831'N	36° 26.389'E
133	FxJj 23	4° 10.315'N	36° 28.565'E
133	FxJj 24	4° 10.451'N	36° 27.813'E

Area	Place	GPS Coordinates	
133	FxJj 25	4° 10.649'N	36° 27.671'E
133	FxJj 26	4° 10.950'N	36° 27.230'E
133	FxJj 27	4° 9.745'N	36° 26.097'E
133	FxJj 28	4° 10.921'N	36° 27.471'E
133	FxJj 29	4° 9.963'N	36° 27.096'E
133	FxJj 53	4° 9.873'N	36° 26.478'E

REFERENCES CITED

1.   Abell, P. I., Awramik, S. M., Osborne, R. H. and Tomellini, S., 1982. Plio-Pleistocene lacustrine stromatolites from Lake Turkana, Kenya: morphology, stratigraphy and stable isotopes. Sedimentary Geology 32, 1-26.

2.   Ahmad, N., 1983. Vertisols. In: Wilding, L. P., Smeck, N. E. and Hall, G. F. (Eds.), Pedogenesis and Soil Taxonomy II: The Soil Orders. Developments in Soil Science 11B, 91-123.

3.   Aitken, J.F. and Flint, S.S., 1995. The application of high-resolution sequence stratigraphy to fluvial systems: a case study from the Upper Carboniferous Breathitt Group, eastern Kentucky, USA. Sedimentology 42, 3 -30.

4.   Allen, J.R.L., 1983. Studies in fluviatile sedimentation: bars, bar complexes and sandstone sheets (low-sinuosity braided streams) in the Brownstones (L. Devonian), Welsh Borders. Sedimentary Geology 33, 237-293.

5.   Allen, P. A., Cabrera, L., Colombo, F. and Matter, A., 1983. Variations in fluvial style on the Eocene-Oligocene alluvial fan of the Scala Dei Group, SE Ebro Basin, Spain. Journal of the Geological Society of London 140, 133-146.

6.   Allen, J.P. and Fielding, C.R., 2007. Sedimentology and stratigraphic architecture of the Late Permian Betts Creek Beds, Queensland, Australia. Sedimentary Geology 202, 5-34.

7.   Asfaw, B., Beyene, Y., Suwa, G., Walter, R.C., White, T.D., WoldeGabriel, G. and Yemane, T., 1992. The earliest Acheulean from Konso-Gardula. Nature 360, 732-735.

8.   Ashley, G.M., 1990. Classification of large-scale subaqueous bedforms: a new look at an old problem. Journal of Sedimentary Petrology 60, 160-172.

9.   Ashworth, P.J., Best, J.L., Roden, J., Bristow, C.S. and Klaassen, G.J., 2000. Morphological evolution and dynamics of a large, sand braid-bar, Jamuna River, Bangladesh. Sedimentology 47, 533-555.

10.   Behrensmeyer, A.K., 1970. Preliminary geologic interpretation of a new hominid site in the Lake Rudolf basin. Nature 226, 225-226.

11.   Bennett, S.J. and Bridge, J.S., 1995. An experimental study of flow, bedload transport and bed topography under conditions of erosion and deposition and comparison with theoretical models. Sedimentology 42, 117-146.

12.   Best, J.L., Ashworth, P.J., Bristow, C.S. and Roden, J., 2003. Three-dimensional sedimentary architecture of a large, mid-channel sand braid bar, Jamuna River, Bangladesh. Journal of Sedimentary Research 73, 516-530.

13.   Blair, T.C., 1987. Sedimentary processes, vertical stratification sequences, and geomorphology of the Roaring River alluvial fan, Rocky Mountain National Park, Colorado. Journal of Sedimentary Petrology 57, 1-18.

14. Blair, T.C. and Bilodeau, W.L., 1988. Development of tectonic cyclothems in rift, pull-apart, and foreland basins: sedimentary response to episodic tectonism. Geology 16, 517-520.

15. Blair, T. and McPherson, J., 1994. Alluvial fans and their natural distinction from rivers based on morphology, hydraulic processes, sedimentary processes and facies assemblages. Journal of Sedimentary Research 64, 450-489.

16. Bluck, B.J., 1980. Structure, generation and preservation of upward fining, braided stream cycles in the Old Red Sandstone of Scotland. Transactions of the Royal Society of Edinburgh 71, 29-46.

17. Boothroyd, J.C. and Ashley, G.M., 1975. Process, bar morphology and sedimentary structures on braided outwash fans, North-eastern Gulf of Alaska. In: Jopling, A.V. and McDonald, B.C. (Eds.), Glaciofluvial and Glaciolacustrine Sedimentation. Society of Economic Paleontologists and Mineralogists Special Publication 23, 193-222.

18. Borchardt, G.A., Aruscavage, P.J. and Millard Jr., H.T., 1972. Correlation of the Bishop Ash, a Pleistocene marker bed, using instrumental neutron activation analysis. Journal of Sedimentary Petrology 42, 301-306.

19. Bowen, B.E. and Vondra, C.F., 1973. Stratigraphical relationships of the Plio-Pleistocene deposits, East Rudolf, Kenya. Nature 242, 391-393.

20. Bown, T.M. and Kraus, M.J., 1987. Integration of channel and floodplain suites in aggrading fluvial systems I: Developmental sequence and lateral

relations of lower Eocene alluvial paleosols, Willwood Formation, Bighorn Basin, Wyoming. Journal of Sedimentary Petrology 57, 587-601.

21.   Braun, D.R., Rogers, M.J., Harris, J.W.K. and Walker, S.J., 2008. Landscape-scale variation in hominin tool use: Evidence from the Developed Oldowan. Journal of Human Evolution 55, 1053-1063.

22.   Bridge, J.S., 1985. Paleochannel patterns inferred from alluvial deposits: a critical evaluation. Sedimentology 55, 579-589.

23.   Bridge, J.S., 1993a. Description and interpretation of fluvial deposits: a critical perspective. Sedimentology 40, 801-810.

24.   Bridge, J.S., 1993b. The interaction between channel geometry, water flow, sediment transport and deposition in braided rivers. In: Best, J.L. and Bristow, C.S. (Eds.), Braided Rivers. Geological Society of London Special Publication 75, 13-71.

25.   Bridge, J.S., 2003. Rivers and Floodplains: Forms, Processes and Sedimentary Record. Blackwell Science, Oxford.

26.   Bridge, J.S., Smith, N.D., Trent, F., Gabel, L. and Bernstein, P., 1986. Sedimentology and morphology of a low-sinuosity river: Calamus River, Nebraska Sand Hills. Sedimentology 33, 851-870.

27.   Brierley, G.J., 1996. Channel morphology and element assemblages: a constructivist approach to facies modeling. In: Carling, P.A. and Dawson, M.R. (Eds.), Advances in Fluvial Dynamics and Stratigraphy. Wiley and Sons, New York, pp. 263-298.

28. Bristow, C.S., 1987. Brahmaputra River: channel migration and deposition. In: Ethridge, F.G., Flores, R.M. and Harvey, M.D. (Eds.), Recent Developments in Fluvial Sedimentology. Society of Economic Paleontologists and Mineralogists Special Publication 39, 63-74.

29. Bristow, C.S. 1996. Reconstructing fluvial channel morphology from sedimentary sequences. In: Carling, P.A. and Dawson, M.R. (Eds.), Advances in Fluvial Dynamics and Stratigraphy. Wiley and Sons, New York, pp. 351-371.

30. Bristow, C.S. and Best, J.L., 1993. Braided rivers: perspectives and problems. In: Best, J.L. and Bristow, C.S. (Eds.), Braided Rivers. Geological Society of London Special Publication 75, 1-11.

31. Bristow, C.S., Skelly, R.L. and Ethridge, F.G., 1999. Crevasse splays from the rapidly aggrading, sand-bed, braided Niobrara River, Nebraska: effect of base-level rise. Sedimentology 46, 1029-1047.

32. Brown, F.H., 1972. Radiometric dating of sedimentary formations in the lower Omo Valley, southern Ethiopia. In: Bishop, W.W. and Miller, J.A. (Eds.), Calibration of Hominid Evolution. Scottish Academic Press, Edinburgh, pp. 273–287.

33. Brown, F.H., 1995. The potential of the Turkana Basin for paleoclimatic reconstruction in East Africa. In: Vrba, E.S., Denton, G.H., Partridge, T.C. and Burckle, L.H. (Eds.), Paleoclimate and evolution with emphasis on human origins. Yale University Press, New Haven, pp. 319-330.

34. Brown, F.H. and Feibel, C.S., 1985. Stratigraphic notes on the Okote Tuff Complex at Koobi Fora. Nature 316, 794-797.

35. Brown, F.H. and Feibel, C.S., 1986. Revision of the lithostratigraphic nomenclature in the Koobi Fora Region, Kenya. Journal of the Geological Society of London 143, 297-310.

36. Brown, F.H. and Feibel, C.S., 1991. Stratigraphy, depositional environments and palaeogeography of the Koobi Fora Formation. In: Harris, J.M. (Ed.), Koobi Fora Research Project Volume 3: stratigraphy, artiodactyls and palaeoenvironments. Clarendon Press, Oxford, pp. 1-30.

37. Brown, F.H. and Gathogo, P.G., 2002. Stratigraphic Relation between Lokalalei 1A and Lokalalei 2C, Pliocene Archaeological Sites in West Turkana, Kenya. Journal of Archaeological Science 29, 699-702.

38. Brown, F.H., Haileab, B. and McDougall, I., 2006. Sequence of tuffs between the KBS Tuff and the Chari Tuff in the Turkana Basin, Kenya and Ethiopia. Journal of Geological Society of London 163, 185-204.

39. Brown, F.H., Sarna-Wojcicki, A.M., Meyer, C.E. and Haileab, B., 1992. Correlation of Pliocene and Pleistocene tephra layers between the Turkana Basin of East Africa and the Gulf of Aden. Quaternary International 13-14, 55-67.

40. Bull, W.B., 1972. Recognition of alluvial fan deposits in the stratigraphic record. In: Rigby, J.K. and Hamblin, W.K. (Eds.), Recognition of Ancient Sedimentary Environments. Society of Economic Paleontologists and Mineralogists Special Publication 16, 63-83.

41. Bunn, H.T., 1981. Archaeological evidence for meat-eating by Plio-Pleistocene hominids from Koobi Fora and Olduvai Gorge. Nature 291, 574-577.

42. Bunn, H.T., 1994. Early Pleistocene hominid foraging strategies along the ancestral Omo River at Koobi Fora, Kenya. Journal of Human Evolution 27, 247-266.

43. Burggraf, D.R., Jr., White, H.J., Frank, H.J. and Vondra, C.F., 1981. Hominid habitats in the Rift Valley Part 2. In: Rapp, G. and Vondra, C.F. (Eds.), Hominid sites: their geologic settings. Westview Press, Boulder, pp. 115-147.

44. Cant, D. J. and Walker, R. G., 1978. Fluvial processes and facies sequences in the sandy braided South Saskatchewan River, Canada. Sedimentology 25, 625-646.

45. Cerling, T.E., 1992. Development of grasslands and savannas in east Africa during the Neogene. Palaeogeography, Palaeoclimatology, Palaeoecology 97, 241-247.

46. Cerling, T. E. and Brown, F.H., 1982. Tuffaceous marker horizons in the Koobi Fora region and the Lower Omo Valley. Nature 299, 216-221.

47. Chorowicz, J., 2005. The East African rift system. Journal of African Earth Sciences 43, 379-410.

48. Collinson, J.D., 1970. Bedforms of the Tana River, Norway. Geografiska Annaler 52A, 31-56.

49. Collinson, J.D. and Thompson, D.B., 1989. Sedimentary Structures (2nd edition). Unwin Hyman, London.

50. Davies, D. K., Vessell, R. K., Miles, R. C., Foley, M. G. and Bonis, S. B., 1978. Fluvial transport and downstream sediment modification in an active volcanic region. In: Miall, A.D. (Ed.), Fluvial Sedimentology. Canadian Society of Petroleum Geologists Memoir 5, 61-84.

51. Davies-Vollum, K.S. and Wing, S.L., 1998. Sedimentological, taphonomic, and climatic aspects of Eocene swamp deposits (Willwood Formation Bighorn Basin, Wyoming). Palaios 13, 28-40.

52. de Heinzelin, J., 1983. The Omo Group. Musée Royal de l'Afrique Centrale, Tervuren, Belgique: Annales, Série 8°, Sciences Géologiques 85.

53. Deluca, J.L. and Eriksson, K.A., 1989. Controls on synchronous ephemeral- and perennial-river sedimentation in the middle sandstone member of the Triassic Chinle Formation, northeastern New Mexico, U.S.A. Sedimentary Geology 61, 155-175.

54. deMenocal, P.B., 2004. African climate change and faunal evolution during the Pliocene-Pleistocene. Earth and Planetary Science Letters 220, 3-24.

55. Dreyer, T., 1993. Quantified fluvial architecture in ephemeral stream deposits of the Esplugafreda Formation (Palaeocene), Tremp-Graus Basin, northern Spain. In: Marzo, M. and Puigdefabregas, C. (Eds.),

Alluvial sedimentation. Special Publication of the International Association of Sedimentologists 17, 337-362.

56. Dunkelman, T.J., Karson, J.A. and Rosendahl, B.R., 1988. Structural style of the Turkana Rift, Kenya. Geology 16, 258-261.

57. Ebinger, C.J., Yemane, T., Harding, D.J., Tesfaye, S., Kelley, S. and Rex, D.C., 2000. Rift deflection, migration, and propagation; linkage of the Ethiopian and Eastern rifts, Africa. Geological Society of America Bulletin 112, 163-176.

58. Eynon, G. and Walker, R.G., 1974. Facies relationships in Pleistocene outwash gravels, southern Ontario: a model for bar growth in braided rivers. Sedimentology 21, 43-70.

59. Farrell, K.M., 1987. Sedimentology and facies architecture of over-bank deposits of the Mississippi River, False River region, Louisiana. In: Ethridge, F.G., Flores, R.M. and Harvey, M.D. (Eds.), Recent Developments in Fluvial Sedimentology. Society of Economic Paleontologists and Mineralogists Special Publication 39, 111-120.

60. Feibel, C.S., 1994. Freshwater stingrays from the Plio-Pleistocene of the Turkana Basin, Kenya and Ethiopia. Lethaia 26, 359-366.

61. Feibel C. S., 1997. Debating the environmental factors in hominid evolution. GSA Today 7, 1-7.

62. Feibel, C.S., 1999. Tephrostratigraphy and geological context in paleoanthropology. Evolutionary Anthropology 8, 87-100.

63. Feibel, C.S. and Brown, F.H., 1986. Depositional history of the Koobi Fora Formation, northern Kenya. In: Proceedings of the Second Conference on the Geology of Kenya.

64. Feibel, C.S. and Brown, F.H. 1993. Microstratigraphy and paleoenvironments. In: Walker, A. and Leakey, R. (Eds.), The Nariokotome *Homo erectus* Skeleton. Harvard University Press, Cambridge, pp. 21-39.

65. Feibel, C.S., Brown, F.H. and McDougall, I., 1989. Stratigraphic context of fossil hominids from the Omo Group deposits, northern Turkana Basin, Kenya and Ethiopia. American Journal of Physical Anthropology 78, 595-622.

66. Feibel, C.S., Harris, J.M. and Brown, F.H., 1991. Neogene palaeoenvironments of the Turkana Basin. In: Harris, J.M. (Ed.), Koobi Fora Research Project Volume 3: stratigraphy, artiodactyls and palaeoenvironments. Claredon, Oxford, pp. 321-370.

67. Findlater, I. C., 1978. Stratigraphy. In: Leakey, M. G. and Leakey, R. E. (Eds.), Koobi Fora Eesearch Project Volume 1: The fossil hominids and an introduction to their context, 1968-1974. Clarendon Press, Oxford, pp. 14-31.

68. Fisher, J.A., Nichols, G.J. and Waltham, D.A., 2007. Unconfined flow deposits in distal sectors of fluvial distributary systems: Examples from the Miocene Luna and Huesca Systems, northern Spain. Sedimentary Geology 195, 55-73.

69. Fitch, F.J., Hooker, P.J., Miller, J.A., Mitchell, T.G. and Watkins, R.T., 1985. Reconnaissance potassium-argon geochronology of the Suregei-Asille district, northern Kenya. Geological Magazine 122, 609-22.

70. Frank, H.J., 1976. Stratigraphy of the upper member, Koobi Fora Formation, northern Karari Escarpment, East Turkana Basin, Kenya. M.S. Thesis, Iowa State University.

71. Friend, P. F., Slater, M. J. and Williams, R. C., 1979. Vertical and lateral building of river sandstone bodies, Ebro Basin, Spain. Journal of the Geological Society of London 136, 39-46.

72. Frostick, L. E. and Reid, I., 1980. Sorting mechanisms in coarse-grained alluvial sediments: fresh evidence from a basalt plateau gravel, Kenya. Journal of the Geological Society 137, 431-441.

73. Frostick, L.E. and Reid, I., 1990. Structural control of sedimentation patterns and implications for the economic potential of the East African rift basins. Journal of African Earth Science 10, 307-318.

74. Frostick, L. E., 1997. The East African Rift basins. In: Selley, R. C. (Ed.), Sedimentary Basins of the World 3: African Basins. Elsevier, Amsterdam, pp. 187-209.

75. Gawthorpe, R.L. and Leeder, M.R., 2000. Tectono-sedimentary evolution of active extensional basins. Basin Research 12, 195-218.

76. Gile, L.H., Hawley, J.W. and Grossman, R.B., 1981. Soils and geomorphology in the Basin and Range area of southern New Mexico—

Guidebook to the Desert Project. New Mexico Bureau Mines and Mineral Resources Memoir 39.

77. Gustavson, T.C., 1978. Bed forms and stratification types of modern gravel meander lobes, Nueces River, Texas. Sedimentology 25, 401-426.

78. Gustavson, T.C., 1991. Arid basin depositional systems and paleosols: Fort Hancock and Camp Rice Formations (Pliocene–Pleistocene), Hueco Bolson, west Texas and adjacent Mexico. Texas Bureau of Economic Geology Report of Investigations 198.

79. Haileab, B., Brown, F.H., McDougall, I. and Gathogo, P.N., 2004. Gombe Group basalts and initiation of Pliocene deposition in the Turkana Depression, northern Kenya and southern Ethiopia. Geological Magazine 141, 41-53.

80. Haile-Selassie, Y., 2001. Late Miocene hominids from the Middle Awash, Ethiopia. Nature 412, 178-181.

81. Harms, J.C., Southard, J.B., Spearing, D.R. and Walker, R.G., 1982. Structures and sequences in clastic rocks. Society of Economic Paleontologists and Mineralogists Short Course 9.

82. Harris, J.M., 1983. Koobi Fora Research Project Volume 2: The Fossil Ungulates: proboscidea, perissodactyla and suidae. Clarendon Press, Oxford.

83. Harris, J.M., Brown, F.H. and Leakey, M.G., 1988. Stratigraphy and paleontology of Pliocene and Pleistocene localities west of Lake Turkana, Kenya. Contributions in Science 399, 1-128.

84. Harris, J.W.K., 1997. Appendix 3A. In: Isaac, G.L. and Isaac, B. (Eds.), Koobi Fora Research Project Volume 5: Plio-Pleistocene Archaeology. Clarendon Press, Oxford, pp. 111-113.

85. Harris, J.W.K,, Isaac, G.L. and Kaufulu, Z.M., 1997. Sites in the upper KBS, Okote, and Chari Members: reports. In: Isaac, G.L. and Isaac, B. (Eds.), Koobi Fora Research Project Volume 5: Plio-Pleistocene Archaeology. Clarendon Press, Oxford, pp. 115-223.

86. Haszeldine, R.S., 1983. Fluvial bars reconstructed from a deep, straight channel, upper Carboniferous coalfield of Northeast England. Journal of Sedimentary Research 53, 1233-1247.

87. Hay, R.L., 1976. Geology of the Olduvai Gorge. University of California Press, Berkeley.

88. Hein, F.J. and Walker, R.G., 1977. Bar evolution and development of stratification in the gravelly, braided Kicking Horse River, British Columbia. Canadian Journal of Earth Sciences 14, 562-570.

89. Heller, P.L. and Paola, C., 1996. Downstream changes in alluvial architecture: an exploration of controls on channel-stacking patterns. Journal of Sedimentary Research 66, 297-306.

90. Hillhouse, J. W., Ndombi, J. W. M., Cox, A. and Brock, A., 1977. Additional results on palaeomagnetic stratigraphy of the Koobi Fora Formation, east of Lake Turkana (Lake Rudolf), Kenya. Nature 265, 411-415.

91. Hillhouse, J.W., Cerling, T.E. and Brown, F.H., 1986. Magnetostratigraphy of the Koobi Fora Formation, Lake Turkana, Kenya. Journal of Geophysical Research 91, 11581-11595.

92. Hjellbakk, A., 1997. Facies and fluvial architecture of a high-energy braided river: the upper Proterozoic Seglodden Member, Baranger Peninsula, northern Norway. Sedimentary Geology 114, 131-161.

93. Holbrook, J., 2001. Origin, genetic interrelationships, and stratigraphy over the continuum of fluvial channel-form bounding surfaces: an illustration from Middle Cretaceous strata, southeastern Colorado. Sedimentary Geology 144, 179-222.

94. Howell, F.C., Haeserts, P. and de Heinzelin, J., 1987. Depositional environments, archaeological occurrences and hominids from members E and F of the Shungura Formation (Omo basin, Ethiopia). Journal of Human Evolution 16, 665-700.

95. Isaac, G.L., 1978. Food sharing and human evolution: Archaeological evidence from the Plio-Pleistocene of East Africa. Journal of Anthropological Research 43, 311-325.

96. Isaac, G.L., 1984. The archaeology of human origins: studies of the Lower Pleistocene in East Africa, 1971–1981. Advances in World Archaeology 3, 1-87.

97. Isaac, G.L. and Harris, J.W.K., 1976. The Karari Industry: Early Pleistocene archaeological evidence from the terrain east of Lake Turkana, Kenya. Nature 262, 102-107.

98.   Isaac, G.L. and Harris, J.W.K., 1978. Archaeology. In: Leaky, M.G. and Leakey, R.E.F. (Eds.), Koobi Fora Research Project Volume 1: The fossil hominids and an introduction to their context, 1968-1974. Clarendon Press, Oxford, pp. 64-85.

99.   Isaac, G.L. and Behrensmeyer, A.K., 1997. Geological context and palaeoenvironments. In: Isaac, G.L. and Isaac, B. (Eds.), Koobi Fora Research Project Volume 5: Plio-Pleistocene Archaeology. Clarendon Press, Oxford, pp. 12-53.

100. Isaac, G.L. and Isaac, B., 1997. Koobi Fora Research Project Volume 5: Plio-Pleistocene Archaeology. Clarendon Press, Oxford.

101. Isaac, G.L, Harris, J.W.K. and Kroll, E.R., 1997. The stone artefact assemblages: a comparative study. In: Isaac, G.L. and Isaac, B. (Eds.), Koobi Fora Research Project Volume 5: Plio-Pleistocene Archaeology. Clarendon Press, Oxford, pp. 262-362.

102. Jo, H.R. and Chough, S. K., 2001. Architectural analysis of fluvial sequences in the northwestern part of Kyongsang Basin (Early Cretaceous), SE Korea. Sedimentary Geology 144, 307-334.

103. Jones, S.J., Frostick, L.E. and Astin, T.R., 2001. Braided stream and flood plain architecture: the Rio Vero Formation, Spanish Pyrenees. Sedimentary Geology 139, 229-260.

104. Katoh, S., Nagaoka, S., WoldeGabriel, G., Renne, P., Snow, M.G., Beyene, Y. and Suwa, G., 2000. Chronostratigraphy and correlation of

the Plio-Pleistocene tephra layers of the Konso Formation, southern Main Ethiopian Rift, Ethiopia. Quaternary Science Reviews 19, 1305-1317.

105. Kaufulu, Z., 1983. The geological context of some early archaeological sites in Kenya, Malawi and Tanzania: microstratigraphy, site formation and interpretation. PhD. Dissertation, University of California (Berkeley).

106. Kibunjia, M., Roche, H., Brown, F. and Leakey, R.E.F., 1992. Pliocene and Pleistocene archaeological sites west of Lake Turkana Kenya. Journal of Human Evolution 23, 431-438.

107. Kimbel, W.H., Walter, R.C., Johanson, D.C., Reed, K.E., Aronson, J.L., Assefa, Z., Marean, C.W., Eck, G.G., Bobe, R., Hovers, E., Rak, Y., Vondra, C., Yemane, T., York, D., Chen, Y., Evensen, N.M. and Smith, P.E., 1994. Late Pliocene *Homo* and Oldowan tools from the Hadar Formation (Kada Hadar Member), Ethiopia. Journal of Human Evolution 31, 549-561.

108. Kirk, M., 1983. Bar development in a fluvial sandstone (Westphalian 'A'), Scotland. Sedimentology 30, 727-742.

109. Kraus, M.J., 1987. Integration of channel and floodplain suites II. Lateral relations of alluvial paleosols. Journal of Sedimentary Petrology 57, 602-612.

110. Kraus, M.J., 1999. Paleosols in clastic sedimentary rocks: their geologic applications. Earth-Science Reviews 47, 41-70.

111. Kraus, M.J., 2002. Basin-scale changes in floodplain paleosols: implications for interpreting alluvial architecture. Journal of Sedimentary Research 72, 500-509.

112. Kraus, M.J. and Aslan, A., 1999. Paleosol sequences in floodplain environments: a hierarchical approach. In: Thiry, M. and Concon, S. (Eds.), Palaeoweathering, Palaeosurfaces and Related Continental Deposits. International Association of Sedimentologists Special Publication 27, 303-321.

113. Kraus, M.J. and Davies-Vollum, K.S., 2004. Mudrock-dominated fills formed in avulsion splay channels: examples from the Willwood Formation, Wyoming. Sedimentology 51, 1127-1144.

114. Le Bas, M.J., Le Maitre, R.W., Streckeisen, A., Zanettin, B. and IUGS Subcommission on the Systematics of Igneous Rocks, 1986. A Chemical Classification of Volcanic Rocks Based on the Total Alkali-Silica Diagram. Journal of Petrology 27, 745-750.

115. Le Maitre, R. W., 1989. A Classification of Igneous Rocks and Glossary of Terms: Recommendations of the International Union of Geological Sciences, Subcommission on the Systematics of Igneous Rocks. Blackwell, Oxford.

116. Leakey, M.D., 1971. Olduvai Gorge, Vol. 3: Excavations in Beds I and II, 1960-1963, Cambridge University Press, Cambridge.

117. Leakey, M.G. and Leakey, R.F., 1978. Koobi Fora Research Project Volume 1: The fossil hominids and an introduction to their context, 1968-1974. Clarendon, Oxford.

118. Leakey, R.E.F., Leakey, M.G. and Behrensmeyer, A.K., 1978. The hominid catalog. In: Leakey, M.G. and Leakey, R.E.F. (Eds.), Koobi Fora Research Project Volume 1: The fossil hominids and an introduction to their context, 1968-1974. Clarendon Press, Oxford, pp. 86-187.

119. Leeder, M.R., Mack, G.H. and Salyards, S.L., 1996. Axial-transverse fluvial interactions in half-graben: Plio-Pleistocene Palomas basin, southern Rio Grande rift, New Mexico, USA. Basin Research 12, 225-241.

120. Leeder, M.R., Harris, T. and Kirkby, M.J., 1998. Sediment supply and climate change: implications for basin stratigraphy. Basin Research 10, 7-18.

121. Leopold, L.B. and Wolman, M.G., 1957. River channel patterns: braided, meandering and straight. U.S. Geological Survey Professional Paper 282B.

122. Lepre, C.J., 2001. Hominid behavior, raw material, and sedimentology from the Okote Member, Koobi Fora Formation, northern Kenya. M.A. Thesis, Rutgers the State University of New Jersey, New Brunswick.

123. Lepre, C.J., Quinn, R.L., Joordens, J.C.A., Swisher III, C.C. and Feibel, C.S., 2007. Plio-Pleistocene facies environments from the KBS Member, Koobi Fora Formation: implications for climate controls on the

development of lake-margin hominin habitats in the northeast Turkana Basin (northwest Kenya). Journal of Human Evolution 53, 504-514.

124. Lourens, L., Hilgen, F., Shackleton, N.J., Laskar, J. and Wilson, D., 2004. The Neogene Period. In: Gradstein, F., Ogg, J. and Smith, A. (Eds.), A Geologic Time Scale. Cambridge University Press, Cambridge, pp. 409-440.

125. Ludwig, B.V. and Harris, J.W.K., 1998. Towards a technological reassessment of East African Plio-Pleistocene lithic assemblages. In: Petraglia, M. and Paddaya, K. (Eds.), The Rise and Diversity of the Lower Paleolithic. Academic Press, New York, pp. 84-106.

126. Lunt, I.A. and Bridge, J.S., 2004. Evolution and deposits of a gravelly braid bar, Sagavanirktok River, Alaska. Sedimentology 51, 415-432.

127. Machette, M.N., 1985. Calcic soils of the southwestern United States. In: Weide, D.L. and Faber, M.L. (Eds.), Soils and Quaternary Geology of the southwestern United States. Geological Society of America Special Paper 203, 1-22.

128. Mack, G.H. and James, W.C., 1992. Calcic paleosols of the Plio-Pleistocene Camp Rice and Palomas Formations, southern Rio Grande rift. Sedimentary Geology 77, 89-109.

129. Mack, G.H. and James, W.C., 1994. Paleoclimate and the global distribution of paleosols. Journal of Geology 102, 360-366.

130. Mack, G.H. and Leeder, M.R., 1999. Climatic and tectonic controls on alluvial-fan and axial-fluvial sedimentation in the Plio-Pleistocene Palomas

half graben, southern Rio Grande Rift. Journal of Sedimentary Research 69, 635-652.

131. Mack, G.H. and Madoff, R.D., 2005. A test of models of fluvial architecture and palaeosol development: Camp Rice Formation (Upper Pliocene-Lower Pleistocene), southern Rio Grande rift, New Mexico, USA. Sedimentology 52, 191-211.

132. Mack, G.H., James, W.C. and Monger, H.C., 1993. Classification of palaeosols. Geological Society of America Bulletin 105, 129-136.

133. Mack, G.H., Macintosh, W.C., Leeder, M.R. and Monger, H.C., 1996. Plio-Pleistocene pumice floods in the ancestral Rio Grande, southern Rio Grande rift, USA. Sedimentary Geology 103, 1-8.

134. Mack, G.H., Cole, D.R., Trevino, L., 2000. The distribution and discrimination of shallow, authigenic carbonate in the Pliocene-Pleistocene Palomas Basin, southern Rio Grande Rift. Geological Society of America Bulletin 112, 643-656.

135. Mackey, S.D. and Bridge, J.S., 1995. Three-dimensional model of alluvial stratigraphy: theory and application. Journal of Sedimentary Research 65, 7-31.

136. Marriott, S.B. and Wright, V.P., 1993. Paleosols as indicators of geomorphic stability in two Old Red Sandstone alluvial suites, South Wales. Journal of the Geological Society of London 150, 1109-1120.

137. McDougall, I., 1985. K-Ar and ^{40}Ar/^{39}Ar dating of the hominid-bearing Pliocene-Pleistocene sequence at Koobi Fora, Lake Turkana, northern Kenya. Geological Society of America Bulletin 96, 159-175.

138. McDougall, I. and Brown, F.H., 2006. Precise ^{40}Ar/^{39}Ar geochronology for the upper Koobi Fora Formation, Turkana Basin, northern Kenya. Journal of the Geological Society of London 163, 205-220.

139. McDougall, I. and Watkins, R.T., 2006. Geochronology of the Nabwal Hills: a record of earliest magmatism in the northern Kenyan Rift Valley. Geological Magazine 143, 25-39.

140. McDougall, I. and Brown, F.H., 2008. Geochronology of the pre-KBS Tuff sequence, Omo Group, Turkana Basin. Journal of the Geological Society 165, 549-562.

141. McDougall, I., F.H., Brown, F.H., Cerling, T.E. and Hillhouse, J.W., 1992. A reappraisal of the geomagnetic polarity time scale to 4 Ma using data from the Turkana Basin, East Africa. Geophysical Research Letters 19, 2349-2352.

142. McHenry, L.J., Mollel, G.F. and Swisher III, C.C., 2008. Compositional and textural correlations between Olduvai Gorge Bed I tephra and volcanic sources in the Ngorongoro Volcanic Highlands, Tanzania. Quaternary International 178, 306-319.

143. McKee, E. D., Crosby, E. J. and Berryhill, H. L., Jr., 1967. Flood deposits, Bijou Creek, Colorado, June 1965. Journal of Sedimentary Petrology 37, 829-851.

144. McLaurin, B.T. and Steel, R.J., 2007. Architecture and origin of an amalgamated fluvial sheet sand, lower Castlegate Formation, Book Cliffs, Utah. Sedimentary Geology 197, 291-311.

145. Miall, A.D., 1977. A review of the braided river depositional environment: Earth-Science Reviews 13, 1-62.

146. Miall, A.D., 1985. Architectural-element analysis: a new method of facies analysis applied to fluvial deposits. Earth-Science Reviews 22, 261-308.

147. Miall, A.D., 1994. Reconstructing fluvial macroform architecture from two-dimensional outcrops: examples from the Castlegate Sandstone, Book Cliffs, Utah. Journal of Sedimentary Research 64, 146-158.

148. Miall, A.D., 1996. The Geology of Fluvial Deposits: sedimentary facies, basin analysis and petroleum geology. Springer, Berlin.

149. Mohrig, D., Heller, P.L., Paola, C. and Lyons, W.J., 2000. Interpreting avulsion process from ancient alluvial sequences: Guadalope–Matarranya system (northern Spain) and Wasatch Formation (western Colorado). Geological Society of America Bulletin 112, 1787-1803.

150. Mollel, G.F., 2002. Petrology and geochemistry of southeastern Ngorongoro Volcanic Highland, and contribution to "sourcing" of stone tools at Olduvai Gorge, Tanzania. M.S. Thesis, Rutgers University the State University of New Jersey, New Brunswick.

151. Morley, C.K., Wescott, W.A., Stone, D.M., Harper, R.M., Wigger, S.T. and Karanja, F.M., 1992. Tectonic evolution of the northern Kenyan Rift. Journal of the Geological Society of London 149, 333-348.

152. Nagaoka, S., Katoh, S., WoldeGabriel, G., Sato, H., Nakaya, H., Beyene, Y. and Suwa, G., 2005. Lithostratigraphy and sedimentary environments of the hominid-bearing Plio–Pleistocene Konso Formation in the southern Main Ethiopian Rift, Ethiopia. Palaeogeography, Palaeoclimatology, Palaeoecology 216, 333-357.

153. Nanson, G.C. and Croke, J.C., 1992. A genetic classification of floodplains. Geomorphology 4, 459-486.

154. Nemec, W. and Steel, R.J., 1984. Alluvial and coastal conglomerates: their significant features and some comments on gravelly mass-flow deposits. In: Koster, E.H. and Steel, R.J. (Eds.), Sedimentology of Gravels and Conglomerates. Canadian Society of Petroleum Geologists Memoir 10, 1-31.

155. Orton, G.J., 1996. Volcanic environments. In: Reading, H.G. (Ed.), Sedimentary Environments: processes, facies and stratigraphy (3rd edition). Blackwell, Oxford, pp. 485–567.

156. Paton, T. R., 1974. Origin and terminology for gilgai in Australia. Geoderma 11, 221-242.

157. Perez-Arlucea, M. and Smith, N.D., 1999. Depositional patterns following the 1870's avulsion of the Saskatchewan River (Cumberland Marshes, Saskatchewan, Canada). Journal of Sedimentary Research 69, 62-73.

158. Perez-Arlucea, M., Mack, G. and Leeder, M., 2000. Reconstructing the ancestral (Plio-Pleistocene) Rio Grande in its active tectonic setting, southern Rio Grande rift, New Mexico, USA. Sedimentology 47, 701-720.

159. Pimentel, N.L., Wright, V.P. and Azevedo, T.M., 1996. Distinguishing early groundwater alteration effects from pedogenesis in ancient alluvial basins: examples from the Palaeogene of southern Portugal. Sedimentary Geology 105, 1-10.

160. Potts, R., 1996. Evolution and Climate Variability. Science 273, 922-923.

161. Potts, R., 1998. Environmental hypotheses of hominid evolution. Yearbook of Physical Anthropology 41, 93-136.

162. Potts, R., Behrensmeyer, A.K. and Ditchfield, P., 1999. Journal of Human Evolution 37, 747-788.

163. Puigdefabregas, C., 1973. Miocene point-bar deposits in the Ebro Basin, northern Spain. Sedimentology 20, 133-144.

164. Quade, J., Levin, L., Semaw, S., Stout, D., Renne, P., Rogers, M. and Simpson, S.W., 2004. Paleoenvironments of the earliest stone toolmakers, Gona, Ethiopia. Geological Society of America Bulletin 116, 1529-1544.

165. Quinn, R.L., Lepre, C.J., Wright, J.D. and Feibel, C.S., 2007. Paleogeographic variations of pedogenic carbonate δ^{13}C values from Koobi Fora, Kenya: implications for floral compositions of Plio-Pleistocene hominin environments. Journal of Human Evolution 53, 560-573.

166. Ramos, A., Sopena, A. and Perez-Arlucea, M., 1986. Evolution of Buntsandstein fluvial sedimentation in the northwest Iberian ranges (Central Spain). Journal of Sedimentary Petrology 56,862-875.

167. Reading, H.G., 1986. Sedimentary Environments: processes, facies and stratigraphy (2nd edition). Blackwell, Oxford.

168. Retallack, G.J., 2001. Soils of the Past (2nd edition). Blackwell, Oxford.

169. Roche, H., Delagnes, A., Brugal, J.-P., Feibel, C., Kibunjia, M., Mourre, V. and Texier, P.-J., 1999. Early hominid stone tool production and technical skill 2.34 Myr ago in West Turkana, Kenya. Nature 399, 57-60.

170. Roche, H., Brugal, J-P., Delagnes, A., Feibel, C., Harmand, S., Kibunjia, M., Prat, S. and Texier, P-J., 2003. Plio-Pleistocene archaeological sites in the Nachukui Formation, West Turkana, Kenya: synthetic results 1997-2001. Comptes Rendus Palevol 2, 663-673.

171. Rogers, M.J. and Sorkowitz, E., 1992. Paleoenvironments and hominid subsistence: new approaches for integrating faunal and lithic archeological remains in the Earth Stone Age of East Africa. Crosscurrents 5, 39-58.

172. Rogers, M.J., Harris, J.W.K. and Feibel, C.S., 1994. Changing patterns of land use by Plio-Pleistocene hominids in the Lake Turkana Basin. Journal of Human Evolution 27, 139-158.

173. Rust, B.R., 1972. Structure and process in a braided river. Sedimentology 18, 221-245.

174. Rust, B.R., 1975. Fabric and structure in glaciofluvial gravels. In: Jopling, A.V. and McDonald, B.C. (Eds.), Glaciofluvial and Glaciolacustrine Sedimentation. Society of Economic Paleontologists and Mineralogists Special Publication 23, 238-248.

175. Rust, B. R., 1978. Depositional models for braided alluvium. In: Miall, A.D. (Ed.), Fluvial Sedimentology. Canadian Society of Petroleum Geologists Memoir 5, 605-625.

176. Rust, B.R., 1984. Proximal braidplain deposits in the Middle Devonian Malbaie Formation of Eastern Gaspe, Quebec, Canada. Sedimentology 31, 675-95.

177. Sarna-Wojcicki, A.M., Meyer, C.E.E., Roth, P.H. and Brown, F.H., 1985. Ages of tuff beds at East African early hominid sites and sediments in the Gulf of Aden. Nature 313, 306-308.

178. Schieber, J., Southard, J. and Thaisen, K., 2007. Accretion of Mudstone Beds from Migrating Floccule Ripples. Science 318, 1760-1763.

179. Semaw, S. Rogers, M., Quade, J., Renne, P., Butler, R.F., Dominguez-Rodrigo, M., Stout, D., Hart, W.S., Pickering T.R. and Simpson, S.W., 2003. 2.6 million-year-old stone tools and associated bones from OGS-6 and OGS-7, Gona, Afar, Ethiopia. Journal of Human Evolution 45, 169-177.

180. Shanley, K.W. and McCabe, P.J., 1994. Perspectives on the sequence stratigraphy of continental strata. American Association of Petroleum Geologists Bulletin 78, 544-568.

181. Slingerland, R. and Smith, N.D., 2004. River avulsions and their deposits. Annual Review of Earth and Planetary Sciences 32, 257-285.

182. Smith, G.A., 1991. Facies sequences and geometries in continental volcaniclastic sediments. In: Fisher, R.V. and Smith, G.A. (Eds.),

Sedimentation in Volcanic Settings. Special Publication of the Society of Economic Paleontologists and Mineralogists 45, 109-121.

183. Smith, N.D., 1974. Sedimentology and bar formation in the upper Kicking Horse River, a braided outwash stream. Journal of Geology 82, 205-23.

184. Smith, N.D., Cross, T.A., Dufficy, J.P. and Clough, S.R., 1989. Anatomy of an avulsion. Sedimentology 36, 1-23.

185. Sneh, A., 1983. Desert stream sequences in the Sinai Peninsula. Journal of Sedimentary Research 53, 1271-1279.

186. Stanistreet, I.G. and McCarthy, T.S., 1993. The Okavango fan and the classification of subaerial fan systems. Sedimentary Geology 85, 115-133.

187. Steel, R.J., 1974. New Red Sandstone floodplain and piedmont sedimentation in the Hebridean Province, Scotland. Journal of Sedimentary Petrology 44, 336-357.

188. Steel, R.J. and Thompson, D.B., 1983. Structures and textures in Triassic braided stream conglomerates ('Bunter' Pebble Beds) in the Sherwood Sandstone Group, North Staffordshire, England. Sedimentology 30, 341-367.

189. Steen-McIntyre, V., 1977. A Manual for Tephrochronology: Collection, Preparation, Petrographic Description and Approximate Dating of Tephra (Volcanic ash). Ph.D. Dissertation, University of Idaho.

190. Stollhofen, H., Stanistreet, I.G., McHenry, L.J., Mollel, G.F., Blumenschine, R.J. and Masao, F.T., 2008. Fingerprinting facies of the

Tuff IF marker, with implications for early hominin palaeoecology, Olduvai Gorge, Tanzania. Palaeogeography, Palaeoclimatology, Palaeoecology 259, 382-409.

191. Suwa, G., Asfaw, B., Beyene, Y., White, T.D., Katoh, S., Nagaoka, S., Nakaya, H., Uzawa, K., Renne, P. and WoldeGabriel, G., 1997. The first skull of *Australopithecus boisei*. Nature 389, 489-492.

192. Toth, N., 1985. The Oldowan reassessed: a close look at early stone artifacts. Journal of Archaeological Science 12, 101-120.

193. Tunbridge, I. P., 1981. Sandy high-energy flood sedimentation: some criteria for recognition, with an example from the Devonian of S.W. England. Sedimentary Geology 28, 79-95.

194. Vondra, C. F. and Burggraf, D. R., Jr., 1978. Fluvial facies of the Plio-Pleistocene Koobi Fora Formation, Karari Ridge, east Lake Turkana, Kenya. In: Miall, A.D. (Ed.), Fluvial Sedimentology. Canadian Society of Petroleum Geologists Memoir 5, 511-529.

195. Vondra, C.F., Johnson, G.D., Bowen, B. E. and Behrensmeyer, A. K., 1971. Preliminary stratigraphical studies of the East Rudolf Basin, Kenya. Nature 231, 245-248.

196. Vrba, E.S., 1995. On the connection between paleoclimate and evolution. In: Vrba, E. S., Denton, G. H., Partridge and T. C., Burckle, L.H. (Eds.), Paleoclimate and Evolution with Emphasis on Human Origins. Yale University Press, New Haven, pp. 24-45.

197. Vrba, E.S., 1999. Habitat Theory in Relation to the Evolution of African Neogene Biota and Hominids. In: Bromage, T.G. and Schrenk, F. (Eds.), African Biogeography, Climate Change, and Human Evolution. Oxford University Press, New York, pp. 19-34.

198. Walker, R.G., 1984. Facies Models: General Introduction. Geoscience Canada Reprint Series 1, 1-10.

199. Watkins, R.T., 1986. Volcano-tectonic control on sedimentation in the Koobi Fora sedimentary basin, Lake Turkana. In: Frostick, L.E., Renaut, R.W., Reid, I. and Tiercelin, J-J. (Eds.), Sedimentation in the African Rifts. Geological Society of London Special Publication 25, 85-95.

200. Wescott, W. A., Morley, C. K. and Karanja, F. M., 1996. Tectonic controls on the development of rift-basin lakes and their sedimentary character: examples from the East African rift system. In: Johnson, T.C. and Odada, E.O. (Eds.), The Limnology, Climatology and Paleoclimatology of the East African Lakes. Gordon and Breach Publishers, Amsterdam, pp. 3-21.

201. White, H.J., Burggraf, D.R., Jr., Bainbridge, R.B., Jr. and Vondra, C.F., 1981. Hominid habitats in the Rift Valley: Part 1. In: Rapp, G., Jr. and Vondra, C.F. (Eds.), Hominid sites: their geologic settings. American Association for the Advancement of Science Selected Symposium 63, Boulder, pp. 57-113.

202. Wilding, L.P. and Ruben, P., 1988. Vertisols: their distribution, properties, classification, and management. Texas A&M University Printing Center, College Station.

203. Williams, G.E., 1971. Flood deposits of the sand-bed ephemeral streams of central Australia. Sedimentology 17, 1-40.

204. Williams, P.F. and Rust, B.R., 1969. The sedimentology of a braided river. Journal of Sedimentary Petrology 39, 649-679.

205. Williamson, P.G., 1982. Molluscan biostratigraphy of the Koobi Fora hominid-bearing deposits. Nature 295, 140-142.

206. Willis, B.J., 1989. Palaeochannel reconstruction from point bar deposits: a three-dimensional perspective. Sedimentology 36, 757-766.

207. Willis, B.J., 1993. Interpretation of bedding geometry within ancient point-bar deposits. In: Marzo, M. and Puigdefabregas, C. (Eds.), Alluvial Sedimentation. International Association of Sedimentologists Special Publication 17, 101-114.

208. Willis, B.J. and Behrensmeyer, A.K., 1994. Architecture of Miocene overbank deposits in northern Pakistan. Journal of Sedimentary Research B64, 60-67.

209. Wilson, M., 1993. Magmatic differentiation. Journal of Geological Society of London 150, 611-624.

210. Wolde-Gabriel, G. and Aronson, J.L., 1987. Chow Bahir Rift: a ''failed'' rift in southern Ethiopia. Geology 15, 430-433.

211. WoldeGabriel, G., Walter, R.C., Aronson, J.L. and Hart, W.K., 1992. Geochronology and distribution of silicic volcanic rocks of Plio–Pleistocene age from the central sector of the Main Ethiopian Rift. Quaternary International 13-14, 69-76.

212. WoldeGabriel, G., Hart, W.K., Katoh, S., Beyene, Y. and Suwa, G., 2005. Correlation of Plio–Pleistocene Tephra in Ethiopian and Kenyan rift basins: Temporal calibration of geological features and hominid fossil records. Journal of Volcanology and Geothermal Research 147, 81-108.

213. Wood, B.A., 1991. Koobi Fora Research Project Volume 4: Hominid Cranial Remains from Koobi Fora. Clarendon, Oxford.

214. Wood, B.A. and Strait, D., 2004. Patterns of resource use in early *Homo* and *Paranthropus*. Journal of Human Evolution 46, 119-237.

215. Wynn, J.G., 1998. Paleopedological characteristics associated with intervals of environmental change from the Neogene Turkana Basin, Northern Kenya. M.S. Thesis, University of Utah.

216. Wynn, J.G., 2000. Paleosols, stable carbon isotopes, and paleoenvironmental interpretation of Kanapoi, Northern Kenya. Journal of Human Evolution 39, 411-432.

217. Wynn, J.G., 2004. Influence of Plio-Pleistocene aridification on human evolution: evidence from paleosols of the Turkana Basin, Kenya. American Journal of Physical Anthropology 123, 106-118.

218. Wynn, J.G. and Feibel, C.S., 1995. Paleoclimatic implications of vertisols within the Koobi Fora Formation, Turkana Basin, northern Kenya. The University of Utah's Journal of Undergraduate Research 6, 32-42.

219. Yaalon, D.H. and Kalmar, D., 1978. Dynamics of cracking and swelling clay soils: displacement of skeletal grains, optimum depth of slickensides, and rate of intra-pedonic turbation. Earth Surface Processes 3, 31-42.

Curriculum Vitae

Christopher John Lepre

1998   Montclair State University, Montclair, New Jersey (USA)

                Bachelor of Arts, Anthropology

2001   Rutgers University, New Brunswick, New Jersey (USA)

                Master of Arts, Anthropology

2009   Rutgers University, New Brunswick, New Jersey (USA)

                Doctor of Philosophy, Anthropology

2002-2009   Part-Time Faculty of Anthropology

                William Paterson University, Wayne, New Jersey (USA)

2007   Leprec, C.J., Quinn, R.L., Joordens, J.C.A., Swisher III, C.C.
                and Feibel, C.S., 2007. Plio-Pleistocene facies
                environments from the KBS Member, Koobi Fora Formation:
                implications for climate controls on the development of lake-
                margin hominin habitats in the northeast Turkana Basin
                (northwest Kenya). Journal of Human Evolution 53, 504-
                514.